Tectonometamorphic evolution of Seram and Ambon, eastern Indonesia: Insights from $^{40}Ar/^{39}Ar$ geochronology

Jonathan M. Pownall[a,b,*], Marnie A. Forster[b], Robert Hall[a], Ian M. Watkinson[a]

[a]*SE Asia Research Group, Department of Earth Sciences, Royal Holloway University of London, Egham TW20 0EX, United Kingdom*
[b]*Research School of Earth Sciences, Australian National University, Canberra, ACT 2601, Australia*
**Corresponding author (e-mail: jonathan.pownall@anu.edu.au)*

Abstract

The island of Seram, eastern Indonesia, experienced a complex Neogene history of multiple metamorphic and deformational events driven by Australia–SE Asia collision. Geological mapping, and structural and petrographic analysis has identified two main phases in the island's tectonic, metamorphic, and magmatic evolution: (1) an initial episode of extreme extension that exhumed hot lherzolites from the subcontinental lithospheric mantle and drove ultrahigh-temperature metamorphism and melting of adjacent continental crust; and (2) subsequent episodes of extensional detachment faulting and strike-slip faulting that further exhumed granulites and mantle rocks across Seram and Ambon. Here we present the results of sixteen $^{40}Ar/^{39}Ar$ furnace step heating experiments on white mica, biotite, and phlogopite for a suite of twelve rocks that were targeted to further unravel Seram's tectonic and metamorphic history. Despite a wide lithological and structural diversity among the samples, there is a remarkable degree of correlation between the $^{40}Ar/^{39}Ar$ ages recorded by different rock types situated in different structural settings, recording thermal events at 16 Ma, 5.7 Ma, 4.5 Ma, and 3.4 Ma. These frequently measured ages are defined, in most instances, by two or more $^{40}Ar/^{39}Ar$

ages that are identical within error. At 16 Ma, a major kyanite-grade metamorphic event affected the Tehoru Formation across western and central Seram, coincident with ultrahigh-temperature metamorphism and melting of granulite-facies rocks comprising the Kobipoto Complex, and the intrusion of lamprophyres. Later, at 5.7 Ma, Kobipoto Complex rocks were exhumed beneath extensional detachment faults on the Kaibobo Peninsula of western Seram, heating and shearing adjacent Tehoru Formation schists to form Taunusa Complex gneisses. Then, at 4.5 Ma, $^{40}Ar/^{39}Ar$ ages record deformation within the Kawa Shear Zone (central Seram) and overprinting of detachment faults in western Seram. Finally, at 3.4 Ma, Kobipoto Complex migmatites were exhumed on Ambon, at the same time as deformation within the Kawa Shear Zone and further overprinting of detachments in western Seram. These ages support there having been multiple synchronised episodes of high-temperature extension and strike-slip faulting, interpreted to be the result of Western Seram having been ripped off from SE Sulawesi, extended, and dragged east by subduction rollback of the Banda Slab.

Keywords: Banda, rollback, extension, mantle exhumation, argon

1. Introduction

The northwestern edge of the Australian continental margin is reconstructed to have collided with SE Asia approximately 23 million years ago (Hall, 2011). Continuing Australia–SE Asia convergence has since been accommodated by a complex tectonic system of multiple subduction zones and shear zones that comprise eastern Indonesia (Fig. 1). The exact geometry and configuration of these subduction zones remains a hotly disputed subject, which has led to multiple tectonic models for the evolution of the region (cf. Hamilton, 1979; Hall, 1996, 2002, 2011, 2012; Charlton, 2000; Milsom, 2001; Hinschberger et al., 2005; Gaina and Müller, 2007; Richards et al., 2007; Spakman and Hall, 2010; Villeneuve et al., 2010; Pownall et al., 2013; Zahirovic et al., 2014; Hall and Spakman, 2015). To decipher the Neogene tectonics of the region it is vital to determine the formation mechanism of the Banda Arc – a 180°-curved string of islands (from Timor round to Buru; see Fig. 1) that connects with the Sunda Arc to its west. The oceanic lithosphere subducted around the arc forms a concave chute that plunges to the west to depths in excess of 650 km (Cardwell and Isacks, 1978; McCaffrey, 1998; Das, 2004; Spakman and Hall, 2010; Pownall et al., 2013; Hall and Spakman, 2015); clearly, this geometry cannot have been created simply by subduction from a straight or low-curvature hinge line. Several authors have suggested that the slab's concave shape is explained by southeastward rollback of a single subduction zone whose curvature progressively tightened (e.g. Hall and Wilson, 2000; Milsom, 2001; Spakman and Hall, 2010; Hall, 2011, 2012; Pownall et al., 2013; Hall and Spakman, 2015). Other authors have instead proposed that the subducted lithosphere beneath the Banda Sea comprises two or more separate slabs that were subducted from different directions (e.g. Cardwell and Isacks, 1978; Das, 2004).

The islands of Seram (Fig. 2), Buru, and the small islands located in the eastern Banda Arc provide the opportunity to understand how subduction developed and proceeded in the Banda Region. Seram was for a long time interpreted to comprise a collisional fold-and-thrust belt incorporating ultramafic thrust sheets of ophiolitic origin (Audley-Charles et al., 1979; Linthout et al., 1996); however, recent geological field investigations on Seram found evidence instead for substantial extension having exhumed the ultramafic rocks from the subcontinental lithospheric mantle (SCLM), alongside granulite-facies migmatites of the Kobipoto Complex (Pownall et al., 2013, 2014, 2016; Pownall and Hall, 2014; Pownall, 2015). Residual granulites from the Kobipoto Complex record evidence for ultrahigh-temperature (UHT: > 900°C) metamorphism at 16 Ma, caused by their juxtaposition with the hot exhuming mantle lherzolites (Pownall et al., 2014; Pownall, 2015). In western Seram, Kobipoto Complex lherzolites and granulite-facies migmatites were exhumed beneath extensional detachment faults, and across central Seram, these rocks have been subsequently incorporated within the major strike-slip Kawa Shear Zone (KSZ; Pownall et al., 2013).

The sense of lithospheric deformation across the island inferred from mapping (broad NNE–SSW extension; WNW–ESE-striking left-lateral strike-slip shearing) is consistent with it having been dragged eastwards into position above a rolling-back slab, as proposed by Spakman and Hall (2010), Hall (2011, 2012), and Pownall et al. (2013, 2014). However, there are many unanswered questions regarding the timing of extreme extension and strike-slip faulting on Seram, and the link between these tectonic events and the recently-identified episode of Middle Miocene UHT metamorphism (Pownall et al., 2014, *in review*; Pownall, 2015).

In this paper, we present (*i*) thirteen new $^{40}Ar/^{39}Ar$ ages for white mica and biotite from Tehoru Formation, Taunusa Complex, and Kobipoto Complex metamorphic rocks and migmatites from western and central Seram; (*ii*) a new $^{40}Ar/^{39}Ar$ age for a Kobipoto Complex diatexite on Ambon; and (*iii*) a new $^{40}Ar/^{39}Ar$ age for a phlogopite lamprophyre found in association with the ultramafic complex exposed in the Kobipoto Mountains. Several rocks were sampled from shear zones associated with Kobipoto Complex exhumation, and from the major Kawa Shear Zone in central Seram. Other rocks were sampled because they record the highest metamorphic grade experienced by their respective metamorphic complex. Some micas have been dated from migmatites for which SHRIMP U–Pb zircon ages have also been acquired (Table 1; Pownall et al., 2014, *in review*) in order to compare the two geochronological systems and assess cooling rates and/or differences in respective closure temperatures. This paper presents interpretations of these $^{40}Ar/^{39}Ar$ ages in the context of microstructural and larger-scale structural observations which help to unravel the sequence of metamorphic, magmatic, and deformational events on Seram.

2. Geological context and sample petrography

Seram exposes several complexes comprising upper-mantle lherzolites and mid/lower-crustal granulite-facies migmatites of the Kobipoto Complex (Pownall, 2015). Granulites from the Kobipoto Mountains, central Seram, record an episode of widespread crustal melting and metamorphism under UHT conditions reaching 925˚C and 9 kbar (Pownall, 2015) shortly before 16 Ma (Pownall et al., 2014). These high-temperature rocks are exposed in western Seram beneath low-angle WNW–ESE-striking detachment faults (Fig. 2c, 3), but in the Kobipoto Mountains of central Seram are incorporated within transpressional pop-up structures (Pownall et al., 2013; Pownall and Hall, 2014; Pownall, 2015). Boudins of serpentinised lherzolites are also located within the Kawa Shear Zone (Fig. 2a) – a strike-slip fault system that traverses the centre of the island. Kobipoto Complex exhumation has evidently been facilitated by different structures at different stages of Seram's tectonic evolution.

In all instances, the Kobipoto Complex has been exhumed beneath or alongside lower grade metamorphic rocks of the Tehoru Formation (Pownall et al., 2013). As noted by Linthout et al. (1989), Tehoru Formation schists and phyllites exposed on the Kaibobo Peninsula in west Seram (Fig. 2c) immediately adjacent to the Kobipoto Complex have been overprinted by a sillimanite-grade shear zone parallel to the Tehoru Formation/Kobipoto Complex contact. Similar field relations are also evident on the neighbouring Hoamoal Peninsula (Fig. 2b). These sheared, sillimanite-grade gneisses were defined by Pownall et al. (2013) as comprising the Taunusa Complex, adapting an earlier definition by Tjokrosapoetro and Budhitrisna (1982). In considering the ultramafic rocks of the Kobipoto Complex to represent an overthrust ophiolite (as implied by Audley-Charles et al., 1979), Linthout et al. (1996) interpreted this metamorphosed shear zone as a sub-ophiolite metamorphic sole. These authors dated biotite and white mica from their 'sole' rocks using an $^{40}Ar/^{39}Ar$ laser step heating method, yielding ages of 6.6–5.4 Ma (Table 1); however, they concluded that these ages related to ophiolite emplacement, as opposed to our view that the ultramafic rocks were exhumed by detachment faulting. Two samples analysed as part of this study (KB11-234 and KB11-374) were taken from similar locations to Linthout et al.'s (1996) sample BK21, within the Taunusa Complex, to enable comparison (Fig. 2c).

As previously mentioned, Kobipoto Complex granulites and lherzolites crop out also in the Kobipoto Mountains of central Seram – a large left-lateral positive flower structure forming the northern extent of the Kawa Shear Zone. The southern extent of this wide shear zone is defined by the topographically prominent Kawa Fault (Fig. 2a), approaching which Tehoru Formation schists become progressively mylonitised. The Kawa Fault juxtaposes Tehoru Formation mylonites against low-grade slates and marbles of the Saku Formation to their north across *c.* 1 km of stranded fault cores and damage zones (Fig. 6; Linthout et al., 1989, 1991; Pownall et al., 2013). Based on mylonitic fabrics, Linthout et al. (1991) interpreted this shear zone as a right-lateral strike-slip system that operated as an antithetic shear within an anticlockwise-rotating 'Buru-Seram Microplate', supporting a reconnaissance paleomagnetic study by Haile (1978), who tentatively suggested that Seram has rotated 74° anticlockwise since 7.6 ± 1.4 Ma (K–Ar age for Kelang pillow basalts; Beckinsale and Nakapadungrat, 1979). Rb–Sr ages of *c.* 3 Ma obtained by Linthout et al. (1991) for Kawa Shear Zone mylonites (Table 1) were interpreted by them as having been reset by hydrothermal fluids that ascended through the antithetic fault network during the hypothesised rotation. However, our fieldwork within the Kawa Shear Zone found evidence for both right- *and* left-lateral shear recorded by the microstructures of alternating mylonite and foliated gouge exposures (Pownall et al., 2013); which do not unambiguously identify an overall shear sense, and instead suggest a history of multiple re-activations with both left- and right-lateral displacement. Furthermore, interpretation of regional topography of the mountains north of the Kawa Fault (i.e., the Kobipoto Mountains pop-up), and Quaternary geomorphology along the fault indicates that left-lateral strike-slip shear was the most recent upper crustal deformation within this zone (Pownall et al., 2013; Pownall and Hall, 2014; Watkinson and Hall, 2016).

2.1. Kobipoto Complex

The Kobipoto Complex (Fig. 4), redefined by Pownall et al. (2013), includes all rocks comprising part of the upper mantle to mid/lower crust exhumed across Seram, Ambon, and possibly islands to the east of Seram (e.g. Kur, Fadol, Kasiui). Exposed granulite-facies migmatites include melanosome-dominated metatexites (including those recording UHT metamorphism; Pownall et al., 2014; Pownall, 2015) and more abundant leucosome-rich cordierite- and garnet-bearing diatexites (described by some previous authors, e.g. Priem et al., 1978, as 'cordierite granites').

Ultramafic rocks, typically lherzolites, accompany the migmatites in every known instance, leading Pownall et al. (2014) to conclude that the extensive crustal melting and granulite-facies metamorphism was driven by the juxtaposition of the hot subcontinental lithospheric mantle with the base of the extended crust.

Kobipoto Complex granulites from the Kobipoto Mountains were described in detail by Pownall (2015), and *c*. 16 Ma SHRIMP U–Pb zircon ages for migmatites exposed in central Seram were presented by Pownall et al. (2014). An $^{40}Ar/^{39}Ar$ biotite age of 16.34 ± 0.04 Ma for a Kobipoto Complex migmatite from the Kobipoto Mountains (Pownall et al., 2014), is within error of the SHRIMP U–Pb zircon age acquired from the same sample (Table 1).

2.1.2. KP11-619 – Grt–Crd–Sil Metatexite

KP11-619 is a metatexite boulder collected from the upstream section of the Wai Tuh in the Kobipoto Mountains and described by Pownall et al. (2014). It contains abundant melanosome comprising cordierite + biotite + garnet + sillimanite. Garnets commonly exceed 5 mm in diameter. Cordierite is typically pinitised, although some of the fresher cordierite contains sprays of sillimanite needles and is associated with two generations of biotite; a dark amorphous generation in direct grain contact with the cordierite and large blebs of ilmenite, and a stubby idioblastic population of biotite that is often is included within the amorphous type (Fig. 4a).

2.1.3. SE10-178 – Cordierite diatexite, Kaibobo Peninsula

This typical ‘cordierite granite’, sampled from the northern body of Kobipoto Complex diatexites on the Kaibobo Peninsula, is characterised by abundant mm-scale sillimanite–spinel schlieren (Fig. 4b), associated with biotite. Cordierite is abundant, partially pinitised, and has white mica reaction rims. Garnet is scarce. Quartz has crystallised into complex subgrains, and plagioclase and K-feldspar are typically idioblastic. Zircon from this sample has been dated by Pownall et al. (*in review*).

2.1.4. KB11-367 – Mylonitised cordierite diatexite, Kaibobo Peninsula

Mylonitised cordierite diatexites are incorporated within a shear zone exposed on the Tanjung Motianai headland of the Kaibobo Peninsula (Fig. 2c; see also Pownall et al., 2013). Mylonitic lineations plunge 12° to the WSW. Cordierite diatexite KB11-367 has a very similar mineralogy to the undeformed diatexites in the centre of the peninsula (e.g. SE10-178). A second generation of biotite has grown along shear bands, wrapping around feldspar clasts and older larger grains of biotite that have acquired fish-type morphologies (Fig. 4c).

2.1.5. AM10-167 – Cordierite diatexite, Ambon

Cordierite diatexite AM10-167 was sampled near to the migmatite–peridotite contact on the southern coast of Latimor, Ambon. This sample is very similar to SE10-178, although biotite is more abundant and spinel + sillimanite schlieren are scarcer.

2.2. Tehoru Formation

Here we follow the definition of the Tehoru Formation given by Audley-Charles et al. (1979), which is approximately equivalent to the 'Formation of Crystalline Schists and Phyllites' described by Valk (1945) and Germeraad (1946). This extensive metamorphic complex (Fig. 5), which crops out over much of western and central Seram, is typified by monotonous greenschist to lower-amphibolite facies metapelites commonly interbanded with metabasic amphibolites. The greenschists are dominantly phyllitic, and the majority of the higher-grade schists contain simple garnet–biotite–muscovite–chlorite assemblages. In addition, staurolite-grade schists and gneisses have also been identified in outcrop, and several authors have reported kyanite-grade schists occurring as float in rivers draining the mountainous interior of the island (Valk, 1945; Audley-Charles et al., 1979; Linthout et al., 1989; Pownall et al., 2013). Linthout et al. (1989) calculated peak metamorphic conditions of ~ 600°C and ~ 5 kbar, followed by cooling and decompression to ~ 500°C and ~ 2 kbar, for staurolite–garnet schists in central Seram based on conventional cation exchange thermobarometry. The protolith of the Tehoru Formation has been assumed to be Paleozoic (Valk, 1945; Audley-Charles et al., 1979; Tjokrosapoetro and Budhitrisna, 1982; Tjokrosapoetro et al., 1993a,b), although Triassic detrital zircon dated by Pownall et al. (2014) from the Kobipoto Complex migmatites, and Jurassic zircon grains recovered from the overlying Kanikeh Formation by Hall and Sevastjanova (2012) demonstrate that this estimate is likely to be too old.

2.2.1. HM11-177 – Hoamoal Peninsula Ky–St–Grt schist

Sample HM11-177 (Fig. 5a–c), a kyanite–staurolite–garnet Tehoru Formation schist, was collected as a small cobble from a stream draining the northwestern portion of the Hoamoal Peninsula. Kyanite-grade schists (representing the highest metamorphic grade of the Tehoru Formation) have not been observed to crop out in this region, so *in situ* sampling was unfortunately not possible. Abundant 1–2 mm-diameter garnet porphyroblasts are wrapped by thick swathes of white mica. Blue kyanite blades are fairly conspicuous in hand sample; staurolite porphyroblasts are also present, although are smaller and scarcer than the garnets. Recrystallised quartz is abundant in the matrix and red-brown rutile grains are present throughout. The garnets are highly poikiloblastic and contain coarse grains of quartz that are concentrated in the cores (Fig. 5b). Many of the garnets display excellent 'snowball' quartz inclusion patterns, providing strong evidence for syn-kinematic growth, and preserving older fabrics. Staurolite is similarly poikiloblastic although does not display such obvious evidence for rotation during growth. There are two distinct populations of white mica present in this schist: (*i*) highly elongate, almost fibrous mats of white mica which form mm-thick, highly crenulated bundles with tight zig-zag folds that wrap around the garnet, staurolite, and kyanite porphyroblasts; and (*ii*) coarser, stubbier, and scarcer grains of white mica that post-date the crenulation, and may have recrystallized from the older crenulated white mica. These two generations of white mica are referred to here as 1st-generation, and 2nd-generation, respectively.

2.2.2. TS11-496 – Kawa Shear Zone Grt mica schist

This mylonite and associated retrograde fault gouges (Fig. 5d–f), formed within the Kawa Shear Zone, was sampled during a river traverse undertaken from the Trans-Seram Highway in central Seram (Fig. 6). Fairly abundant (~10 vol.%) mm-scale garnet porphyroblasts contain curved trails of quartz inclusions. They are partly wrapped round by biotite and/or white mica or flanked by abundant quartz. White mica also forms highly-crenulated aggregates that are concentrated along minor shear bands. Based on cross-cutting relationships, the white mica appears to be slightly older than the biotite, which also defines the shear bands. σ-type garnet porphyroblasts indicate a left-lateral shear sense.

2.2.3. SER-26C – Kawa Shear Zone Grt–Hbl mica schist

This schist (Fig. 5g–i) was sampled north of the village of Tehoru from a NW–SE-striking strike-slip shear zone within the Tehoru Formation. It is characterised by abundant 0.1–1.0 mm subhedral garnet and hornblende porphyroblasts found in association with coarse grains of biotite. Coarse grains of plagioclase are found in other domains of the rock; finely-recrystallised quartz is abundant throughout. Many of the hornblendes have sigmoidal geometries that are aligned with the biotite grains. Narrow biotite-rich shear bands are oriented parallel to the C-planes of an S–C′ fabric that is weakly defined by hornblende and biotite crenulation (Fig. 5i). The hornblende and biotite define the same fabric in the rock, but the hornblende appears to predate biotite formation.

2.3. Saku Formation

Low-grade slates and marbles of the Saku Formation (Hartono and Tjokrosapoetro, 1984) are located north of the Kawa Fault (Fig. 2a). Their protolith is thought to have overlain the protolith of the Tehoru Formation (Tjokrosapoetro et al., 1993a). No rocks sampled from the Saku Formation were suitable for $^{40}Ar/^{39}Ar$ dating.

2.4. Taunusa Complex

The Taunusa Complex (Fig. 6) is considered here and by Pownall et al. (2013) as a high-T overprint of the Tehoru Formation in response to heating and shearing by the Kobipoto Complex peridotites and migmatites. Sillimanite-bearing schists and gneisses comprising the hanging wall above exhumed Kobipoto Complex rocks on the Kaibobo Peninsula (Pownall et al., 2013, *in review*) were shown by Linthout et al. (1989) to have been metamorphosed at temperatures surpassing 700˚C (at 4–5 kbar) – around 100˚C hotter than they determined for the Tehoru Formation. Similar contact relations are observed on the nearby Hoamoal Peninsula, where Taunusa Complex rocks separate the Kobipoto Complex and Tehoru Formation (Pownall et al., 2013).

2.4.1. KB11-234 – Kaibobo Peninsula Sil gneiss

This gneiss (Fig. 6a–c), sampled from the hanging wall above the Kaibobo Detachment (Fig. 2c), comprises alternating quartzofeldspathic and biotite-rich bands that have been crosscut by narrow shear bands comprising fibrous sillimanite and biotite. These shear bands define a weak S–C fabric, enclosing sigmoidal microlithons (Fig. 6b). Scarce relict garnet poikiloblasts are heavily altered and partly pseudomorphed by biotite. Large white mica grains are present in the quartzofeldspathic domains, where quartz has recrystallised between large K-feldspars. Growth of sillimanite is interpreted to have been caused by high-T shearing during Kobipoto Complex exhumation.

2.4.2. KB11-374 – Kaibobo Peninsula Sil–mica gneiss

This Taunusa Complex gneiss (Fig. 6d–f), sampled ~ 1 km west of KP11-234, was also heated and sheared by the high-T exhumation of the adjacent Kobipoto Complex. Bands of recrystallised quartz host plagioclase grains and large (up to 5 mm) white mica 'fish' indicating top-to-the-north shear (Fig. 6d,e). As also observed by Linthout et al. (1996) in a similar nearby sample BK21 (Fig. 2c), these white mica fish contain inclusions of folded fibrolitic sillimanite, demonstrating that white mica crystallization must have occurred during the latter stages of high-T shearing. Coarse white mica grains within the more mafic segregations of the gneiss define an S–C fabric, again indicative of top-to-the-north shear. Here, the white mica is frequently boudinaged, with biotite having formed in the strain shadows (Fig. 6d).

Porphyroblastic minerals are absent from this rock.

2.4.3. SER-7 – Hoamoal Peninsula And–Sil–Bt schist

This schist was sampled from the west coast of the Hoamoal Peninsula adjacent to Kobipoto Complex lherzolites and scarce diatexites that have been exhumed in the vicinity of Luhu village (Fig. 2b). Here, the contact is a steep reverse fault, and the schists in the vicinity of sample SER-7 indicate top-to-the-NNW shear sense (Fig. 6g). SER-7 (Fig. 6g–i) comprises quartz bands of various grain sizes interspersed with narrow biotite-rich zones hosting mm-scale andalusite crystals, with an elongate morphology characteristic of pseudomorphs after kyanite. This inference is supported by the presence of blue kyanite rods in an adjacent outcrop. The biotite exists mainly as small partially chloritised stubby flakes formed between quartz grains, but more rarely larger elongate grains are present. Chloritised white mica is also present. Narrow anastomosing trails of sillimanite traverse the rock subparallel to the main foliation, defining minor shear bands. Fine intergrowths of sillimanite and biotite suggest some of the biotite must have formed during or shortly after the high-T (sillimanite-grade) metamorphic peak, when the rock is thought to have been heated and sheared by exhumation of the neighboring Kobipoto Complex in a similar manner to KB11-234 and KB11-374.

2.4.4. KP11-581D – Kobipoto Mountains Grt–Sil metatexite

This sample (Fig. 6j–l) was collected as a small boulder in the Wai Sapolewa, Kobipoto Mountains. In contrast to the metamorphic rocks of the Kobipoto Complex, this sample has not been metamorphosed in the granulite facies, although it has experienced considerable partial melting. The melanosome comprises large garnet phenocrysts wrapped by tightly-folded swathes of white mica and sillimanite, which is more characteristic of samples belonging to the Taunusa Complex than the Tehoru Formation. The leucosome comprises coarse recrystallised quartz with highly sutured subgrains grown around randomly-oriented mm-scale (up to 5 mm long) laths of white mica. Large apatite grains are also present.

2.5. Lamprophyric rocks

Several phlogopite-rich lamprophyric rocks were observed to intrude the lherzolites exposed within the Kobipoto Mountains (Fig. 2a). This may be the same rock type referred to by Germeraad (1946), who described an "apatite biotitite" comprising 82 vol.% biotite from the same region (collected by L.M.R. Rutten and W. Hotz between 1917 and 1919).

2.5.1. KP11-593 – Phlogopite Minette

A phlogopite-rich lamprophyre was found as a boulder in the Wai Tuh, Kobipoto Mountains (Fig. 7a). Very similar lithologies were also observed as intrusions within metre-scale lherzolite boulders (Fig. 7b). Bronze-coloured phlogopite crystals attain lengths sometimes in excess of 2 cm (Fig. 7c). Smaller and far scarcer apatite grains also feature as phenocrysts. The groundmass comprises K-feldspar, plagioclase, and smaller biotites. Quartz is absent, although so are feldspathoids. We have interpreted this lamprophyre as a minette (following Le Maitre, 2002) based on the dominant phlogopite–K-feldspar mineralogy, and its K- and Na-rich bulk chemistry (3.38 wt.% K_2O; 3.83 wt.% Na_2O), high Mg (16.82 wt.% MgO), and low silica content (49.95 wt.% SiO_2) determined by X-ray fluorescence (XRF) spectroscopy (see Supplementary Data File 1). As these lamprophyres formed by melting of the ultramafic complex, $^{40}Ar/^{39}Ar$ dating of the phlogopite indicates the time of lherzolite exhumation and/or cooling.

3. $^{40}Ar/^{39}Ar$ geochronology

Sixteen mica separates (9 biotite, 6 white mica, and 1 phlogopite) were dated from twelve rocks, as listed in Table 2. The Taunusa Complex samples are all from the hanging wall directly above the exhumed Kobipoto Complex rocks. The Tehoru Formation samples are taken either from the Kawa Shear Zone, or were sampled on the basis that they have experienced kyanite-grade metamorphism, representing the highest grade achieved by this metamorphic unit. The Kobipoto Complex diatexites, as previously mentioned, are from the Kobipoto Mountains, the Kaibobo Peninsula, and from Ambon. Phlogopite was dated from the lamprophyre sampled from the Kobipoto Mountains that was found to intrude the ultramafic complex. The relative structural locations and metamorphic classifications for all samples are shown schematically in Figure 8.

3.1. Methods

Two different methods were used to separate the micas from their host rock (as noted in Table 2), at Royal Holloway University of London. *Method 1* involved removing the mica from an uncrushed hand sample by splitting the rock along its cleavage and carving out selected mica-dominated microstructures with a sharp knife; *Method 2* involved crushing the sample to a fine gravel size and then wet sieving this sample to extract 63–250 μm grains before separating the grains based on their magnetic susceptibilities using a Frantz magnetic barrier separator. Both methods required subsequent 'papering' and hand picking under a binocular microscope to increase the purity of the separates. Method 1 was our preference as it allowed individual microstructures to be targeted for analysis; however, the relatively scarce and fine-grained nature of mica made it necessary to use Method 2 for some of the samples.

The samples were irradiated in two separate batches alongside CaF_2 and K-glass standards. Biotite samples SER-7, SER-26C, SE10-178, and AM10-167 were packed into Cd-shielded canister number 'ANU#7' and were irradiated by the McMaster reactor, Ontario, in for 8 MWh. The other 12 samples were packed into Cd-shielded canister number 'ANU#13' and were irradiated by the United States Geological Survey TRIGA reactor, Denver, for 12 MWh. Fish Canyon Tuff sanidine (28.10 ± 0.04 Ma K–Ar age; Spell and McDougall, 2003) was used as the flux monitor for the ANU#7 samples, and biotite standard GA-1550 (98.5 ± 0.8 Ma K–Ar age; Spell and McDougall, 2003) was used as the flux monitor for the ANU#13 samples.

All irradiated samples were repackaged and analysed at the Research School of Earth Sciences (Australian National University) Argon Laboratory using the *in vacuo* furnace step-heating method described previously by Forster and Lister (2010, 2014). The samples were dropped into a tantalum crucible within a double-vacuum resistance furnace, and raised to increasingly higher thermostatically controlled temperatures for 15-minute durations, between which the furnace was left to cool to a 350°C resting temperature. Typically, 21 to 23 heating steps were performed on each sample, with a minimum difference between successive heating steps of +30°C. A final heating step at 1450°C ensured all gas was released from the sample, and an extensive cleaning procedure involving evacuating and heating the empty furnace to 1450°C (repeated three times) minimised the risk of cross-sample contamination.

Gas incrementally released from the samples during the step-heating procedure was released through an ultrahigh-vacuum extraction line to a VG1200 gas-source mass spectrometer that measured the abundances of ^{36}Ar, ^{37}Ar, ^{38}Ar, ^{39}Ar, and ^{40}Ar with a 7.6×10^{-17} mol mV^{-1} sensitivity. The flux monitors were degassed using a Coherent infrared diode laser and analysed using the same extraction line and mass spectrometer.

The data were reduced using *Noble v1.8* software in accordance with the correction factors and J-factors listed in Appendix A. Correction factors were calculated from the analyses of CaF_2 and K-glass, and J-factors were calculated from analysis of the flux monitors, all of which were irradiated at known distances from the samples. ^{40}K abundances and decay constants are taken from standard values recommended by the IUGS subcommission on geochronology (Steiger and Jäger, 1977). The decay factor of ^{40}K ($\lambda^{40}K$) for all age calculations was set at 5.5430×10^{-10} yr^{-1}.

Results tables for each step heating experiment are presented in Appendix A, with a summary of these ages and their interpretations presented in the final column of Table 2.

3.2. Interpretation of apparent age spectra

The apparent age spectra for the 16 samples are presented in Figure 9 (for ages < 12 Ma) and Figure 10 (for ages *c*. 16 Ma). Errors are presented at a 1σ level (displayed by bar thickness for individual heating steps, and by orange error bars for interpreted ages), and the mean square weighted deviation (MSWD) is also displayed for each interpreted age. The apparent age spectrum for diatexite KP11-619 (Fig. 10b) is reproduced after Pownall et al. (2014). Other previously published ages are shown in part 'a' of both figures for comparison. The spectra are arranged to allow comparison between similar ages, rather than being grouped by rock type. Results tables for each step heating experiment (including their respective J-factors) are presented in Appendix A.

Many spectra feature a single wide, flat plateau; other spectra reveal more complex behaviour due to mixing of different gas populations. In this second instance, the spectra were analysed using the Method of Asymptotes and Limits, as devised by Forster and Lister (2004). This method recognises that a single apparent age spectrum may be produced by the mixing of distinct gas populations from two or more microstructural and/or microchemical reservoirs of different ages. For instance, for Figure 9c, we interpret the upward-sloping yellow 'staircase' (between 20 and 40% ^{39}Ar release) that converges on limits aged 4.47 ± 0.02 Ma and 5.43 ± 0.09 Ma to result from the mixing of two different argon reservoirs with those respective ages. By means of microstructural and/or microchemical analysis of the dated mineral grains, it is often possible to attribute a sequence of two or more $^{40}Ar/^{39}Ar$ ages to a history of crystallisation, recrystallisation, and deformation during which new argon reservoirs were formed, or older ones fully or partially degassed and therefore reset (Forster and Lister, 2004, 2014).

Our interpretations for the ages indicated by each step heating experiment are shown in the last column of Table 2. A discussion of the possible meanings of these ages from a tectonic and/or metamorphic standpoint is presented in Section 4.

4. Geological interpretation of $^{40}Ar/^{39}Ar$ ages

As summarised in Figures 11 and 12, several frequently measured ages have emerged from this study: 16 Ma, 5.7 Ma, 4.5 Ma, and 3.4 Ma. Interestingly, single samples often record two of these ages, demonstrating a history of overprinting tectonic events affecting much of Seram. For instance, biotite from Taunusa Complex sample KB11-234 (Fig. 9c) has recorded a 5.43 Ma $^{40}Ar/^{39}Ar$ age interpreted to be related to extensional exhumation of hot Kobipoto Complex rocks in western Seram, as well as a younger 4.47 Ma $^{40}Ar/^{39}Ar$ age interpreted to record movement of the Kawa Shear Zone. These and other events are discussed in detail below.

4.1. The 16 Ma metamorphic–magmatic event

The oldest-known event recorded by the $^{40}Ar/^{39}Ar$ system on Seram is that which drove ultrahigh-temperature (UHT) metamorphism of the Kobipoto Complex granulites at 16 Ma (Pownall et al., 2014; Pownall, 2015). As previously reported by Pownall et al. (2014), the 16.34 ± 0.04 Ma $^{40}Ar/^{39}Ar$ age of biotite from Kobipoto Complex diatexite KP11-619 is identical-within-error to the 16.00 ± 0.52 Ma $^{206}Pb/^{238}U$ zircon age determined for the same rock. Biotite in this sample, as discussed by Pownall et al. (2014), most likely formed as a high-T retrograde product during the early stages of decompression and cooling from UHT conditions. Therefore, it is entirely plausible that it formed at very similar P–T conditions to the zircon, especially if, as suggested by Pownall (2015): (*i*) the thin 16 Ma zircon rims crystallised in response to Zr-liberating (i.e. garnet-consuming) reactions during the rock's retrogression, rather than recording the age of peak metamorphism (cf. Kelsey et al., 2008; Sajeev et al., 2010; Kelsey & Powell, 2011; Kohn et al., 2015), (*ii*) the closure temperature of the mica was higher than conventionally assumed (cf. Forster and Lister, 2014), and (*iii*) cooling, and therefore exhumation, was very rapid. The apparent age spectrum for KP11-619 biotite additionally indicates mixing with a younger 14.83 ± 0.29 Ma gas population, the origin of which is unclear, but may have been released by the amorphous recrystallised generation of biotite observed in thin section (Fig. 4a).

Sample HM11-177, the kyanite–staurolite–garnet schist from the Hoamoal Peninsula, also records *c.* 16 Ma ages. Crenulated white mica (1st-generation) produced a spectrum with a single wide plateau at 16.60 ± 0.06 Ma (Fig. 10f), whereas the uncrenulated white mica (2nd-generation) inferred from the microstructure to be younger, exhibited mixing between this age and a slightly younger gas population at 15.88 ± 0.10 Ma (Fig. 10e). Incredibly, this younger age is identical within error to the $^{40}Ar/^{39}Ar$ age yielded by white mica from sillimanite gneiss sample KP11-581D from the Kobipoto Mountains (Fig. 10d), over 150 km further east (Fig. 12). This extremely close similarity of $^{40}Ar/^{39}Ar$ ages over such a long distance suggests that a kyanite-grade metamorphic event at 16 Ma, which evidently affected Tehoru Formation schists across the entirety of western and central Seram, was a short and intense event. Furthermore, this evidence for a regionally significant metamorphic event at 16 Ma greatly strengthens the argument that the 16 Ma $^{206}Pb/^{238}U$ zircon ages from the Kobipoto Complex migmatites (Pownall et al., 2014) record UHT metamorphism, as opposed to being related to subsequent localised re-melting or metasomatism of the migmatite complex.

In the light of the age correlations shown in Figures 11 and 12, we interpret UHT metamorphism of the Kobipoto Complex, and the accompanying melting that was necessary to dehydrate the residual high-temperature assemblages (Vielzeuf et al., 1990; White and Powell, 2002), to have been contemporaneous with kyanite-grade metamorphism of parts of the Tehoru Formation at *c.* 16 Ma. Large prismatic sillimanite crystals occurring in the Kobipoto Complex granulites are interpreted as pseudomorphs after kyanite (Pownall, 2015), demonstrating a similar mineralogy for the Kobipoto Complex and Tehoru Formation, which might share a common protolith (Pownall et al., 2013).

It follows that metamorphic grade was therefore dictated by proximity to the exhuming subcontinental lithospheric mantle, where the geotherm would locally have been elevated. It should be clarified that the classifications for the Tehoru Formation, Kobipoto Complex, and Taunusa Complex outlined by Pownall et al. (2013) and illustrated in Figure 8 are effectively based on each units' relationships to the detachment faults that facilitated crustal extension and mantle exhumation. The Kobipoto Complex granulite-facies migmatites represent the partially-melted mid/lower crust (30–35 km depth; Pownall, 2015) exhumed alongside the upper SCLM beneath the detachment faults; the Tehoru Formation includes the vast majority of Seram's metamorphosed rocks comprising greenschist to upper-amphibolite facies (kyanite-grade) schists and basic amphibolites, which form the hanging walls of the detachments; and the Taunusa Complex is simply a localised overprint of those Tehoru Formation rocks that lie immediately above the detachments – a high temperature, high strain zone characterised by the occurrence of fibrolitic sillimanite and very localised partial melting.

4.2. Lamprophyric volcanism at 15 Ma

Phlogopite phenocrysts from lamprophyre sample KP11-593 yielded an $^{40}Ar/^{39}Ar$ age of 15.07 ± 0.08 Ma, as defined by a single, very wide plateau (80% of ^{39}Ar release) on the apparent age spectrum (Fig. 10c). As previously described (Pownall et al., 2013), this and other lamprophyric rocks were emplaced as dykes through the lherzolites exposed in the Kobipoto Mountains (Fig. 7b), thus demonstrating a genetic relationship between these ultramafic rock units. This *c*. 15 Ma age for lamprophyric volcanism demonstrates that melting of the fertile mantle occurred more-or-less contemporaneously with UHT metamorphism and melting of the continental crust. Further evidence is therefore provided for lithosphere-scale extension and the resulting exhumation of hot, fertile mantle having driven the UHT metamorphic event at *c*. 16 Ma.

4.3. Kobipoto Complex exhumation in western Seram

White mica and biotite from the two Taunusa Complex gneisses sampled from the Kaibobo Peninsula (KB11-234 and KB11-374) all yielded $^{40}Ar/^{39}Ar$ ages of *c*. 5.5 Ma (Fig. 11, 13). Aside from KB11-234 biotite, all apparent age spectra feature wide plateaux that record single ages. As previously mentioned, the spectrum from KB11-234 biotite shows a rising profile that converges on an upper 5.43 ± 0.09 Ma plateau and a lower 4.47 ± 0.02 Ma limit. We interpret this as due to mixing between two gas populations of those respective ages: the older age correlating with the other samples; the younger age possibly to a second generation of amorphous recrystallised biotite. In both instances, the white mica $^{40}Ar/^{39}Ar$ age is very slightly older than the biotite $^{40}Ar/^{39}Ar$ age from the same rock (by ~ 0.2 Myr), which is due either to the fact that in both instances the white mica is microstructurally older than biotite (Fig. 6c, d), and/or that the white mica closed to appreciable argon diffusion at a slightly higher temperature.

Inclusions of sillimanite within the white mica 'fish' (Fig. 6f), and the occurrence of sillimanite also within the shear bands (Fig. 6c, h), demonstrates that the white mica most probably grew during high temperature shearing of the gneiss (as previously concluded by Linthout et al., 1996). Therefore, we interpret the white mica $^{40}Ar/^{39}Ar$ ages to date movement on the shear zone. Biotite, which has formed in the strain shadows between the white mica fish (Fig. 6d), or has otherwise grown around the white mica (Fig. 6c) is by association also related to the high-temperature shearing. These $^{40}Ar/^{39}Ar$ ages therefore provide information on the timing of Kobipoto Complex exhumation on the Kaibobo Peninsula, since the Taunusa Complex formed in response to the extensional exhumation of the hot lherzolites and migmatites beneath the Kaibobo Detachment (Pownall et al., 2013).

Kobipoto Complex diatexites similarly yielded *c.* 5.5 Ma $^{40}Ar/^{39}Ar$ ages, demonstrating a correlation with the age of mylonitisation of the Taunusa Complex gneisses comprising the hanging wall. Biotite from cordierite diatexite sample SE10-178 produced a humped apparent age spectrum with a plateau at 5.88 ± 0.05 Ma peaking at 6.69 ± 0.13 Ma at 65% total ^{39}Ar release. Biotite from mylonitised cordierite diatexite sample KB11-367 also yielded a 5.40 ± 0.21 Ma $^{40}Ar/^{39}Ar$ age, as well as a younger 3.30 ± 0.04 Ma age. This younger age likely relates to argon released from the younger generation of biotite grown within the shear bands (described in Section 2.1.4), which cross-cut the older biotite-bearing fabric. The main phase of activity of the shear zone exposed on Tanjung Motianai is therefore shown to post-date movement of the Kobipoto Detachment by ~ 2 Myr (Fig. 11, 13). 'Motianai Shear Zone' movement appears to instead coincide with deformation within the Kawa Shear Zone at *c.* 3.5 Ma (cf. sample SER-26C).

Previous work on the Kaibobo Peninsula by Linthout et al. (1996) obtained $^{40}Ar/^{39}Ar$ white mica and biotite ages also of *c.* 5.5 Ma (see Table 1) using a laser step heating method for a sillimanite gneiss sampled from the same structural position as our Tehoru formation rocks (Fig. 2c). Although these authors also interpreted their ages to relate to shearing, they instead attributed the cause of the shearing to obduction of the ultramafic complex, which they interpreted to comprise part of an ophiolite (Linthout et al., 1989). Nevertheless, these previously published $^{40}Ar/^{39}Ar$ ages (Table 1) are in close agreement with our results (Fig. 11), and although they have larger uncertainties provide additional age constraints on timing of shear zone operation.

4.4. Kawa Shear Zone activity

The Kawa Shear Zone (KSZ), based on its geomorphological expression, operated most recently and perhaps to the present day with a left-lateral shear sense (Pownall et al., 2013; Pownall and Hall, 2014; Watkinson and Hall, 2016). However, the incorporation of ultramafic rock slivers within fault gouges (Fig. 5f), and the occurrence of both left- and right-lateral outcrop-scale shear-sense indicators, demonstrate a more complex history. It has previously been suggested that the Kawa Fault, and associated faults within the KSZ, may have originated as low-angle detachments (similar to those exposed in western Seram) that were later re-activated as thrust/reverse faults with strong strike-slip shear components (Pownall et al., 2013). This interpretation was based on the occurrence of ultramafic slivers in the KSZ, and the observation that the KSZ and the Kaibobo Detachment (western Seram) share the same strike (120–300°). These new $^{40}Ar/^{39}Ar$ ages support this proposal, as they reveal 3 distinct events (at 5.6 Ma, 4.5 Ma, and 3.3 Ma) associated with the detachment on the Kaibobo Peninsula; the younger two of these ages relating to events also recorded in the KSZ (Fig. 14).

Sample TS11-496, a mylonitised garnet-mica schist from the central part of the KSZ, yielded a 10.2 Ma age (white mica) in addition to a significantly younger 4.5 Ma age (white mica and biotite). We interpret these ages as recording two separate deformational events, as opposed to a single period of slow cooling. This interpretation is supported by microstructural evidence (Section 2.2.2) for biotite crystallisation having post-dated white mica formation. Interestingly, the 4.5 Ma age is also recorded by Taunusa Complex samples SER-7 (biotite) from the southern Hoamoal Peninsula, and, as previously mentioned, by KB11-234 (biotite) from the Kaibobo Peninsula. Again, samples at > 100 km separation distances gave $^{40}Ar/^{39}Ar$ ages that are identical within error (4.47 ± 0.02 Ma, 4.47 ± 0.16 Ma, 4.48 ± 0.09 Ma, and 4.49 ± 0.08 Ma; see Figs. 11 and 12). Sample SER-26C, a garnet mylonite 60 km further southeast, provided a younger 3.5 Ma biotite $^{40}Ar/^{39}Ar$ age. Although the correlation is less strong, this age is within 0.2 Myr of the $^{40}Ar/^{39}Ar$ biotite ages recorded by the mylonitised cordierite diatexite on the Kaibobo Peninsula (KB11-367), and the cordierite diatexite on Ambon (AM10-167).

These results demonstrate that (*i*) the KSZ may have been active, in some form, as early as 10.2 Ma (if the 10.2 Ma age dates mylonitisation); (*ii*) deformation that was absorbed by the KSZ at 4.5 Ma also affected Taunusa Complex gneisses in the central Kaibobo Peninsula; and (*iii*) subsequent movement of the KSZ at 3.5 Ma was coincident with operation of the Tanjung Motianai Shear Zone on the southern Kaibobo Peninsula.

4.5. Ambon

Biotite from cordierite diatexite AM10-167 produced a single $^{40}Ar/^{39}Ar$ age of 3.63 ± 0.04 Ma, which we interpret to record exhumation and cooling of the Kobipoto Complex on Ambon. This is similar to the 3.3 ± 0.1 Ma Rb–Sr age reported by Priem et al. (1979) and the 4.1–3.4 Ma K–Ar ages reported by Honthaas et al. (1999) for similar 'cordierite granites' sampled from the island. As previously mentioned, this new $^{40}Ar/^{39}Ar$ age correlates with the timing of shearing within the

KSZ and southern Kaibobo Peninsula (samples SER-26C and KB11-367, respectively). Ambonites—cordierite-garnet dacites presumably sourced from the Kobipoto Complex migmatites (Whitford and Jezek, 1979; Linthout and Helmers, 1994; Pownall et al., *in review*)—were erupted on Ambon around 1 Myr later, from *c.* 2.3 Ma (Honthaas et al., 1999).

5. Implications for Banda Arc tectonics

According to plate reconstructions by Spakman and Hall (2010) and Hall (2002, 2011, 2012), the highly arcuate Banda Arc (and the highly concave Banda Slab) formed by rollback of a single slab into a pre-existing Jurassic D-shaped oceanic 'Banda Embayment' in the Australian continental margin (Fig. 15). The embayment is inferred to have originally been enclosed along its northern extent by a promontory of Australian crust called the Sula Spur (Klompé, 1954), which fragmented sometime after its collision with SE Asia (*c.* 23 Ma; Hall, 2011) to form Seram, Ambon, Buru, and parts of eastern Sulawesi. The timing of rollback depicted by the reconstruction is based, in part, on the dating of ocean-floor basalts and the interpretation of ocean-floor magnetic stripes that formed behind the rolling-back arc, which demonstrate that back-arc spreading must have opened the North Banda Basin between 12.5–7.2 Ma (Réhault et al., 1994; Hinschberger et al., 2000, 2003), and the South Banda Basin between 6.5–3.5 Ma (Honthaas et al., 1998; Hinschberger et al., 2001). Based on these constraints, the reconstructions show the eastern extent of the Java Trench beginning to rapidly roll back southeastwards into the Banda Embayment to form the Banda Arc from the Middle Miocene (15 Ma). A horizontal tear in the slab beneath Buru interpreted from seismic tomography (Hall and

Spakman, 2015) implies that at some point the slab tore from its northern margin after having driven extension and fragmentation of the adjacent Sula Spur as rollback advanced southeastwards (Spakman and Hall, 2010). The new $^{40}Ar/^{39}Ar$ ages presented in this study document a history of protracted crustal extension and strike-slip faulting across Seram, thus providing insights into how Banda slab rollback affected the geology of the Sula Spur as it tore into the Banda Embayment.

Several lines of geochronological evidence now indicate a regionally significant episode of high- to ultrahigh-temperature metamorphism and melting at *c.* 16 Ma on Seram: (*i*) 16 Ma SHRIMP U–Pb ages for metamorphic zircon from the Kobipoto Mountains granulites (Pownall et al., 2014); (*ii*) the 16 Ma biotite $^{40}Ar/^{39}Ar$ age for Kobipoto Complex diatexite KP11-619 (Fig. 10b), attributed to high-T retrogression of the granulites; (*iii*) the 17–16 Ma white mica $^{40}Ar/^{39}Ar$ ages for kyanite-grade Tehoru Formation schist HM11-177 (Fig. 10e,f) and Taunusa Complex gneiss KP11-581D (Fig. 10d); and (*iv*) the 15 Ma phlogopite $^{40}Ar/^{39}Ar$ age for lamprophyre sample KP11-593 (Fig. 10c), which was sourced from and intruded through the hot lherzolites. These ages document an episode of rapid cooling of the Kobipoto Complex granulites from UHT conditions involving post-peak zircon growth (likely in response to garnet breakdown at 850–900 °C; Pownall, 2015) and crystallisation of retrograde biotite, both at *c.* 16 Ma (Pownall et al., 2014). Kyanite-grade metamorphism of Tehoru Formation schists, which occurred across western and central Seram, is shown by the 17–16 Ma $^{40}Ar/^{39}Ar$ white mica ages of samples HM11-177 and KP11-581D to have occurred more-or-less simultaneously with UHT metamorphism and melting of the Kobipoto Complex migmatites. We thus interpret an episode of regional high-grade metamorphism and melting, producing both UHT granulite-facies migmatites and kyanite-grade schists at different structural levels, to have affected Seram soon after (or just before?) the Banda slab began rolling back to the southeast.

In order that rocks now in western Seram were extended by the Banda slab rollback at 16 Ma, western Seram must at that time have been positioned closer to eastern Sulawesi (Fig. 15), as opposed to having been affected by the 16 Ma event in its current location relative to Australia. Furthermore, *c.* 16 Ma metamorphic ages identified further afield suggest that there was extension of a large part of the upper plate and the metamorphic event probably affected a broad region. Advokaat et al. (2014) presented SHRIMP U–Pb ages for metamorphic zircon of 15.4 Ma from gneisses on Sulawesi's North Arm, which were interpreted to date a period of significant extension predating the exhumation of core complexes. Also, 17.6 and 16.9 Ma K–Ar ages from K-feldspar and biotite, respectively, from Kur island in the easternmost Banda Arc (Honthaas et al., 1997) reinforce the idea that products from this Early-Middle Miocene event were transported far into the Banda Embayment. A 17.0 Ma ^{40}Ar/^{39}Ar hornblende age from the Aileu Complex, Timor-Leste (Ely et al., 2014), would also appear to correlate with the 16 Ma event on western and central Seram, which is potentially explained by fragments of the Australian Sula Spur having been transported across the Banda Embayment and colliding with different Australian continental rocks on the Timor side (Bowin et al., 1980; Hall, 2011; Ely et al., 2014). In contrast, northern and eastern Seram likely occupied a similar position, with respect to the Bird's Head (West Papua), throughout the Neogene (Fig. 15).

The opening of the North Banda Basin (Fig. 1) between 12.5–7.15 Ma (Réhault et al., 1994; Hinschberger et al., 2000, 2003) places a minimum age on the time by which Banda rollback separated Seram from Sulawesi, which was described by Hall (2011) as the first phase of E–W extension in the Banda Arc's evolution. This time interval corresponds to the gap shown in Figure 11 where no major events were recorded on Seram by this ^{40}Ar/^{39}Ar study, suggesting that extension behind the rolling-back slab at that time was accommodated primarily by oceanic spreading between Sulawesi and Buru, without the requirement to extend the lithosphere beneath Seram.

Around 1 Myr after the North Banda Basin is dated to have ceased spreading, extension was transferred to the detachment faults in western Seram (Fig. 13). This forced Kobipoto Complex lherzolites and granulite-facies migmatites generated during the 16 Ma UHT event to be juxtaposed against lower-grade Tehoru Formation rocks at shallower structural levels. The heat retained by the Kobipoto Complex during its exhumation was sufficient to metamorphose and deform adjacent rocks comprising the hanging wall, originally part of the Tehoru Formation, to produce the observed Taunusa Complex sillimanite-grade shear zone (Figs. 8, 13). The $^{40}Ar/^{39}Ar$ ages determined by this study for the two Taunusa Complex samples (KB11-234 and KB11-374) demonstrate that one such high-T shear zone now exposed on the Kaibobo Peninsula (the 'Kaibobo Detachment'; Fig. 2c, 13) was active at 5.8–5.6 Ma.

Further exhumation of the Kobipoto Complex migmatites and lherzolites on Seram was later facilitated by transpression within the Kawa Shear Zone (KSZ), shown here to have operated from 4.4 Ma. As suggested by Pownall et al. (2013), the strike-slip faults comprising the KSZ are overprinted and steepened originally low-angle lithospheric detachment faults akin to those preserved in western Seram (Fig. 12) and they also incorporate peridotites and share the same 120°–300° strike. This interpretation is further supported by the $^{40}Ar/^{39}Ar$ ages presented in this study, as the main phase of KSZ operation is shown to post-date movement along the detachment faults exposed in western Seram by around 1 Myr. Also, sample KB11-234 from the Taunusa Complex of the Kaibobo Peninsula records both events (Fig. 11, 12), demonstrating that also in western Seram shear zones were reactivated at 4.4 Ma, but perhaps not with a strong strike-slip component. Sample SER-7 from a peridotite-bounding shear zone on the southern Hoamoal Peninsula, also recorded this 4.4 Ma age. The overprinting of former extensional faults by strike-slip faults in central Seram would have contributed further to the net elongation of Seram, as depicted by Figure 14, as rollback progressed further east.

At 3.5 Ma, Kobipoto Complex rocks were exhumed on Ambon (sample AM10-167), which was accompanied by further deformation within low-angle shear zones in western Seram (sample KB11-367) and shear within the southeastern portion of the KSZ (sample SER-26C). This event was contemporaneous also with extension across northern and central Sulawesi that drove rapid subsidence of Gorontalo Bay and the rapid exhumation of adjacent metamorphic core complexes (Cottam et al., 2011; Watkinson, 2011; Pholbud et al., 2012; Advokaat et al., 2014; Hennig et al., 2012, 2014, 2015; Pezzati et al., 2014, 2015; Rudyawan et al., 2014; van Leeuwen et al., 2007, 2016). Although it remains unclear if (or how) the two regions operated as parts of the same tectonic system, it is interesting to note in both instances the dominance of extensional tectonics in the early stages of collision.

This extreme extension documented on Seram from 16 Ma until present possibly affected other islands now comprising the northern Banda Arc, such as Buru and the small island chain immediately SE of Seram. Lherzolites and/or high-grade metamorphic rocks have been reported from Buru, Gorong, Manawoka, Kasiui, Tioor, Watubela, Kur, and Fadol (Bowin et al., 1980; Charlton et al., 1991; Hamilton, 1979; Honthaas et al., 1997; Pownall et al., 2016), which likely share similar histories to those exposed on Seram (Pownall et al., 2016). Our working hypothesis is that highly-extended lithosphere exists all around the northern portion of the Banda Arc, on the inner side of the collisional fold-and-thrust belts comprising the Seram and Aru troughs.

6. Conclusions

Our new $^{40}Ar/^{39}Ar$ ages, in the context of previous field-based studies on Seram and Ambon, suggest the following sequence of tectonic and metamorphic–magmatic events having affected the islands:

(1) Substantial lithospheric extension juxtaposed hot lherzolites against the mid/lower crust (~33 km depth; Pownall, 2015), driving HT–UHT metamorphism and melting just prior to *c.* 16 Ma to form the Kobipoto Complex migmatites. This event was accompanied by kyanite-grade metamorphism of the Tehoru Formation and the intrusion of lamprophyric melts sourced from the exhumed lherzolites. Seram was very likely located adjacent to eastern Sulawesi at this time, prior to being drawn eastwards by rollback of the Banda slab into the Banda Embayment.

(2) After the 16 Ma Middle Miocene metamorphic event, extension behind the rolling-back slab was accommodated by spreading of the North Banda Basin between Sulawesi and Buru (12.5–7.2 Ma; Hinschberger et al., 2000) with no major deformation recorded on Seram.

(3) The Kobipoto Complex was exhumed between 5.8–5.6 Ma to shallower structural levels across western Seram, as facilitated by the Kaibobo Detachment and similar low-angle normal faults during continued southeastward slab rollback ~1 Myr after North Banda Basin spreading ceased.

(4) From 4.5 Ma, the Kawa Shear Zone, central Seram, operated with a strike-slip sense and exhumed slivers of peridotite, possibly having overprinted similar low-angle extensional structures to those currently preserved in western Seram.

(5) Further strike-slip deformation within the Kawa Shear Zone occurred at 3.5 Ma, coincident with exhumation of Kobipoto Complex diatexites on Ambon and further deformation within shear zones in western Seram.

The very close correlation of several $^{40}Ar/^{39}Ar$ ages interpreted from the apparent age spectra demonstrate a tight synchronicity between tectonic events recorded over the width of Seram, with several samples having recorded two of these frequently measured ages. These ages document a protracted history of extension and strike-slip faulting, consistent with Seram having been extended and sheared above the rolling-back Banda Slab from 16 Ma until 3.5 Ma. This study demonstrates the utility of microstructurally-focused argon geochronology in assessing the timing of tectonic processes in multiply-deformed terranes, and showcases the rapidity and synchronicity of extensional tectonics in the modern Earth.

Appendix A. $^{40}Ar/^{39}Ar$ step heating results

$^{40}Ar/^{39}Ar$ step heating results are presented in Supplementary Data File 2, which can be found online at >>>>>>>.

Acknowledgements

We are extremely grateful to Yasinto Priastomo and Ramadhan Adhitama (Institut Teknologi Bandung) for assistance in the field. Matthew Thirlwall and Christina Manning are thanked for assistance with XRF analysis. We also thank Chris Morley and Tony Barber for their reviews, and Alan Collins for his editorial assistance. $^{40}Ar/^{39}Ar$ geochronology was undertaken at the RSES Argon Laboratory, Australian National University. This research was funded by the SE Asia Research Group (Royal Holloway University of London), Australian Research Council (ARC) grant DP0877274 awarded to MAF, and ARC grant DE160100128 awarded to JMP.

References

Advokaat, E. L., Hall, R., White, L. T., Armstrong, R., Kohn, B., BouDagher-Fadel, M. K., 2014. Neogene extension and exhumation in NW Sulawesi. AGU Fall Meeting 2014, T43A-4701.

Audley-Charles, M.G., Carter, D.J., Barber, A.J., Norvick, M.S., Tjokrosapoetro, S., 1979. Reinterpretation of the geology of Seram: implications for the Banda Arcs and northern Australia. Journal of the Geological Society 136, 547–566.

Beckinsale, R.D., Nakapadungrat, S., 1978. A late Miocene K-Ar age for the lavas of Pulau Kelang, Seram, Indonesia. Journal of physics of the Earth 26, 199–201.

Bowin, C., Purdy, G.M., Johnston, C., Shor, G., Lawyer, L., Hartono, H., Jezek, P., 1980. Arc-continent collision in the Banda Sea region. AAPG Bulletin 64, 868–915.

Cardwell, R.K., Isacks, B.L., 1978. Geometry of the subducted lithosphere beneath the Banda Sea in eastern Indonesia from seismicity and fault plane solutions. Journal of Geophysical Research: Solid Earth (1978–2012) 83, 2825–2838. doi:10.1029/JB083iB06p02825

Charlton, T.R., Kaye, S.J., Samodra, H., Sardjono, 1991. Geology of the Kai Islands: implications for the evolution of the Aru Trough and Weber Basin, Banda Arc, Indonesia. Marine and Petroleum Geology 8, 62–69. doi:10.1016/0264-8172(91)90045-3

Charlton, T.R., 2000. Tertiary evolution of the Eastern Indonesia Collision Complex. Journal of Asian Earth Sciences 18, 603–631.

Cottam, M.A., Hall, R., Forster, M.A., Boudagher-Fadel, M.K., 2011. Basement character and basin formation in Gorontalo Bay, Sulawesi, Indonesia: new observations from the Togian Islands. In: Hall, R., Cottam, M.A., Wilson, M.E.J. (Eds.), The SE Asian Gateway: History and Tectonics of the Australia-Asia Collision. The Geological Society, Special Publication 355, 177–202. doi:10.1144/SP355.9

Das, S., 2004. Seismicity gaps and the shape of the seismic zone in the Banda Sea region from relocated hypocenters. J. Geophys. Res. 109, B12303. doi:10.1029/2004JB003192

Ely, K.S., Sandiford, M., Phillips, D., Boger, S.D., 2014. Detrital zircon U–Pb and $^{40}Ar/^{39}Ar$ hornblende ages from the Aileu Complex, Timor-Leste: provenance and metamorphic cooling history. Journal of the Geological Society 171, 299–309. doi:10.1144/jgs2012-065

Forster, M.A., Lister, G.S., 2004. The interpretation of $^{40}Ar/^{39}Ar$ apparent age spectra produced by mixing: application of the method of asymptotes and limits. Journal of Structural Geology 26, 287–305. doi:10.1016/j.jsg.2003.10.004

Forster, M.A., Lister, G.S., 2010. Argon enters the retentive zone: reassessment of diffusion parameters for K-feldspar in the South Cyclades Shear Zone, Ios, Greece. Geological Society, London, Special Publications 332, 17–34. doi:10.1144/SP332.2

Forster, M.A., Lister, G.S., 2014. $^{40}Ar/^{39}Ar$ geochronology and the diffusion of ^{39}Ar in phengite-muscovite intergrowths during step-heating experiments *in vacuo*.

Geological Society, London, Special Publications 378, 117–135. doi:10.1144/SP378.16

Gaina, C., Müller, D., 2007. Cenozoic tectonic and depth/age evolution of the Indonesian gateway and associated back-arc basins. Earth Science Reviews 83, 177–203. doi:10.1016/j.earscirev.2007.04.004

Germeraad, J.H., 1946. Geology of central Seran, in: Rutten, L., Hotz, W. (Eds.), Geological, Petrographical, and Palaeontological Results of Explorations, Carried Out From September 1917 Till June 1919 in the Island of Ceram. De Bussy, Amsterdam, p. 135.

Haile, N.S., 1978. Paleomagnetic evidence for the rotation of Seram, Indonesia. Journal of physics of the Earth 26, 191–198.

Hall, R., 1996. Reconstructing Cenozoic SE Asia, in: Hall, R., Blundell, D. (Eds.), Tectonic Evolution of Southeast Asia. Geological Society of London Special Publications, pp. 153–184. doi:10.1144/GSL.SP.1996.106.01.11

Hall, R., 2002. Cenozoic geological and plate tectonic evolution of SE Asia and the SW Pacific: computer-based reconstructions, model and animations. Journal of Asian Earth Sciences 20, 353–431. doi:10.1016/S1367-9120(01)00069-4

Hall, R., 2011. Australia-SE Asia collision: plate tectonics and crustal flow. In: Hall, R., Cottam, M.A., Wilson, M.E.J. (Eds.), The SE Asian Gateway: History and Tectonics of the Australia-Asia Collision. Geological Society, London, Special Publications 355, 75–109. doi:10.1144/SP355.5

Hall, R., 2012. Late Jurassic–Cenozoic reconstructions of the Indonesian region and the Indian Ocean. Tectonophysics 570-571, 1–41. doi:10.1016/j.tecto.2012.04.021

Hall, R., Wilson, M.E.J., 2000. Neogene sutures in eastern Indonesia. Journal of Asian Earth Sciences 18, 781–808.

Hall, R., Sevastjanova, I., 2012. Australian crust in Indonesia. Australian Journal of Earth Sciences 59, 827–844. doi:10.1080/08120099.2012.692335

Hall, R., Spakman, W., 2015. Mantle structure and tectonic history of SE Asia. Tectonophysics. doi:10.1016/j.tecto.2015.07.003

Hamilton, W., 1979. Tectonics of the Indonesian region. US Geological Survey Professional Paper 1078, 345 pp.

Hartono, H.M.S., Tjokrosapoetro S., 1984. Preliminary account and reconstruction of Indonesian terranes. Proceedings of the Indonesian Petroleum Association 13, 185–226.

Hennig, J., Hall, R., Watkinson, I.M., Forster, M., 2012. Timing and Mechanisms of Exhumation in West Central Sulawesi. AGU Fall Meeting, T43E-2713.

Hennig, J., Advokaat, E., Rudyawan, A., Hall, R., 2014. Large Sediment Accumulations and Major Subsidence Offshore; Rapid Uplift on Land: Consequences of Extension of Gorontalo Bay and Northern Sulawesi. Indonesian Petroleum Association, Proceedings 38, IPA14-G-304.

Hennig, J., Hall, R., Armstrong, R.A., 2015. U–Pb zircon geochronology of rocks from west Central Sulawesi, Indonesia: Extension-related metamorphism and magmatism during the early stages of mountain building. Gondwana Research. doi:10.1016/j.gr.2014.12.012.

Hinschberger, F., Malod, J.-A., Réhault, J.-P., Dyment, J., Honthaas, C., Villeneuve, M., Burhanuddin, S., 2000. Origine et evolution du basin Nord-Banda (Indonésie): apport des données magnétiques. Comptes Rendus de l'Académie des Sciences, Série IIA: Sciences de la Terre et des Planètes 331, 507–514.

Hinschberger, F., Malod, J.-A., Dyment, J., Honthaas, C., Réhault, J.-P., Burhanuddin, S., 2001. Magnetic lineations constraints for the back-arc opening of the Late Neogene South Banda Basin (eastern Indonesia). Tectonophysics 333, 47–59. doi:10.1016/S0040-1951(00)00266-3

Hinschberger, F., Malod, J.-A., Réhault, J.-P., Burhanuddin, S., 2003. Apport de la bathymétrie et de la géomorphologie à la géodynamique des mers de l'Est-indonésien. Bulletin de la Société Géologique de France 174, 545–560.

Hinschberger, F., Malod, J.-A., Réhault, J.-P., Villeneuve, M., Royer, J.-Y., Burhanuddin, S., 2005. Late Cenozoic geodynamic evolution of eastern Indonesia. Tectonophysics 404, 91–118. doi:10.1016/j.tecto.2005.05.005

Honthaas, C., Villeneuve, M., Réhault, J.-P., Bellon, H., Cornee, J.-J., Saint-Marc, P., Butterlin, J., Gravelle, M., Burhanuddin, S., 1997. L'île de Kur: géologie du flanc oriental du bassin de Weber (Indonésie orientale). Comptes Rendus de l'Académie des Sciences, Série IIA: Sciences de la Terre et des Planètes 325, 883–890.

Honthaas, C., Réhault, J.-P., Maury, R.C., Bellon, H., Hémond, C., Malod, J.-A., Cornée, J.-J., Villeneuve, M., Cotten, J., Burhanuddin, S., Guillou, H., Arnaud, N., 1998. A Neogene back-arc origin for the Banda Sea basins: geochemical and geochronological constraints from the Banda ridges (East Indonesia). Tectonophysics 298, 297–317. doi:10.1016/S0040-1951(98)00190-5

Honthaas, C., Maury, R.C., Priadi, B., Bellon, H., Cotten, J., 1999. The Plio–Quaternary Ambon arc, Eastern Indonesia. Tectonophysics 301, 261–281. doi:10.1016/S0040-1951(98)00227-3

Kelsey, D.E., Powell, R., 2011. Progress in linking accessory mineral growth and breakdown to major mineral evolution in metamorphic rocks: a thermodynamic approach in the Na_2O-CaO-K_2O-FeO-MgO-Al_2O_3-SiO_2-H_2O-TiO_2-ZrO_2 system. Journal of Metamorphic Geology 29, 151–166.

Kelsey, D.E., Clark, C., Hand, M., 2008. Thermobarometric modelling of zircon and monazite growth in melt-bearing systems: examples using model metapelitic and metapsammitic granulites. Journal of Metamorphic Geology 26, 199–212.

Klompé, T.H.F., 1954. The structural importance of the Sula Spur (Indonesia). Indonesian Journal of Natural Sciences 110, 21–40.

Kohn, M.J., Corrie, S.L., Markley, C., 2015. The fall and rise of metamorphic zircon. American Mineralogist 100, 897–908.

Le Maitre, R.W., 2002. Igneous Rocks: A Classification and Glossary of Terms. Cambridge University Press, Cambridge, pp. 1–236.

Linthout, K., Helmers, H., 1994. Pliocene obducted, rotated and migrated ultramafic rocks and obduction-induced anatectic granite, SW Seram and Ambon, Eastern Indonesia. Journal of Southeast Asian Earth Sciences 9, 95–109. doi:10.1016/0743-9547(94)90068-X

Linthout, K., Helmers, H., Sopaheluwakan, J., Nila, E.S., 1989. Metamorphic complexes in Buru and Seram, Northern Banda Arc. Netherlands Journal of Sea Research 24, 345–356. doi:10.1016/0077-7579(89)90160-9

Linthout, K., Helmers, H., Andriessen, P., 1991. Dextral strike-slip in Central Seram and 3-4.5 Ma Rb/Sr ages in pre-triassic metamorphics related to early Pliocene counterclockwise rotation of the Buru-Seram microplate (E. Indonesia). Journal of Southeast Asian Earth Sciences 6, 335–342. doi:10.1016/0743-9547(91)90079-D

Linthout, K., Helmers, H., Wijbrans, J.R., Van Wees, J.D.A.M., 1996. $^{40}Ar/^{39}Ar$ constraints on obduction of the Seram ultramafic complex: consequences for the evolution of the southern Banda Sea. Geological Society, London, Special Publications 106, 455–464. doi:10.1144/GSL.SP.1996.106.01.28

McCaffrey, R., 1988. Active tectonics of the eastern Sunda and Banda arcs. Geophysics 93, 15163–15182.

Milsom, J., 2001. Subduction in eastern Indonesia: how many slabs? Tectonophysics 338, 167–178. doi:10.1016/S0040-1951(01)00137-8

Pezzati, G., Hall, R., Burgess, P., Pérez-Gussinyé, M., 2014. The Poso Basin in Gorontalo Bay, Sulawesi: Extension related to core complex formation on land. Indonesian Petroleum Association, Proceedings 38, IPA14-G-297.

Pezzati, G., Hennig, J., Advokaat, E., Hall, R., Burgess, P., Pérez-Gussinyé, M., 2015. Subsidence in Gorontalo Bay, Sulawesi (Indonesia) and metamorphic core complex exhumation on land. EGU General Assembly 2015, 7476.

Pholbud, P., Hall, R., Advokaat, E., Burgess, P., Rudyawan, A., 2012. A new interpretation of Gorontalo Bay, Sulawesi. Indonesian Petroleum Association, Proceedings 36, IPA12-G-039.

Pownall, J.M., 2015. UHT metamorphism on Seram, eastern Indonesia: reaction microstructures and P–T evolution of spinel-bearing garnet–sillimanite granulites from the Kobipoto Complex. Journal of Metamorphic Geology 33, 909–935. doi:10.1111/jmg.12153

Pownall, J.M., Hall, R., 2014. Neogene extension on Seram: A new tectonic model for the northern Banda Arc. Indonesian Petroleum Association, Proceedings 38, IPA14-G-305.

Pownall, J.M., Hall, R., Watkinson, I.M., 2013. Extreme extension across Seram and Ambon, eastern Indonesia: evidence for Banda slab rollback. Solid Earth 4, 277–314. doi:10.5194/se-4-277-2013

Pownall, J.M., Hall, R., Armstrong, R.A., Forster, M.A., 2014. Earth's youngest known ultrahigh-temperature granulites discovered on Seram, eastern Indonesia. Geology 42, 279–282. doi:10.1130/G35230.1

Pownall, J.M., Hall, R., Lister, G.S., 2016. Rolling open Earth's deepest forearc basin. Geology 44, 947–950. doi:10.1130/G38051.1.

Pownall, J.M., Hall, R., Armstrong, R.A., *in review*. Hot lherzolite exhumation, UHT migmatite formation, and acid volcanism driven by Miocene rollback of the Banda Arc, eastern Indonesia. Submitted to Gondwana Research.

Priem, H.N.A., Andriessen, P.A.M., Boelrijk, N.A.I.M., Hebeda, E.H., Hutchinson, C.S., Verdurmen, E.A.T., Versschure, R.H., 1978. Isotopic evidence for a middle to late Pliocene age of the cordierite granite on Ambon, Indonesia. Geologie en Mijnbouw 57, 441–443.

Réhault, J.-P., Maury, R.C., Bellon, H., Sarmili, L., Burhanuddin, S., Joron, J.-L., Cotten, J., Malod, J.-A., 1994. La Mer de Banda Nord (Indonésie): un bassin arrière-arc du Miocène supérieur. Comptes Rendus de l'Académie des Sciences, Série IIA: Sciences de la Terre et des Planètes 318, 969–976.

Richards, S., Lister, G., Kennett, B., 2007. A slab in depth: Three-dimensional geometry and evolution of the Indo-Australian plate. Geochemistry, Geophysics, Geosystems 8. doi:10.1029/2007GC001657

Rudyawan, A., Hall, R., White, L., 2014. Neogene extension of the Central North Arm of Sulawesi, Indonesia. AGU Fall Meeting 2014, T43A-4681.

Ryan, W.B.F., Carbotte, S.M., Coplan, J.O., O'Hara, S., Melkonian, A., Arko, R., Weissel, R.A., Ferrini, V., Goodwillie, A., Nitsche, F., Bonczkowski, J., Zemsky, R., 2009. Global Multi-Resolution Topography synthesis. Geochemistry, Geophysics, Geosystems 10. doi:10.1029/2008GC002332

Sajeev, K., Williams, I.S., Osanai, Y., 2010. Sensitive high-resolution ion microprobe U-Pb dating of prograde and retrograde ultrahigh-temperature metamorphism as exemplified by Sri Lankan granulites. Geology 38, 971–974.

Spakman, W., Hall, R., 2010. Surface deformation and slab-mantle interaction during Banda arc subduction rollback. Nature Geoscience 3, 562–566. doi:10.1038/ngeo917

Spell, T.L., McDougall, I., 2003. Characterization and calibration of Ar-40/Ar-39 dating standards. Chemical Geology 198, 189–211.

Steiger, R.H., Jäger, E., 1977. Subcommission on geochronology: Convention on the use of decay constants in geo- and cosmoschronology. Earth and Planetary Science Letters 36, 359–362.

Tjokrosapoetro, S., Budhitrisna, T., 1982. Geology and Tectonics of the northern Banda Arc. Bulletin of the Indonesian Geological Research and Development Centre 6, 1–17.

Tjokrosapoetro, S., Achdan, A., Suwitodirdjo, K., Rusmana, E., Abidin, H.Z., 1993a. Geological map of the Masohi quadrangle, Maluku, 1:250,000. Geological Research and Development Centre, Bandung, Indonesia.

Tjokrosapoetro, S., Budhitrisna, T., Rusmana, E., 1993b. Geology of the Buru Quadrangle, Maluku, 1:250,000. Geological Research and Development Centre, Bandung.

Valk, W., 1945. Contributions to the geology of West Seran, in: Rutten, L., Hotz, W. (Eds.), Geological, Petrographical, and Palaeontological Results of Explorations, Carried Out From September 1917 Till June 1919 in the Island of Ceram. De Bussy, Amsterdam, p. 104.

van Leeuwen, T., Allen, C.M., Kadarusman, A., Elburg, M., Palin, J.M., Muhardjo, Suwijanto, 2007. Petrologic, isotopic, and radiometric age constraints on the origin and tectonic history of the Malino Metamorphic Complex, NW Sulawesi, Indonesia. Journal of Asian Earth Sciences 29, 751–777. doi:10.1016/j.jseaes.2006.05.002

van Leeuwen, T., Allen, C.M., Elburg, M., Massonne, H.-J., Palin, J.M, Hennig, J., 2016. The Palu Metamorphic Complex, NW Sulawesi, Indonesia: Origin and evolution of a young metamorphic terrane with links to Gondwana and Sundaland. Journal of Asian Earth Sciences 115, 133–152.

Vielzeuf, D., Clemens, J.D., Pin, C., Moinet, E., 1990. Granites, granulites, and crustal differentiation. In: Vielzeuf, D., Vidal, Ph. (Eds.), Granulites and Crustal Evolution. pp. 59–85. Springer, Netherlands

Villeneuve, M., Martini, R., Bellon, H., Réhault, J.-P., Cornee, J.-J., Bellier, O., Burhannuddin, S., Hinschberger, F., Honthaas, C., Monnier, C., 2010. Deciphering of six blocks of Gondwanan origin within Eastern Indonesia (South East Asia). Gondwana Research 18, 420–437. doi:10.1016/j.gr.2009.12.011

Watkinson, I.M., 2011. Ductile flow in the metamorphic rocks of central Sulawesi. In: Hall, R., Cottam, M.A., Wilson, M.E.J. (Eds.), The SE Asian Gateway: History and Tectonics of the Australia-Asia Collision. Geological Society, London, Special Publications 355, 157–176. doi:10.1144/SP355.8

Watkinson, I.M., Hall, R., 2016. Fault systems of the eastern Indonesian triple junction: evaluation of Quaternary activity and implications for seismic hazards. In: Cummins, P. R, Meilano, I. (Eds.), Geohazards in Indonesia: Earth Science for Disaster Risk Reduction. Geological Society of London Special Publication.

White, R.W., Powell, R., 2002. Melt loss and the preservation of granulite facies mineral assemblages. Journal of Metamorphic Geology 20, 621–632.

Whitford, D.J., Jezek, P.A., 1979. Origin of late Cenozoic lavas from the Banda Arc, Indonesia: trace elements and Sr isotope evidence. Contributions to Mineralogy and Petrology 68, 141–150.

Zahirovic, S., Seton, M., Müller, R.D., 2014. The Cenozoic and Cretaceous tectonic evolution of Southeast Asia. Solid Earth 5, 227–273.

Figure Captions

Fig. 1 Tectonic map of Eastern Indonesia and the surrounding region showing the location of Seram and Ambon, located in the northern limb of the Banda Arc. Subduction zones and major faults are modified from Hall (2012). The location of the Banda Detachment, flooring the Weber Deep, is taken from Pownall et al. (2016). The digital elevation model uses Global Multi-Resolution Topography (GMRT) data from Ryan et al. (2009).

Fig. 2 (a) Geological map of Seram and Ambon (after Pownall et al., 2013), showing enlargements of (b) the southern Hoamoal Peninsula, and (c) the Kaibobo Peninsula. The key to all parts of the figure is shown bottom left. Sample locations (listed in Table 2) are marked on each part of the figure. Samples BK21 and BK18 are those of Linthout et al. (1996). Cross-section X–X′–X″, marked in part (c), is shown in Figure 13.

Fig. 3 Panoramic photo of the northern Kaibobo Peninsula taken from Gunung Hemahuhui, overlain with the approximate traces of geological contacts. Note that cordierite diatexites and lherzolites (comprising the Kobipoto Complex) are structurally below the Taunusa Complex, which forms the hanging wall to the Kaibobo Detachment.

Fig. 4 Kobipoto Complex samples. (a) Two generations of biotite growth in metatexite KP11-619 from the Kobipoto Mountains; (b) Spinel–sillimanite scheliere in diatexite SE10-178 from the Kaibobo Peninsula; (c) Mylonitised granite KB11-367 from the Tanjung Motianai Shear Zone (Kaibobo Peninsula) featuring biotite 'fish' (bt1) and biotite growth along the shear bands (bt2). See Table 2 for further sample information.

Fig. 5 Tehoru Formation samples. (a–c) Kyanite-staurolite-garnet schist HM11-177 featuring tightly crenulated white mica (wm1) and coarser white mica aggregates (wm2); (d, e) Garnet-biotite mylonite TS11-496 containing σ-type garnet porphyroblasts indicative of left-lateral shear; (f) Serpentinite boudin from the Kawa Shear Zone, located < 1 km to the north of sample TS11-496; (g–i) Garnet mylonite SER-26C, sampled from the shear zone south of Teluk Taluti (g). σ-type garnets and S–C fabric (which incorporates biotite in both S- and C-planes) is consistent with a left-lateral shear sense. The dashed white lines represent the strike of the schistosity. Photomicrographs in parts a–c are taken under cross-polarised light. See Table 2 for further sample information.

Fig. 6 Taunusa Complex samples. (a–c) Sillimanite-garnet gneiss KB11-234 containing fibrolitic sillimanite concentrated in shear bands. White mica growth is shown to predate biotite formation (c). (d–f) Sillimanite-garnet gneiss KB11-374 featuring large white mica fish (e) containing inclusions of sillimanite (f) and biotite grown in the strain shadows (d). (g–i) Andalusite-sillimanite-biotite schist SER-7 featuring the characteristic sillimanite-defined shear bands (h). (j–l) Garnet-cordierite-sillimanite metatexite KP11-581D, with coarse white mica grown in the leucosome, and crenulated white mica and sillimanite present in the melanosome. Photomicrographs in parts c, e, f, i, k, and l are taken under cross-polarised light. See Table 2 for further sample information.

Fig. 7 Lamprophyric rocks of the Kobipoto Mountians. (a) Phlogopite minette sample KP11-593 showing huge laths of bronze-coloured phlogopite. Note pen for scale. (b) Phlogopite-rich minette existing as veins through serpentinised lherzolites. (c) Photomicrograph of sample KP11-593 (XPL) showing very large euhedral phlogopite grains within a finer-grained groundmass predominantly of K-feldspar and apatite. See Table 2 for further sample information.

Fig. 8 Schematic cross-section demonstrating the main field relationships interpreted for Seram, showing the relationship between the Tehoru, Taunusa, and Kobipoto metamorphic complexes (after Pownall et al., 2013). The location of samples is purely diagrammatic.

Fig. 9 Apparent $^{40}Ar/^{39}Ar$ age spectra for samples younger than 12 Ma. (a) $^{40}Ar/^{39}Ar$ ages determined by Linthout et al. (1996) for Taunusa Complex gneiss (BK21) and Kobipoto Complex cordierite diatexite (BK18) from the Kaibobo Peninsula. (b–l) Apparent age spectra for 11 samples, interpreted using the method of Asymptotes and Limits (Forster and Lister, 2004). In instances where a single plateau age has been interpreted, the steps used to calculate this age are highlighted in dark blue. In instances where limits have been interpreted resulting from mixing of two gas populations, steps used to calculate each limit are marked in dark blue and light blue, respectively. Orange error bars are shown at 1σ. Yellow steps are not used in age calculations. The spectra are arranged to demonstrate cross-correlation of frequently measured ages. See Table 2 for individual interpretations. MSWD—mean square of weighted deviates.

Fig. 10 Apparent $^{40}Ar/^{39}Ar$ age spectra for samples recording *c.* 16 Ma ages. (a) $^{206}Pb/^{238}U$ zircon ages determined by Pownall et al. (2014) for Kobipoto Complex migmatites from the Kobipoto Mountains. (b–f) Apparent age spectra for 5 samples, interpreted using the method of Asymptotes and Limits (Forster and Lister, 2004). In instances where a single plateau age has been interpreted, the steps used to calculate this age are highlighted in dark blue. In instances where limits have been interpreted resulting from mixing of two gas populations, steps used to calculate each limit are marked in dark blue and light blue, respectively. Orange error bars are shown at 1σ. Yellow steps are not used in age calculations. The spectra are arranged to demonstrate cross-correlation of frequently measured ages. See Table 2 for individual interpretations. MSWD—mean square of weighted deviates.

Fig. 11 A comparison of $^{40}Ar/^{39}Ar$ ages determined by this study, $^{40}Ar/^{39}Ar$ ages published by Linthout et al. (1996), and $^{206}Pb/^{238}U$ zircon ages determined by Pownall et al. (2014). Error bars are shown at 1σ. Note the clustering of frequently measured ages at *c.* 16 Ma, 5.8–5.6 Ma, 4.5–4.4 Ma, and 3.5–3.4 Ma. The timings of North Banda Basin opening (12.5–7.15 Ma) and South Banda Basin opening (6.5–3.5 Ma) are taken from Hinschberger et al. (2000) and Hinschberger et al. (2001), respectively.

Fig. 12 Tectonic map of Seram (from Pownall et al., 2013) annotated with $^{40}Ar/^{39}Ar$ ages determined by this study. The ages support the interpretation that the strike-slip faults (red) in central Seram post-date movement along the detachment faults (green) in western Seram, and that the Kawa Shear Zone may therefore have overprinted similar extensional detachments in central Seram. Frequently measured ages, often demonstrating a remarkable degree of correlation between samples with large separation distances, are coloured as follows: red—*c*. 16 Ma, blue—5.8–5.6 Ma, purple—4.5–4.4 Ma, and green—3.5–3.4 Ma.

Fig. 13 Cross-section X–X′–X′′ across the Kaibobo Detachment, Kaibobo Peninsula, annotated with photomicrographs labelled with respective $^{40}Ar/^{39}Ar$ ages for biotite and white mica. See Fig. 2c for location of the section.

Fig. 14 Block model for Seram and Ambon (adapted from Pownall et al., 2014) showing the timing of UHT metamorphism, detachment faulting, and strike-slip shearing as determined by this $^{40}Ar/^{39}Ar$ study. KSZ—Kawa Shear Zone; SCLM–Subcontinental lithospheric mantle.

Fig. 15 Tectonic reconstruction of Eastern Indonesia from Australia–SE Asia collision at *c*. 23 Ma (based on Hall, 2012) representing graphically the events correlated in Figure 11. NBB—North Banda Basin; SBB—South Banda Basin; BR—Banda Ridges.

Tables

Table 1: Previously-published ages for metamorphic rocks on Seram and Buru

Table 2: $^{40}Ar/^{39}Ar$ geochronology sample list and interpretation of apparent age spectra

Supplementary Data

Supplementary Data File 1: XRF analysis of lamprophyre sample KP11-593

Supplementary Data File 2: $^{40}Ar/^{39}Ar$ geochronology data tables

Tectonometamorphic evolution of Seram and Ambon, eastern Indonesia: Insights from $^{40}Ar/^{39}Ar$ geochronology

Jonathan M. Pownall[a,b,*], Marnie A. Forster[b], Robert Hall[a], Ian M. Watkinson[a]

[a]SE Asia Research Group, Department of Earth Sciences, Royal Holloway University of London, Egham TW20 0EX, United Kingdom
[b]Research School of Earth Sciences, Australian National University, Canberra, ACT 2601, Australia
**Corresponding author (e-mail: jonathan.pownall@anu.edu.au)*

Abstract

The island of Seram, eastern Indonesia, experienced a complex Neogene history of multiple metamorphic and deformational events driven by Australia–SE Asia collision. Geological mapping, and structural and petrographic analysis has identified two main phases in the island's tectonic, metamorphic, and magmatic evolution: (1) an initial episode of extreme extension that exhumed hot lherzolites from the subcontinental lithospheric mantle and drove ultrahigh-temperature metamorphism and melting of adjacent continental crust; and (2) subsequent episodes of extensional detachment faulting and strike-slip faulting that further exhumed granulites and mantle rocks across Seram and Ambon. Here we present the results of sixteen $^{40}Ar/^{39}Ar$ furnace step heating experiments on white mica, biotite, and phlogopite for a suite of twelve rocks that were targeted to further unravel Seram's tectonic and metamorphic history. Despite a wide lithological and structural diversity among the samples, there is a remarkable degree of correlation between the $^{40}Ar/^{39}Ar$ ages recorded by different rock types situated in different structural settings, recording thermal events at 16 Ma, 5.7 Ma, 4.5 Ma, and 3.4 Ma. These frequently measured ages are defined, in most instances, by two or more $^{40}Ar/^{39}Ar$

ages that are identical within error. At 16 Ma, a major kyanite-grade metamorphic event affected the Tehoru Formation across western and central Seram, coincident with ultrahigh-temperature metamorphism and melting of granulite-facies rocks comprising the Kobipoto Complex, and the intrusion of lamprophyres. Later, at 5.7 Ma, Kobipoto Complex rocks were exhumed beneath extensional detachment faults on the Kaibobo Peninsula of western Seram, heating and shearing adjacent Tehoru Formation schists to form Taunusa Complex gneisses. Then, at 4.5 Ma, $^{40}Ar/^{39}Ar$ ages record deformation within the Kawa Shear Zone (central Seram) and overprinting of detachment faults in western Seram. Finally, at 3.4 Ma, Kobipoto Complex migmatites were exhumed on Ambon, at the same time as deformation within the Kawa Shear Zone and further overprinting of detachments in western Seram. These ages support there having been multiple synchronised episodes of high-temperature extension and strike-slip faulting, interpreted to be the result of Western Seram having been ripped off from SE Sulawesi, extended, and dragged east by subduction rollback of the Banda Slab.

Keywords: Banda, rollback, extension, mantle exhumation, argon

1. Introduction

The northwestern edge of the Australian continental margin is reconstructed to have collided with SE Asia approximately 23 million years ago (Hall, 2011). Continuing Australia–SE Asia convergence has since been accommodated by a complex tectonic system of multiple subduction zones and shear zones that comprise eastern Indonesia (Fig. 1). The exact geometry and configuration of these subduction zones remains a hotly disputed subject, which has led to multiple tectonic models for the evolution of the region (cf. Hamilton, 1979; Hall, 1996, 2002, 2011, 2012; Charlton, 2000; Milsom, 2001; Hinschberger et al., 2005; Gaina and Müller, 2007; Richards et al., 2007; Spakman and Hall, 2010; Villeneuve et al., 2010; Pownall et al., 2013; Zahirovic et al., 2014; Hall and Spakman, 2015). To decipher the Neogene tectonics of the region it is vital to determine the formation mechanism of the Banda Arc – a 180°-curved string of islands (from Timor round to Buru; see Fig. 1) that connects with the Sunda Arc to its west. The oceanic lithosphere subducted around the arc forms a concave chute that plunges to the west to depths in excess of 650 km (Cardwell and Isacks, 1978; McCaffrey, 1998; Das, 2004; Spakman and Hall, 2010; Pownall et al., 2013; Hall and Spakman, 2015); clearly, this geometry cannot have been created simply by subduction from a straight or low-curvature hinge line. Several authors have suggested that the slab's concave shape is explained by southeastward rollback of a single subduction zone whose curvature progressively tightened (e.g. Hall and Wilson, 2000; Milsom, 2001; Spakman and Hall, 2010; Hall, 2011, 2012; Pownall et al., 2013; Hall and Spakman, 2015). Other authors have instead proposed that the subducted lithosphere beneath the Banda Sea comprises two or more separate slabs that were subducted from different directions (e.g. Cardwell and Isacks, 1978; Das, 2004).

The islands of Seram (Fig. 2), Buru, and the small islands located in the eastern Banda Arc provide the opportunity to understand how subduction developed and proceeded in the Banda Region. Seram was for a long time interpreted to comprise a collisional fold-and-thrust belt incorporating ultramafic thrust sheets of ophiolitic origin (Audley-Charles et al., 1979; Linthout et al., 1996); however, recent geological field investigations on Seram found evidence instead for substantial extension having exhumed the ultramafic rocks from the subcontinental lithospheric mantle (SCLM), alongside granulite-facies migmatites of the Kobipoto Complex (Pownall et al., 2013, 2014, 2016; Pownall and Hall, 2014; Pownall, 2015). Residual granulites from the Kobipoto Complex record evidence for ultrahigh-temperature (UHT: > 900°C) metamorphism at 16 Ma, caused by their juxtaposition with the hot exhuming mantle lherzolites (Pownall et al., 2014; Pownall, 2015). In western Seram, Kobipoto Complex lherzolites and granulite-facies migmatites were exhumed beneath extensional detachment faults, and across central Seram, these rocks have been subsequently incorporated within the major strike-slip Kawa Shear Zone (KSZ; Pownall et al., 2013).

The sense of lithospheric deformation across the island inferred from mapping (broad NNE–SSW extension; WNW–ESE-striking left-lateral strike-slip shearing) is consistent with it having been dragged eastwards into position above a rolling-back slab, as proposed by Spakman and Hall (2010), Hall (2011, 2012), and Pownall et al. (2013, 2014). However, there are many unanswered questions regarding the timing of extreme extension and strike-slip faulting on Seram, and the link between these tectonic events and the recently-identified episode of Middle Miocene UHT metamorphism (Pownall et al., 2014, *in review*; Pownall, 2015).

In this paper, we present (*i*) thirteen new $^{40}Ar/^{39}Ar$ ages for white mica and biotite from Tehoru Formation, Taunusa Complex, and Kobipoto Complex metamorphic rocks and migmatites from western and central Seram; (*ii*) a new $^{40}Ar/^{39}Ar$ age for a Kobipoto Complex diatexite on Ambon; and (*iii*) a new $^{40}Ar/^{39}Ar$ age for a phlogopite lamprophyre found in association with the ultramafic complex exposed in the Kobipoto Mountains. Several rocks were sampled from shear zones associated with Kobipoto Complex exhumation, and from the major Kawa Shear Zone in central Seram. Other rocks were sampled because they record the highest metamorphic grade experienced by their respective metamorphic complex. Some micas have been dated from migmatites for which SHRIMP U–Pb zircon ages have also been acquired (Table 1; Pownall et al., 2014, *in review*) in order to compare the two geochronological systems and assess cooling rates and/or differences in respective closure temperatures. This paper presents interpretations of these $^{40}Ar/^{39}Ar$ ages in the context of microstructural and larger-scale structural observations which help to unravel the sequence of metamorphic, magmatic, and deformational events on Seram.

2. Geological context and sample petrography

Seram exposes several complexes comprising upper-mantle lherzolites and mid/lower-crustal granulite-facies migmatites of the Kobipoto Complex (Pownall, 2015). Granulites from the Kobipoto Mountains, central Seram, record an episode of widespread crustal melting and metamorphism under UHT conditions reaching 925˚C and 9 kbar (Pownall, 2015) shortly before 16 Ma (Pownall et al., 2014). These high-temperature rocks are exposed in western Seram beneath low-angle WNW–ESE-striking detachment faults (Fig. 2c, 3), but in the Kobipoto Mountains of central Seram are incorporated within transpressional pop-up structures (Pownall et al., 2013; Pownall and Hall, 2014; Pownall, 2015). Boudins of serpentinised lherzolites are also located within the Kawa Shear Zone (Fig. 2a) – a strike-slip fault system that traverses the centre of the island. Kobipoto Complex exhumation has evidently been facilitated by different structures at different stages of Seram's tectonic evolution.

In all instances, the Kobipoto Complex has been exhumed beneath or alongside lower grade metamorphic rocks of the Tehoru Formation (Pownall et al., 2013). As noted by Linthout et al. (1989), Tehoru Formation schists and phyllites exposed on the Kaibobo Peninsula in west Seram (Fig. 2c) immediately adjacent to the Kobipoto Complex have been overprinted by a sillimanite-grade shear zone parallel to the Tehoru Formation/Kobipoto Complex contact. Similar field relations are also evident on the neighbouring Hoamoal Peninsula (Fig. 2b). These sheared, sillimanite-grade gneisses were defined by Pownall et al. (2013) as comprising the Taunusa Complex, adapting an earlier definition by Tjokrosapoetro and Budhitrisna (1982). In considering the ultramafic rocks of the Kobipoto Complex to represent an overthrust ophiolite (as implied by Audley-Charles et al., 1979), Linthout et al. (1996) interpreted this metamorphosed shear zone as a sub-ophiolite metamorphic sole. These authors dated biotite and white mica from their 'sole' rocks using an $^{40}Ar/^{39}Ar$ laser step heating method, yielding ages of 6.6–5.4 Ma (Table 1); however, they concluded that these ages related to ophiolite emplacement, as opposed to our view that the ultramafic rocks were exhumed by detachment faulting. Two samples analysed as part of this study (KB11-234 and KB11-374) were taken from similar locations to Linthout et al.'s (1996) sample BK21, within the Taunusa Complex, to enable comparison (Fig. 2c).

As previously mentioned, Kobipoto Complex granulites and lherzolites crop out also in the Kobipoto Mountains of central Seram – a large left-lateral positive flower structure forming the northern extent of the Kawa Shear Zone. The southern extent of this wide shear zone is defined by the topographically prominent Kawa Fault (Fig. 2a), approaching which Tehoru Formation schists become progressively mylonitised. The Kawa Fault juxtaposes Tehoru Formation mylonites against low-grade slates and marbles of the Saku Formation to their north across *c.* 1 km of stranded fault cores and damage zones (Fig. 6; Linthout et al., 1989, 1991; Pownall et al., 2013). Based on mylonitic fabrics, Linthout et al. (1991) interpreted this shear zone as a right-lateral strike-slip system that operated as an antithetic shear within an anticlockwise-rotating 'Buru-Seram Microplate', supporting a reconnaissance paleomagnetic study by Haile (1978), who tentatively suggested that Seram has rotated 74° anticlockwise since 7.6 ± 1.4 Ma (K–Ar age for Kelang pillow basalts; Beckinsale and Nakapadungrat, 1979). Rb–Sr ages of *c.* 3 Ma obtained by Linthout et al. (1991) for Kawa Shear Zone mylonites (Table 1) were interpreted by them as having been reset by hydrothermal fluids that ascended through the antithetic fault network during the hypothesised rotation. However, our fieldwork within the Kawa Shear Zone found evidence for both right- *and* left-lateral shear recorded by the microstructures of alternating mylonite and foliated gouge exposures (Pownall et al., 2013); which do not unambiguously identify an overall shear sense, and instead suggest a history of multiple re-activations with both left- and right-lateral displacement. Furthermore, interpretation of regional topography of the mountains north of the Kawa Fault (i.e., the Kobipoto Mountains pop-up), and Quaternary geomorphology along the fault indicates that left-lateral strike-slip shear was the most recent upper crustal deformation within this zone (Pownall et al., 2013; Pownall and Hall, 2014; Watkinson and Hall, 2016).

2.1. Kobipoto Complex

The Kobipoto Complex (Fig. 4), redefined by Pownall et al. (2013), includes all rocks comprising part of the upper mantle to mid/lower crust exhumed across Seram, Ambon, and possibly islands to the east of Seram (e.g. Kur, Fadol, Kasiui). Exposed granulite-facies migmatites include melanosome-dominated metatexites (including those recording UHT metamorphism; Pownall et al., 2014; Pownall, 2015) and more abundant leucosome-rich cordierite- and garnet-bearing diatexites (described by some previous authors, e.g. Priem et al., 1978, as 'cordierite granites').

Ultramafic rocks, typically lherzolites, accompany the migmatites in every known instance, leading Pownall et al. (2014) to conclude that the extensive crustal melting and granulite-facies metamorphism was driven by the juxtaposition of the hot subcontinental lithospheric mantle with the base of the extended crust.

Kobipoto Complex granulites from the Kobipoto Mountains were described in detail by Pownall (2015), and *c*. 16 Ma SHRIMP U–Pb zircon ages for migmatites exposed in central Seram were presented by Pownall et al. (2014). An $^{40}Ar/^{39}Ar$ biotite age of 16.34 ± 0.04 Ma for a Kobipoto Complex migmatite from the Kobipoto Mountains (Pownall et al., 2014), is within error of the SHRIMP U–Pb zircon age acquired from the same sample (Table 1).

2.1.2. KP11-619 – Grt–Crd–Sil Metatexite

KP11-619 is a metatexite boulder collected from the upstream section of the Wai Tuh in the Kobipoto Mountains and described by Pownall et al. (2014). It contains abundant melanosome comprising cordierite + biotite + garnet + sillimanite. Garnets commonly exceed 5 mm in diameter. Cordierite is typically pinitised, although some of the fresher cordierite contains sprays of sillimanite needles and is associated with two generations of biotite; a dark amorphous generation in direct grain contact with the cordierite and large blebs of ilmenite, and a stubby idioblastic population of biotite that is often is included within the amorphous type (Fig. 4a).

2.1.3. SE10-178 – Cordierite diatexite, Kaibobo Peninsula

This typical 'cordierite granite', sampled from the northern body of Kobipoto Complex diatexites on the Kaibobo Peninsula, is characterised by abundant mm-scale sillimanite–spinel schlieren (Fig. 4b), associated with biotite. Cordierite is abundant, partially pinitised, and has white mica reaction rims. Garnet is scarce. Quartz has crystallised into complex subgrains, and plagioclase and K-feldspar are typically idioblastic. Zircon from this sample has been dated by Pownall et al. (*in review*).

2.1.4. KB11-367 – Mylonitised cordierite diatexite, Kaibobo Peninsula

Mylonitised cordierite diatexites are incorporated within a shear zone exposed on the Tanjung Motianai headland of the Kaibobo Peninsula (Fig. 2c; see also Pownall et al., 2013). Mylonitic lineations plunge 12° to the WSW. Cordierite diatexite KB11-367 has a very similar mineralogy to the undeformed diatexites in the centre of the peninsula (e.g. SE10-178). A second generation of biotite has grown along shear bands, wrapping around feldspar clasts and older larger grains of biotite that have acquired fish-type morphologies (Fig. 4c).

2.1.5. AM10-167 – Cordierite diatexite, Ambon

Cordierite diatexite AM10-167 was sampled near to the migmatite–peridotite contact on the southern coast of Latimor, Ambon. This sample is very similar to SE10-178, although biotite is more abundant and spinel + sillimanite schlieren are scarcer.

2.2. Tehoru Formation

Here we follow the definition of the Tehoru Formation given by Audley-Charles et al. (1979), which is approximately equivalent to the 'Formation of Crystalline Schists and Phyllites' described by Valk (1945) and Germeraad (1946). This extensive metamorphic complex (Fig. 5), which crops out over much of western and central Seram, is typified by monotonous greenschist to lower-amphibolite facies metapelites commonly interbanded with metabasic amphibolites. The greenschists are dominantly phyllitic, and the majority of the higher-grade schists contain simple garnet–biotite–muscovite–chlorite assemblages. In addition, staurolite-grade schists and gneisses have also been identified in outcrop, and several authors have reported kyanite-grade schists occurring as float in rivers draining the mountainous interior of the island (Valk, 1945; Audley-Charles et al., 1979; Linthout et al., 1989; Pownall et al., 2013). Linthout et al. (1989) calculated peak metamorphic conditions of ~ 600˚C and ~ 5 kbar, followed by cooling and decompression to ~ 500˚C and ~ 2 kbar, for staurolite–garnet schists in central Seram based on conventional cation exchange thermobarometry. The protolith of the Tehoru Formation has been assumed to be Paleozoic (Valk, 1945; Audley-Charles et al., 1979; Tjokrosapoetro and Budhitrisna, 1982; Tjokrosapoetro et al., 1993a,b), although Triassic detrital zircon dated by Pownall et al. (2014) from the Kobipoto Complex migmatites, and Jurassic zircon grains recovered from the overlying Kanikeh Formation by Hall and Sevastjanova (2012) demonstrate that this estimate is likely to be too old.

2.2.1. HM11-177 – Hoamoal Peninsula Ky–St–Grt schist

Sample HM11-177 (Fig. 5a–c), a kyanite–staurolite–garnet Tehoru Formation schist, was collected as a small cobble from a stream draining the northwestern portion of the Hoamoal Peninsula. Kyanite-grade schists (representing the highest metamorphic grade of the Tehoru Formation) have not been observed to crop out in this region, so *in situ* sampling was unfortunately not possible. Abundant 1–2 mm-diameter garnet porphyroblasts are wrapped by thick swathes of white mica. Blue kyanite blades are fairly conspicuous in hand sample; staurolite porphyroblasts are also present, although are smaller and scarcer than the garnets. Recrystallised quartz is abundant in the matrix and red-brown rutile grains are present throughout. The garnets are highly poikiloblastic and contain coarse grains of quartz that are concentrated in the cores (Fig. 5b). Many of the garnets display excellent 'snowball' quartz inclusion patterns, providing strong evidence for syn-kinematic growth, and preserving older fabrics. Staurolite is similarly poikiloblastic although does not display such obvious evidence for rotation during growth. There are two distinct populations of white mica present in this schist: (*i*) highly elongate, almost fibrous mats of white mica which form mm-thick, highly crenulated bundles with tight zig-zag folds that wrap around the garnet, staurolite, and kyanite porphyroblasts; and (*ii*) coarser, stubbier, and scarcer grains of white mica that post-date the crenulation, and may have recrystallized from the older crenulated white mica. These two generations of white mica are referred to here as 1st-generation, and 2nd-generation, respectively.

2.2.2. TS11-496 – Kawa Shear Zone Grt mica schist

This mylonite and associated retrograde fault gouges (Fig. 5d–f), formed within the Kawa Shear Zone, was sampled during a river traverse undertaken from the Trans-Seram Highway in central Seram (Fig. 6). Fairly abundant (~10 vol.%) mm-scale garnet porphyroblasts contain curved trails of quartz inclusions. They are partly wrapped round by biotite and/or white mica or flanked by abundant quartz. White mica also forms highly-crenulated aggregates that are concentrated along minor shear bands. Based on cross-cutting relationships, the white mica appears to be slightly older than the biotite, which also defines the shear bands. σ-type garnet porphyroblasts indicate a left-lateral shear sense.

2.2.3. SER-26C – Kawa Shear Zone Grt–Hbl mica schist

This schist (Fig. 5g–i) was sampled north of the village of Tehoru from a NW–SE-striking strike-slip shear zone within the Tehoru Formation. It is characterised by abundant 0.1–1.0 mm subhedral garnet and hornblende porphyroblasts found in association with coarse grains of biotite. Coarse grains of plagioclase are found in other domains of the rock; finely-recrystallised quartz is abundant throughout. Many of the hornblendes have sigmoidal geometries that are aligned with the biotite grains. Narrow biotite-rich shear bands are oriented parallel to the C-planes of an S–C′ fabric that is weakly defined by hornblende and biotite crenulation (Fig. 5i). The hornblende and biotite define the same fabric in the rock, but the hornblende appears to predate biotite formation.

2.3. Saku Formation

Low-grade slates and marbles of the Saku Formation (Hartono and Tjokrosapoetro, 1984) are located north of the Kawa Fault (Fig. 2a). Their protolith is thought to have overlain the protolith of the Tehoru Formation (Tjokrosapoetro et al., 1993a). No rocks sampled from the Saku Formation were suitable for $^{40}Ar/^{39}Ar$ dating.

2.4. Taunusa Complex

The Taunusa Complex (Fig. 6) is considered here and by Pownall et al. (2013) as a high-T overprint of the Tehoru Formation in response to heating and shearing by the Kobipoto Complex peridotites and migmatites. Sillimanite-bearing schists and gneisses comprising the hanging wall above exhumed Kobipoto Complex rocks on the Kaibobo Peninsula (Pownall et al., 2013, *in review*) were shown by Linthout et al. (1989) to have been metamorphosed at temperatures surpassing 700˚C (at 4–5 kbar) – around 100˚C hotter than they determined for the Tehoru Formation. Similar contact relations are observed on the nearby Hoamoal Peninsula, where Taunusa Complex rocks separate the Kobipoto Complex and Tehoru Formation (Pownall et al., 2013).

2.4.1. KB11-234 – Kaibobo Peninsula Sil gneiss

This gneiss (Fig. 6a–c), sampled from the hanging wall above the Kaibobo Detachment (Fig. 2c), comprises alternating quartzofeldspathic and biotite-rich bands that have been crosscut by narrow shear bands comprising fibrous sillimanite and biotite. These shear bands define a weak S–C fabric, enclosing sigmoidal microlithons (Fig. 6b). Scarce relict garnet poikiloblasts are heavily altered and partly pseudomorphed by biotite. Large white mica grains are present in the quartzofeldspathic domains, where quartz has recrystallised between large K-feldspars. Growth of sillimanite is interpreted to have been caused by high-T shearing during Kobipoto Complex exhumation.

2.4.2. KB11-374 – Kaibobo Peninsula Sil–mica gneiss

This Taunusa Complex gneiss (Fig. 6d–f), sampled ~ 1 km west of KP11-234, was also heated and sheared by the high-T exhumation of the adjacent Kobipoto Complex. Bands of recrystallised quartz host plagioclase grains and large (up to 5 mm) white mica 'fish' indicating top-to-the-north shear (Fig. 6d,e). As also observed by Linthout et al. (1996) in a similar nearby sample BK21 (Fig. 2c), these white mica fish contain inclusions of folded fibrolitic sillimanite, demonstrating that white mica crystallization must have occurred during the latter stages of high-T shearing. Coarse white mica grains within the more mafic segregations of the gneiss define an S–C fabric, again indicative of top-to-the-north shear. Here, the white mica is frequently boudinaged, with biotite having formed in the strain shadows (Fig. 6d).

Porphyroblastic minerals are absent from this rock.

2.4.3. SER-7 – Hoamoal Peninsula And–Sil–Bt schist

This schist was sampled from the west coast of the Hoamoal Peninsula adjacent to Kobipoto Complex lherzolites and scarce diatexites that have been exhumed in the vicinity of Luhu village (Fig. 2b). Here, the contact is a steep reverse fault, and the schists in the vicinity of sample SER-7 indicate top-to-the-NNW shear sense (Fig. 6g). SER-7 (Fig. 6g–i) comprises quartz bands of various grain sizes interspersed with narrow biotite-rich zones hosting mm-scale andalusite crystals, with an elongate morphology characteristic of pseudomorphs after kyanite. This inference is supported by the presence of blue kyanite rods in an adjacent outcrop. The biotite exists mainly as small partially chloritised stubby flakes formed between quartz grains, but more rarely larger elongate grains are present. Chloritised white mica is also present. Narrow anastomosing trails of sillimanite traverse the rock subparallel to the main foliation, defining minor shear bands. Fine intergrowths of sillimanite and biotite suggest some of the biotite must have formed during or shortly after the high-T (sillimanite-grade) metamorphic peak, when the rock is thought to have been heated and sheared by exhumation of the neighboring Kobipoto Complex in a similar manner to KB11-234 and KB11-374.

2.4.4. KP11-581D – Kobipoto Mountains Grt–Sil metatexite

This sample (Fig. 6j–l) was collected as a small boulder in the Wai Sapolewa, Kobipoto Mountains. In contrast to the metamorphic rocks of the Kobipoto Complex, this sample has not been metamorphosed in the granulite facies, although it has experienced considerable partial melting. The melanosome comprises large garnet phenocrysts wrapped by tightly-folded swathes of white mica and sillimanite, which is more characteristic of samples belonging to the Taunusa Complex than the Tehoru Formation. The leucosome comprises coarse recrystallised quartz with highly sutured subgrains grown around randomly-oriented mm-scale (up to 5 mm long) laths of white mica. Large apatite grains are also present.

2.5. Lamprophyric rocks

Several phlogopite-rich lamprophyric rocks were observed to intrude the lherzolites exposed within the Kobipoto Mountains (Fig. 2a). This may be the same rock type referred to by Germeraad (1946), who described an "apatite biotitite" comprising 82 vol.% biotite from the same region (collected by L.M.R. Rutten and W. Hotz between 1917 and 1919).

2.5.1. KP11-593 – Phlogopite Minette

A phlogopite-rich lamprophyre was found as a boulder in the Wai Tuh, Kobipoto Mountains (Fig. 7a). Very similar lithologies were also observed as intrusions within metre-scale lherzolite boulders (Fig. 7b). Bronze-coloured phlogopite crystals attain lengths sometimes in excess of 2 cm (Fig. 7c). Smaller and far scarcer apatite grains also feature as phenocrysts. The groundmass comprises K-feldspar, plagioclase, and smaller biotites. Quartz is absent, although so are feldspathoids. We have interpreted this lamprophyre as a minette (following Le Maitre, 2002) based on the dominant phlogopite–K-feldspar mineralogy, and its K- and Na-rich bulk chemistry (3.38 wt.% K_2O; 3.83 wt.% Na_2O), high Mg (16.82 wt.% MgO), and low silica content (49.95 wt.% SiO_2) determined by X-ray fluorescence (XRF) spectroscopy (see Supplementary Data File 1). As these lamprophyres formed by melting of the ultramafic complex, $^{40}Ar/^{39}Ar$ dating of the phlogopite indicates the time of lherzolite exhumation and/or cooling.

3. $^{40}Ar/^{39}Ar$ geochronology

Sixteen mica separates (9 biotite, 6 white mica, and 1 phlogopite) were dated from twelve rocks, as listed in Table 2. The Taunusa Complex samples are all from the hanging wall directly above the exhumed Kobipoto Complex rocks. The Tehoru Formation samples are taken either from the Kawa Shear Zone, or were sampled on the basis that they have experienced kyanite-grade metamorphism, representing the highest grade achieved by this metamorphic unit. The Kobipoto Complex diatexites, as previously mentioned, are from the Kobipoto Mountains, the Kaibobo Peninsula, and from Ambon. Phlogopite was dated from the lamprophyre sampled from the Kobipoto Mountains that was found to intrude the ultramafic complex. The relative structural locations and metamorphic classifications for all samples are shown schematically in Figure 8.

3.1. Methods

Two different methods were used to separate the micas from their host rock (as noted in Table 2), at Royal Holloway University of London. *Method 1* involved removing the mica from an uncrushed hand sample by splitting the rock along its cleavage and carving out selected mica-dominated microstructures with a sharp knife; *Method 2* involved crushing the sample to a fine gravel size and then wet sieving this sample to extract 63–250 μm grains before separating the grains based on their magnetic susceptibilities using a Frantz magnetic barrier separator. Both methods required subsequent 'papering' and hand picking under a binocular microscope to increase the purity of the separates. Method 1 was our preference as it allowed individual microstructures to be targeted for analysis; however, the relatively scarce and fine-grained nature of mica made it necessary to use Method 2 for some of the samples.

The samples were irradiated in two separate batches alongside CaF_2 and K-glass standards. Biotite samples SER-7, SER-26C, SE10-178, and AM10-167 were packed into Cd-shielded canister number 'ANU#7' and were irradiated by the McMaster reactor, Ontario, in for 8 MWh. The other 12 samples were packed into Cd-shielded canister number 'ANU#13' and were irradiated by the United States Geological Survey TRIGA reactor, Denver, for 12 MWh. Fish Canyon Tuff sanidine (28.10 ± 0.04 Ma K–Ar age; Spell and McDougall, 2003) was used as the flux monitor for the ANU#7 samples, and biotite standard GA-1550 (98.5 ± 0.8 Ma K–Ar age; Spell and McDougall, 2003) was used as the flux monitor for the ANU#13 samples.

All irradiated samples were repackaged and analysed at the Research School of Earth Sciences (Australian National University) Argon Laboratory using the *in vacuo* furnace step-heating method described previously by Forster and Lister (2010, 2014). The samples were dropped into a tantalum crucible within a double-vacuum resistance furnace, and raised to increasingly higher thermostatically controlled temperatures for 15-minute durations, between which the furnace was left to cool to a 350˚C resting temperature. Typically, 21 to 23 heating steps were performed on each sample, with a minimum difference between successive heating steps of +30˚C. A final heating step at 1450˚C ensured all gas was released from the sample, and an extensive cleaning procedure involving evacuating and heating the empty furnace to 1450˚C (repeated three times) minimised the risk of cross-sample contamination.

Gas incrementally released from the samples during the step-heating procedure was released through an ultrahigh-vacuum extraction line to a VG1200 gas-source mass spectrometer that measured the abundances of ^{36}Ar, ^{37}Ar, ^{38}Ar, ^{39}Ar, and ^{40}Ar with a 7.6×10^{-17} mol mV^{-1} sensitivity. The flux monitors were degassed using a Coherent infrared diode laser and analysed using the same extraction line and mass spectrometer.

The data were reduced using *Noble v1.8* software in accordance with the correction factors and J-factors listed in Appendix A. Correction factors were calculated from the analyses of CaF_2 and K-glass, and J-factors were calculated from analysis of the flux monitors, all of which were irradiated at known distances from the samples. ^{40}K abundances and decay constants are taken from standard values recommended by the IUGS subcommission on geochronology (Steiger and Jäger, 1977). The decay factor of ^{40}K ($\lambda^{40}K$) for all age calculations was set at 5.5430×10^{-10} yr^{-1}.

Results tables for each step heating experiment are presented in Appendix A, with a summary of these ages and their interpretations presented in the final column of Table 2.

3.2. Interpretation of apparent age spectra

The apparent age spectra for the 16 samples are presented in Figure 9 (for ages < 12 Ma) and Figure 10 (for ages *c*. 16 Ma). Errors are presented at a 1σ level (displayed by bar thickness for individual heating steps, and by orange error bars for interpreted ages), and the mean square weighted deviation (MSWD) is also displayed for each interpreted age. The apparent age spectrum for diatexite KP11-619 (Fig. 10b) is reproduced after Pownall et al. (2014). Other previously published ages are shown in part ‘a’ of both figures for comparison. The spectra are arranged to allow comparison between similar ages, rather than being grouped by rock type. Results tables for each step heating experiment (including their respective J-factors) are presented in Appendix A.

Many spectra feature a single wide, flat plateau; other spectra reveal more complex behaviour due to mixing of different gas populations. In this second instance, the spectra were analysed using the Method of Asymptotes and Limits, as devised by Forster and Lister (2004). This method recognises that a single apparent age spectrum may be produced by the mixing of distinct gas populations from two or more microstructural and/or microchemical reservoirs of different ages. For instance, for Figure 9c, we interpret the upward-sloping yellow ‘staircase’ (between 20 and 40% ^{39}Ar release) that converges on limits aged 4.47 ± 0.02 Ma and 5.43 ± 0.09 Ma to result from the mixing of two different argon reservoirs with those respective ages. By means of microstructural and/or microchemical analysis of the dated mineral grains, it is often possible to attribute a sequence of two or more ^{40}Ar/^{39}Ar ages to a history of crystallisation, recrystallisation, and deformation during which new argon reservoirs were formed, or older ones fully or partially degassed and therefore reset (Forster and Lister, 2004, 2014).

Our interpretations for the ages indicated by each step heating experiment are shown in the last column of Table 2. A discussion of the possible meanings of these ages from a tectonic and/or metamorphic standpoint is presented in Section 4.

4. Geological interpretation of ^{40}Ar/^{39}Ar ages

As summarised in Figures 11 and 12, several frequently measured ages have emerged from this study: 16 Ma, 5.7 Ma, 4.5 Ma, and 3.4 Ma. Interestingly, single samples often record two of these ages, demonstrating a history of overprinting tectonic events affecting much of Seram. For instance, biotite from Taunusa Complex sample KB11-234 (Fig. 9c) has recorded a 5.43 Ma $^{40}Ar/^{39}Ar$ age interpreted to be related to extensional exhumation of hot Kobipoto Complex rocks in western Seram, as well as a younger 4.47 Ma $^{40}Ar/^{39}Ar$ age interpreted to record movement of the Kawa Shear Zone. These and other events are discussed in detail below.

4.1. The 16 Ma metamorphic–magmatic event

The oldest-known event recorded by the $^{40}Ar/^{39}Ar$ system on Seram is that which drove ultrahigh-temperature (UHT) metamorphism of the Kobipoto Complex granulites at 16 Ma (Pownall et al., 2014; Pownall, 2015). As previously reported by Pownall et al. (2014), the 16.34 ± 0.04 Ma $^{40}Ar/^{39}Ar$ age of biotite from Kobipoto Complex diatexite KP11-619 is identical-within-error to the 16.00 ± 0.52 Ma $^{206}Pb/^{238}U$ zircon age determined for the same rock. Biotite in this sample, as discussed by Pownall et al. (2014), most likely formed as a high-T retrograde product during the early stages of decompression and cooling from UHT conditions. Therefore, it is entirely plausible that it formed at very similar P–T conditions to the zircon, especially if, as suggested by Pownall (2015): (*i*) the thin 16 Ma zircon rims crystallised in response to Zr-liberating (i.e. garnet-consuming) reactions during the rock's retrogression, rather than recording the age of peak metamorphism (cf. Kelsey et al., 2008; Sajeev et al., 2010; Kelsey & Powell, 2011; Kohn et al., 2015), (*ii*) the closure temperature of the mica was higher than conventionally assumed (cf. Forster and Lister, 2014), and (*iii*) cooling, and therefore exhumation, was very rapid. The apparent age spectrum for KP11-619 biotite additionally indicates mixing with a younger 14.83 ± 0.29 Ma gas population, the origin of which is unclear, but may have been released by the amorphous recrystallised generation of biotite observed in thin section (Fig. 4a).

Sample HM11-177, the kyanite–staurolite–garnet schist from the Hoamoal Peninsula, also records *c.* 16 Ma ages. Crenulated white mica (1st-generation) produced a spectrum with a single wide plateau at 16.60 ± 0.06 Ma (Fig. 10f), whereas the uncrenulated white mica (2nd-generation) inferred from the microstructure to be younger, exhibited mixing between this age and a slightly younger gas population at 15.88 ± 0.10 Ma (Fig. 10e). Incredibly, this younger age is identical within error to the $^{40}Ar/^{39}Ar$ age yielded by white mica from sillimanite gneiss sample KP11-581D from the Kobipoto Mountains (Fig. 10d), over 150 km further east (Fig. 12). This extremely close similarity of $^{40}Ar/^{39}Ar$ ages over such a long distance suggests that a kyanite-grade metamorphic event at 16 Ma, which evidently affected Tehoru Formation schists across the entirety of western and central Seram, was a short and intense event. Furthermore, this evidence for a regionally significant metamorphic event at 16 Ma greatly strengthens the argument that the 16 Ma $^{206}Pb/^{238}U$ zircon ages from the Kobipoto Complex migmatites (Pownall et al., 2014) record UHT metamorphism, as opposed to being related to subsequent localised re-melting or metasomatism of the migmatite complex.

In the light of the age correlations shown in Figures 11 and 12, we interpret UHT metamorphism of the Kobipoto Complex, and the accompanying melting that was necessary to dehydrate the residual high-temperature assemblages (Vielzeuf et al., 1990; White and Powell, 2002), to have been contemporaneous with kyanite-grade metamorphism of parts of the Tehoru Formation at *c.* 16 Ma. Large prismatic sillimanite crystals occurring in the Kobipoto Complex granulites are interpreted as pseudomorphs after kyanite (Pownall, 2015), demonstrating a similar mineralogy for the Kobipoto Complex and Tehoru Formation, which might share a common protolith (Pownall et al., 2013).

It follows that metamorphic grade was therefore dictated by proximity to the exhuming subcontinental lithospheric mantle, where the geotherm would locally have been elevated. It should be clarified that the classifications for the Tehoru Formation, Kobipoto Complex, and Taunusa Complex outlined by Pownall et al. (2013) and illustrated in Figure 8 are effectively based on each units' relationships to the detachment faults that facilitated crustal extension and mantle exhumation. The Kobipoto Complex granulite-facies migmatites represent the partially-melted mid/lower crust (30–35 km depth; Pownall, 2015) exhumed alongside the upper SCLM beneath the detachment faults; the Tehoru Formation includes the vast majority of Seram's metamorphosed rocks comprising greenschist to upper-amphibolite facies (kyanite-grade) schists and basic amphibolites, which form the hanging walls of the detachments; and the Taunusa Complex is simply a localised overprint of those Tehoru Formation rocks that lie immediately above the detachments – a high temperature, high strain zone characterised by the occurrence of fibrolitic sillimanite and very localised partial melting.

4.2. Lamprophyric volcanism at 15 Ma

Phlogopite phenocrysts from lamprophyre sample KP11-593 yielded an $^{40}Ar/^{39}Ar$ age of 15.07 ± 0.08 Ma, as defined by a single, very wide plateau (80% of ^{39}Ar release) on the apparent age spectrum (Fig. 10c). As previously described (Pownall et al., 2013), this and other lamprophyric rocks were emplaced as dykes through the lherzolites exposed in the Kobipoto Mountains (Fig. 7b), thus demonstrating a genetic relationship between these ultramafic rock units. This *c*. 15 Ma age for lamprophyric volcanism demonstrates that melting of the fertile mantle occurred more-or-less contemporaneously with UHT metamorphism and melting of the continental crust. Further evidence is therefore provided for lithosphere-scale extension and the resulting exhumation of hot, fertile mantle having driven the UHT metamorphic event at *c*. 16 Ma.

4.3. Kobipoto Complex exhumation in western Seram

White mica and biotite from the two Taunusa Complex gneisses sampled from the Kaibobo Peninsula (KB11-234 and KB11-374) all yielded $^{40}Ar/^{39}Ar$ ages of *c*. 5.5 Ma (Fig. 11, 13). Aside from KB11-234 biotite, all apparent age spectra feature wide plateaux that record single ages. As previously mentioned, the spectrum from KB11-234 biotite shows a rising profile that converges on an upper 5.43 ± 0.09 Ma plateau and a lower 4.47 ± 0.02 Ma limit. We interpret this as due to mixing between two gas populations of those respective ages: the older age correlating with the other samples; the younger age possibly to a second generation of amorphous recrystallised biotite. In both instances, the white mica $^{40}Ar/^{39}Ar$ age is very slightly older than the biotite $^{40}Ar/^{39}Ar$ age from the same rock (by ~ 0.2 Myr), which is due either to the fact that in both instances the white mica is microstructurally older than biotite (Fig. 6c, d), and/or that the white mica closed to appreciable argon diffusion at a slightly higher temperature.

Inclusions of sillimanite within the white mica 'fish' (Fig. 6f), and the occurrence of sillimanite also within the shear bands (Fig. 6c, h), demonstrates that the white mica most probably grew during high temperature shearing of the gneiss (as previously concluded by Linthout et al., 1996). Therefore, we interpret the white mica $^{40}Ar/^{39}Ar$ ages to date movement on the shear zone. Biotite, which has formed in the strain shadows between the white mica fish (Fig. 6d), or has otherwise grown around the white mica (Fig. 6c) is by association also related to the high-temperature shearing. These $^{40}Ar/^{39}Ar$ ages therefore provide information on the timing of Kobipoto Complex exhumation on the Kaibobo Peninsula, since the Taunusa Complex formed in response to the extensional exhumation of the hot lherzolites and migmatites beneath the Kaibobo Detachment (Pownall et al., 2013).

Kobipoto Complex diatexites similarly yielded *c.* 5.5 Ma $^{40}Ar/^{39}Ar$ ages, demonstrating a correlation with the age of mylonitisation of the Taunusa Complex gneisses comprising the hanging wall. Biotite from cordierite diatexite sample SE10-178 produced a humped apparent age spectrum with a plateau at 5.88 ± 0.05 Ma peaking at 6.69 ± 0.13 Ma at 65% total ^{39}Ar release. Biotite from mylonitised cordierite diatexite sample KB11-367 also yielded a 5.40 ± 0.21 Ma $^{40}Ar/^{39}Ar$ age, as well as a younger 3.30 ± 0.04 Ma age. This younger age likely relates to argon released from the younger generation of biotite grown within the shear bands (described in Section 2.1.4), which cross-cut the older biotite-bearing fabric. The main phase of activity of the shear zone exposed on Tanjung Motianai is therefore shown to post-date movement of the Kobipoto Detachment by ~ 2 Myr (Fig. 11, 13). 'Motianai Shear Zone' movement appears to instead coincide with deformation within the Kawa Shear Zone at *c.* 3.5 Ma (cf. sample SER-26C).

Previous work on the Kaibobo Peninsula by Linthout et al. (1996) obtained $^{40}Ar/^{39}Ar$ white mica and biotite ages also of *c.* 5.5 Ma (see Table 1) using a laser step heating method for a sillimanite gneiss sampled from the same structural position as our Tehoru formation rocks (Fig. 2c). Although these authors also interpreted their ages to relate to shearing, they instead attributed the cause of the shearing to obduction of the ultramafic complex, which they interpreted to comprise part of an ophiolite (Linthout et al., 1989). Nevertheless, these previously published $^{40}Ar/^{39}Ar$ ages (Table 1) are in close agreement with our results (Fig. 11), and although they have larger uncertainties provide additional age constraints on timing of shear zone operation.

4.4. Kawa Shear Zone activity

The Kawa Shear Zone (KSZ), based on its geomorphological expression, operated most recently and perhaps to the present day with a left-lateral shear sense (Pownall et al., 2013; Pownall and Hall, 2014; Watkinson and Hall, 2016). However, the incorporation of ultramafic rock slivers within fault gouges (Fig. 5f), and the occurrence of both left- and right-lateral outcrop-scale shear-sense indicators, demonstrate a more complex history. It has previously been suggested that the Kawa Fault, and associated faults within the KSZ, may have originated as low-angle detachments (similar to those exposed in western Seram) that were later re-activated as thrust/reverse faults with strong strike-slip shear components (Pownall et al., 2013). This interpretation was based on the occurrence of ultramafic slivers in the KSZ, and the observation that the KSZ and the Kaibobo Detachment (western Seram) share the same strike (120–300°). These new $^{40}Ar/^{39}Ar$ ages support this proposal, as they reveal 3 distinct events (at 5.6 Ma, 4.5 Ma, and 3.3 Ma) associated with the detachment on the Kaibobo Peninsula; the younger two of these ages relating to events also recorded in the KSZ (Fig. 14).

Sample TS11-496, a mylonitised garnet-mica schist from the central part of the KSZ, yielded a 10.2 Ma age (white mica) in addition to a significantly younger 4.5 Ma age (white mica and biotite). We interpret these ages as recording two separate deformational events, as opposed to a single period of slow cooling. This interpretation is supported by microstructural evidence (Section 2.2.2) for biotite crystallisation having post-dated white mica formation. Interestingly, the 4.5 Ma age is also recorded by Taunusa Complex samples SER-7 (biotite) from the southern Hoamoal Peninsula, and, as previously mentioned, by KB11-234 (biotite) from the Kaibobo Peninsula. Again, samples at > 100 km separation distances gave $^{40}Ar/^{39}Ar$ ages that are identical within error (4.47 ± 0.02 Ma, 4.47 ± 0.16 Ma, 4.48 ± 0.09 Ma, and 4.49 ± 0.08 Ma; see Figs. 11 and 12). Sample SER-26C, a garnet mylonite 60 km further southeast, provided a younger 3.5 Ma biotite $^{40}Ar/^{39}Ar$ age. Although the correlation is less strong, this age is within 0.2 Myr of the $^{40}Ar/^{39}Ar$ biotite ages recorded by the mylonitised cordierite diatexite on the Kaibobo Peninsula (KB11-367), and the cordierite diatexite on Ambon (AM10-167).

These results demonstrate that (*i*) the KSZ may have been active, in some form, as early as 10.2 Ma (if the 10.2 Ma age dates mylonitisation); (*ii*) deformation that was absorbed by the KSZ at 4.5 Ma also affected Taunusa Complex gneisses in the central Kaibobo Peninsula; and (*iii*) subsequent movement of the KSZ at 3.5 Ma was coincident with operation of the Tanjung Motianai Shear Zone on the southern Kaibobo Peninsula.

4.5. Ambon

Biotite from cordierite diatexite AM10-167 produced a single $^{40}Ar/^{39}Ar$ age of 3.63 ± 0.04 Ma, which we interpret to record exhumation and cooling of the Kobipoto Complex on Ambon. This is similar to the 3.3 ± 0.1 Ma Rb–Sr age reported by Priem et al. (1979) and the 4.1–3.4 Ma K–Ar ages reported by Honthaas et al. (1999) for similar 'cordierite granites' sampled from the island. As previously mentioned, this new $^{40}Ar/^{39}Ar$ age correlates with the timing of shearing within the

KSZ and southern Kaibobo Peninsula (samples SER-26C and KB11-367, respectively). Ambonites—cordierite-garnet dacites presumably sourced from the Kobipoto Complex migmatites (Whitford and Jezek, 1979; Linthout and Helmers, 1994; Pownall et al., *in review*)—were erupted on Ambon around 1 Myr later, from *c*. 2.3 Ma (Honthaas et al., 1999).

5. Implications for Banda Arc tectonics

According to plate reconstructions by Spakman and Hall (2010) and Hall (2002, 2011, 2012), the highly arcuate Banda Arc (and the highly concave Banda Slab) formed by rollback of a single slab into a pre-existing Jurassic D-shaped oceanic 'Banda Embayment' in the Australian continental margin (Fig. 15). The embayment is inferred to have originally been enclosed along its northern extent by a promontory of Australian crust called the Sula Spur (Klompé, 1954), which fragmented sometime after its collision with SE Asia (*c*. 23 Ma; Hall, 2011) to form Seram, Ambon, Buru, and parts of eastern Sulawesi. The timing of rollback depicted by the reconstruction is based, in part, on the dating of ocean-floor basalts and the interpretation of ocean-floor magnetic stripes that formed behind the rolling-back arc, which demonstrate that back-arc spreading must have opened the North Banda Basin between 12.5–7.2 Ma (Réhault et al., 1994; Hinschberger et al., 2000, 2003), and the South Banda Basin between 6.5–3.5 Ma (Honthaas et al., 1998; Hinschberger et al., 2001). Based on these constraints, the reconstructions show the eastern extent of the Java Trench beginning to rapidly roll back southeastwards into the Banda Embayment to form the Banda Arc from the Middle Miocene (15 Ma). A horizontal tear in the slab beneath Buru interpreted from seismic tomography (Hall and

Spakman, 2015) implies that at some point the slab tore from its northern margin after having driven extension and fragmentation of the adjacent Sula Spur as rollback advanced southeastwards (Spakman and Hall, 2010). The new ^{40}Ar/^{39}Ar ages presented in this study document a history of protracted crustal extension and strike-slip faulting across Seram, thus providing insights into how Banda slab rollback affected the geology of the Sula Spur as it tore into the Banda Embayment.

Several lines of geochronological evidence now indicate a regionally significant episode of high- to ultrahigh-temperature metamorphism and melting at *c.* 16 Ma on Seram: (*i*) 16 Ma SHRIMP U–Pb ages for metamorphic zircon from the Kobipoto Mountains granulites (Pownall et al., 2014); (*ii*) the 16 Ma biotite ^{40}Ar/^{39}Ar age for Kobipoto Complex diatexite KP11-619 (Fig. 10b), attributed to high-T retrogression of the granulites; (*iii*) the 17–16 Ma white mica ^{40}Ar/^{39}Ar ages for kyanite-grade Tehoru Formation schist HM11-177 (Fig. 10e,f) and Taunusa Complex gneiss KP11-581D (Fig. 10d); and (*iv*) the 15 Ma phlogopite ^{40}Ar/^{39}Ar age for lamprophyre sample KP11-593 (Fig. 10c), which was sourced from and intruded through the hot lherzolites. These ages document an episode of rapid cooling of the Kobipoto Complex granulites from UHT conditions involving post-peak zircon growth (likely in response to garnet breakdown at 850–900°C; Pownall, 2015) and crystallisation of retrograde biotite, both at *c.* 16 Ma (Pownall et al., 2014). Kyanite-grade metamorphism of Tehoru Formation schists, which occurred across western and central Seram, is shown by the 17–16 Ma ^{40}Ar/^{39}Ar white mica ages of samples HM11-177 and KP11-581D to have occurred more-or-less simultaneously with UHT metamorphism and melting of the Kobipoto Complex migmatites. We thus interpret an episode of regional high-grade metamorphism and melting, producing both UHT granulite-facies migmatites and kyanite-grade schists at different structural levels, to have affected Seram soon after (or just before?) the Banda slab began rolling back to the southeast.

In order that rocks now in western Seram were extended by the Banda slab rollback at 16 Ma, western Seram must at that time have been positioned closer to eastern Sulawesi (Fig. 15), as opposed to having been affected by the 16 Ma event in its current location relative to Australia. Furthermore, *c.* 16 Ma metamorphic ages identified further afield suggest that there was extension of a large part of the upper plate and the metamorphic event probably affected a broad region. Advokaat et al. (2014) presented SHRIMP U–Pb ages for metamorphic zircon of 15.4 Ma from gneisses on Sulawesi's North Arm, which were interpreted to date a period of significant extension predating the exhumation of core complexes. Also, 17.6 and 16.9 Ma K–Ar ages from K-feldspar and biotite, respectively, from Kur island in the easternmost Banda Arc (Honthaas et al., 1997) reinforce the idea that products from this Early-Middle Miocene event were transported far into the Banda Embayment. A 17.0 Ma $^{40}Ar/^{39}Ar$ hornblende age from the Aileu Complex, Timor-Leste (Ely et al., 2014), would also appear to correlate with the 16 Ma event on western and central Seram, which is potentially explained by fragments of the Australian Sula Spur having been transported across the Banda Embayment and colliding with different Australian continental rocks on the Timor side (Bowin et al., 1980; Hall, 2011; Ely et al., 2014). In contrast, northern and eastern Seram likely occupied a similar position, with respect to the Bird's Head (West Papua), throughout the Neogene (Fig. 15).

The opening of the North Banda Basin (Fig. 1) between 12.5–7.15 Ma (Réhault et al., 1994; Hinschberger et al., 2000, 2003) places a minimum age on the time by which Banda rollback separated Seram from Sulawesi, which was described by Hall (2011) as the first phase of E–W extension in the Banda Arc's evolution. This time interval corresponds to the gap shown in Figure 11 where no major events were recorded on Seram by this $^{40}Ar/^{39}Ar$ study, suggesting that extension behind the rolling-back slab at that time was accommodated primarily by oceanic spreading between Sulawesi and Buru, without the requirement to extend the lithosphere beneath Seram.

Around 1 Myr after the North Banda Basin is dated to have ceased spreading, extension was transferred to the detachment faults in western Seram (Fig. 13). This forced Kobipoto Complex lherzolites and granulite-facies migmatites generated during the 16 Ma UHT event to be juxtaposed against lower-grade Tehoru Formation rocks at shallower structural levels. The heat retained by the Kobipoto Complex during its exhumation was sufficient to metamorphose and deform adjacent rocks comprising the hanging wall, originally part of the Tehoru Formation, to produce the observed Taunusa Complex sillimanite-grade shear zone (Figs. 8, 13). The $^{40}Ar/^{39}Ar$ ages determined by this study for the two Taunusa Complex samples (KB11-234 and KB11-374) demonstrate that one such high-T shear zone now exposed on the Kaibobo Peninsula (the 'Kaibobo Detachment'; Fig. 2c, 13) was active at 5.8–5.6 Ma.

Further exhumation of the Kobipoto Complex migmatites and lherzolites on Seram was later facilitated by transpression within the Kawa Shear Zone (KSZ), shown here to have operated from 4.4 Ma. As suggested by Pownall et al. (2013), the strike-slip faults comprising the KSZ are overprinted and steepened originally low-angle lithospheric detachment faults akin to those preserved in western Seram (Fig. 12) and they also incorporate peridotites and share the same 120°–300° strike. This interpretation is further supported by the $^{40}Ar/^{39}Ar$ ages presented in this study, as the main phase of KSZ operation is shown to post-date movement along the detachment faults exposed in western Seram by around 1 Myr. Also, sample KB11-234 from the Taunusa Complex of the Kaibobo Peninsula records both events (Fig. 11, 12), demonstrating that also in western Seram shear zones were reactivated at 4.4 Ma, but perhaps not with a strong strike-slip component. Sample SER-7 from a peridotite-bounding shear zone on the southern Hoamoal Peninsula, also recorded this 4.4 Ma age. The overprinting of former extensional faults by strike-slip faults in central Seram would have contributed further to the net elongation of Seram, as depicted by Figure 14, as rollback progressed further east.

At 3.5 Ma, Kobipoto Complex rocks were exhumed on Ambon (sample AM10-167), which was accompanied by further deformation within low-angle shear zones in western Seram (sample KB11-367) and shear within the southeastern portion of the KSZ (sample SER-26C). This event was contemporaneous also with extension across northern and central Sulawesi that drove rapid subsidence of Gorontalo Bay and the rapid exhumation of adjacent metamorphic core complexes (Cottam et al., 2011; Watkinson, 2011; Pholbud et al., 2012; Advokaat et al., 2014; Hennig et al., 2012, 2014, 2015; Pezzati et al., 2014, 2015; Rudyawan et al., 2014; van Leeuwen et al., 2007, 2016). Although it remains unclear if (or how) the two regions operated as parts of the same tectonic system, it is interesting to note in both instances the dominance of extensional tectonics in the early stages of collision.

This extreme extension documented on Seram from 16 Ma until present possibly affected other islands now comprising the northern Banda Arc, such as Buru and the small island chain immediately SE of Seram. Lherzolites and/or high-grade metamorphic rocks have been reported from Buru, Gorong, Manawoka, Kasiui, Tioor, Watubela, Kur, and Fadol (Bowin et al., 1980; Charlton et al., 1991; Hamilton, 1979; Honthaas et al., 1997; Pownall et al., 2016), which likely share similar histories to those exposed on Seram (Pownall et al., 2016). Our working hypothesis is that highly-extended lithosphere exists all around the northern portion of the Banda Arc, on the inner side of the collisional fold-and-thrust belts comprising the Seram and Aru troughs.

6. Conclusions

Our new $^{40}Ar/^{39}Ar$ ages, in the context of previous field-based studies on Seram and Ambon, suggest the following sequence of tectonic and metamorphic–magmatic events having affected the islands:

(1) Substantial lithospheric extension juxtaposed hot lherzolites against the mid/lower crust (~33 km depth; Pownall, 2015), driving HT–UHT metamorphism and melting just prior to *c.* 16 Ma to form the Kobipoto Complex migmatites. This event was accompanied by kyanite-grade metamorphism of the Tehoru Formation and the intrusion of lamprophyric melts sourced from the exhumed lherzolites. Seram was very likely located adjacent to eastern Sulawesi at this time, prior to being drawn eastwards by rollback of the Banda slab into the Banda Embayment.

(2) After the 16 Ma Middle Miocene metamorphic event, extension behind the rolling-back slab was accommodated by spreading of the North Banda Basin between Sulawesi and Buru (12.5–7.2 Ma; Hinschberger et al., 2000) with no major deformation recorded on Seram.

(3) The Kobipoto Complex was exhumed between 5.8–5.6 Ma to shallower structural levels across western Seram, as facilitated by the Kaibobo Detachment and similar low-angle normal faults during continued southeastward slab rollback ~1 Myr after North Banda Basin spreading ceased.

(4) From 4.5 Ma, the Kawa Shear Zone, central Seram, operated with a strike-slip sense and exhumed slivers of peridotite, possibly having overprinted similar low-angle extensional structures to those currently preserved in western Seram.

(5) Further strike-slip deformation within the Kawa Shear Zone occurred at 3.5 Ma, coincident with exhumation of Kobipoto Complex diatexites on Ambon and further deformation within shear zones in western Seram.

The very close correlation of several $^{40}Ar/^{39}Ar$ ages interpreted from the apparent age spectra demonstrate a tight synchronicity between tectonic events recorded over the width of Seram, with several samples having recorded two of these frequently measured ages. These ages document a protracted history of extension and strike-slip faulting, consistent with Seram having been extended and sheared above the rolling-back Banda Slab from 16 Ma until 3.5 Ma. This study demonstrates the utility of microstructurally-focused argon geochronology in assessing the timing of tectonic processes in multiply-deformed terranes, and showcases the rapidity and synchronicity of extensional tectonics in the modern Earth.

Appendix A. $^{40}Ar/^{39}Ar$ step heating results

$^{40}Ar/^{39}Ar$ step heating results are presented in Supplementary Data File 2, which can be found online at >>>>>>>.

Acknowledgements

We are extremely grateful to Yasinto Priastomo and Ramadhan Adhitama (Institut Teknologi Bandung) for assistance in the field. Matthew Thirlwall and Christina Manning are thanked for assistance with XRF analysis. We also thank Chris Morley and Tony Barber for their reviews, and Alan Collins for his editorial assistance. $^{40}Ar/^{39}Ar$ geochronology was undertaken at the RSES Argon Laboratory, Australian National University. This research was funded by the SE Asia Research Group (Royal Holloway University of London), Australian Research Council (ARC) grant DP0877274 awarded to MAF, and ARC grant DE160100128 awarded to JMP.

References

Advokaat, E. L., Hall, R., White, L. T., Armstrong, R., Kohn, B., BouDagher-Fadel, M. K., 2014. Neogene extension and exhumation in NW Sulawesi. AGU Fall Meeting 2014, T43A-4701.

Audley-Charles, M.G., Carter, D.J., Barber, A.J., Norvick, M.S., Tjokrosapoetro, S., 1979. Reinterpretation of the geology of Seram: implications for the Banda Arcs and northern Australia. Journal of the Geological Society 136, 547–566.

Beckinsale, R.D., Nakapadungrat, S., 1978. A late Miocene K-Ar age for the lavas of Pulau Kelang, Seram, Indonesia. Journal of physics of the Earth 26, 199–201.

Bowin, C., Purdy, G.M., Johnston, C., Shor, G., Lawyer, L., Hartono, H., Jezek, P., 1980. Arc-continent collision in the Banda Sea region. AAPG Bulletin 64, 868–915.

Cardwell, R.K., Isacks, B.L., 1978. Geometry of the subducted lithosphere beneath the Banda Sea in eastern Indonesia from seismicity and fault plane solutions. Journal of Geophysical Research: Solid Earth (1978–2012) 83, 2825–2838. doi:10.1029/JB083iB06p02825

Charlton, T.R., Kaye, S.J., Samodra, H., Sardjono, 1991. Geology of the Kai Islands: implications for the evolution of the Aru Trough and Weber Basin, Banda Arc, Indonesia. Marine and Petroleum Geology 8, 62–69. doi:10.1016/0264-8172(91)90045-3

Charlton, T.R., 2000. Tertiary evolution of the Eastern Indonesia Collision Complex. Journal of Asian Earth Sciences 18, 603–631.

Cottam, M.A., Hall, R., Forster, M.A., Boudagher-Fadel, M.K., 2011. Basement character and basin formation in Gorontalo Bay, Sulawesi, Indonesia: new observations from the Togian Islands. In: Hall, R., Cottam, M.A., Wilson, M.E.J. (Eds.), The SE Asian Gateway: History and Tectonics of the Australia-Asia Collision. The Geological Society, Special Publication 355, 177–202. doi:10.1144/SP355.9

Das, S., 2004. Seismicity gaps and the shape of the seismic zone in the Banda Sea region from relocated hypocenters. J. Geophys. Res. 109, B12303. doi:10.1029/2004JB003192

Ely, K.S., Sandiford, M., Phillips, D., Boger, S.D., 2014. Detrital zircon U–Pb and $^{40}Ar/^{39}Ar$ hornblende ages from the Aileu Complex, Timor-Leste: provenance and metamorphic cooling history. Journal of the Geological Society 171, 299–309. doi:10.1144/jgs2012-065

Forster, M.A., Lister, G.S., 2004. The interpretation of $^{40}Ar/^{39}Ar$ apparent age spectra produced by mixing: application of the method of asymptotes and limits. Journal of Structural Geology 26, 287–305. doi:10.1016/j.jsg.2003.10.004

Forster, M.A., Lister, G.S., 2010. Argon enters the retentive zone: reassessment of diffusion parameters for K-feldspar in the South Cyclades Shear Zone, Ios, Greece. Geological Society, London, Special Publications 332, 17–34. doi:10.1144/SP332.2

Forster, M.A., Lister, G.S., 2014. $^{40}Ar/^{39}Ar$ geochronology and the diffusion of ^{39}Ar in phengite-muscovite intergrowths during step-heating experiments *in vacuo*.

Geological Society, London, Special Publications 378, 117–135. doi:10.1144/SP378.16

Gaina, C., Müller, D., 2007. Cenozoic tectonic and depth/age evolution of the Indonesian gateway and associated back-arc basins. Earth Science Reviews 83, 177–203. doi:10.1016/j.earscirev.2007.04.004

Germeraad, J.H., 1946. Geology of central Seran, in: Rutten, L., Hotz, W. (Eds.), Geological, Petrographical, and Palaeontological Results of Explorations, Carried Out From September 1917 Till June 1919 in the Island of Ceram. De Bussy, Amsterdam, p. 135.

Haile, N.S., 1978. Paleomagnetic evidence for the rotation of Seram, Indonesia. Journal of physics of the Earth 26, 191–198.

Hall, R., 1996. Reconstructing Cenozoic SE Asia, in: Hall, R., Blundell, D. (Eds.), Tectonic Evolution of Southeast Asia. Geological Society of London Special Publications, pp. 153–184. doi:10.1144/GSL.SP.1996.106.01.11

Hall, R., 2002. Cenozoic geological and plate tectonic evolution of SE Asia and the SW Pacific: computer-based reconstructions, model and animations. Journal of Asian Earth Sciences 20, 353–431. doi:10.1016/S1367-9120(01)00069-4

Hall, R., 2011. Australia-SE Asia collision: plate tectonics and crustal flow. In: Hall, R., Cottam, M.A., Wilson, M.E.J. (Eds.), The SE Asian Gateway: History and Tectonics of the Australia-Asia Collision. Geological Society, London, Special Publications 355, 75–109. doi:10.1144/SP355.5

Hall, R., 2012. Late Jurassic–Cenozoic reconstructions of the Indonesian region and the Indian Ocean. Tectonophysics 570-571, 1–41. doi:10.1016/j.tecto.2012.04.021

Hall, R., Wilson, M.E.J., 2000. Neogene sutures in eastern Indonesia. Journal of Asian Earth Sciences 18, 781–808.

Hall, R., Sevastjanova, I., 2012. Australian crust in Indonesia. Australian Journal of Earth Sciences 59, 827–844. doi:10.1080/08120099.2012.692335

Hall, R., Spakman, W., 2015. Mantle structure and tectonic history of SE Asia. Tectonophysics. doi:10.1016/j.tecto.2015.07.003

Hamilton, W., 1979. Tectonics of the Indonesian region. US Geological Survey Professional Paper 1078, 345 pp.

Hartono, H.M.S., Tjokrosapoetro S., 1984. Preliminary account and reconstruction of Indonesian terranes. Proceedings of the Indonesian Petroleum Association 13, 185–226.

Hennig, J., Hall, R., Watkinson, I.M., Forster, M., 2012. Timing and Mechanisms of Exhumation in West Central Sulawesi. AGU Fall Meeting, T43E-2713.

Hennig, J., Advokaat, E., Rudyawan, A., Hall, R., 2014. Large Sediment Accumulations and Major Subsidence Offshore; Rapid Uplift on Land: Consequences of Extension of Gorontalo Bay and Northern Sulawesi. Indonesian Petroleum Association, Proceedings 38, IPA14-G-304.

Hennig, J., Hall, R., Armstrong, R.A., 2015. U–Pb zircon geochronology of rocks from west Central Sulawesi, Indonesia: Extension-related metamorphism and magmatism during the early stages of mountain building. Gondwana Research. doi:10.1016/j.gr.2014.12.012.

Hinschberger, F., Malod, J.-A., Réhault, J.-P., Dyment, J., Honthaas, C., Villeneuve, M., Burhanuddin, S., 2000. Origine et evolution du basin Nord-Banda (Indonésie): apport des données magnétiques. Comptes Rendus de l'Académie des Sciences, Série IIA: Sciences de la Terre et des Planètes 331, 507–514.

Hinschberger, F., Malod, J.-A., Dyment, J., Honthaas, C., Réhault, J.-P., Burhanuddin, S., 2001. Magnetic lineations constraints for the back-arc opening of the Late Neogene South Banda Basin (eastern Indonesia). Tectonophysics 333, 47–59. doi:10.1016/S0040-1951(00)00266-3

Hinschberger, F., Malod, J.-A., Réhault, J.-P., Burhanuddin, S., 2003. Apport de la bathymétrie et de la géomorphologie à la géodynamique des mers de l'Est-indonésien. Bulletin de la Société Géologique de France 174, 545–560.

Hinschberger, F., Malod, J.-A., Réhault, J.-P., Villeneuve, M., Royer, J.-Y., Burhanuddin, S., 2005. Late Cenozoic geodynamic evolution of eastern Indonesia. Tectonophysics 404, 91–118. doi:10.1016/j.tecto.2005.05.005

Honthaas, C., Villeneuve, M., Réhault, J.-P., Bellon, H., Cornee, J.-J., Saint-Marc, P., Butterlin, J., Gravelle, M., Burhanuddin, S., 1997. L'île de Kur: géologie du flanc oriental du bassin de Weber (Indonésie orientale). Comptes Rendus de l'Académie des Sciences, Série IIA: Sciences de la Terre et des Planètes 325, 883–890.

Honthaas, C., Réhault, J.-P., Maury, R.C., Bellon, H., Hémond, C., Malod, J.-A., Cornée, J.-J., Villeneuve, M., Cotten, J., Burhanuddin, S., Guillou, H., Arnaud, N., 1998. A Neogene back-arc origin for the Banda Sea basins: geochemical and geochronological constraints from the Banda ridges (East Indonesia). Tectonophysics 298, 297–317. doi:10.1016/S0040-1951(98)00190-5

Honthaas, C., Maury, R.C., Priadi, B., Bellon, H., Cotten, J., 1999. The Plio–Quaternary Ambon arc, Eastern Indonesia. Tectonophysics 301, 261–281. doi:10.1016/S0040-1951(98)00227-3

Kelsey, D.E., Powell, R., 2011. Progress in linking accessory mineral growth and breakdown to major mineral evolution in metamorphic rocks: a thermodynamic approach in the Na_2O-CaO-K_2O-FeO-MgO-Al_2O_3-SiO_2-H_2O-TiO_2-ZrO_2 system. Journal of Metamorphic Geology 29, 151–166.

Kelsey, D.E., Clark, C., Hand, M., 2008. Thermobarometric modelling of zircon and monazite growth in melt-bearing systems: examples using model metapelitic and metapsammitic granulites. Journal of Metamorphic Geology 26, 199–212.

Klompé, T.H.F., 1954. The structural importance of the Sula Spur (Indonesia). Indonesian Journal of Natural Sciences 110, 21–40.

Kohn, M.J., Corrie, S.L., Markley, C., 2015. The fall and rise of metamorphic zircon. American Mineralogist 100, 897–908.

Le Maitre, R.W., 2002. Igneous Rocks: A Classification and Glossary of Terms. Cambridge University Press, Cambridge, pp. 1–236.

Linthout, K., Helmers, H., 1994. Pliocene obducted, rotated and migrated ultramafic rocks and obduction-induced anatectic granite, SW Seram and Ambon, Eastern Indonesia. Journal of Southeast Asian Earth Sciences 9, 95–109. doi:10.1016/0743-9547(94)90068-X

Linthout, K., Helmers, H., Sopaheluwakan, J., Nila, E.S., 1989. Metamorphic complexes in Buru and Seram, Northern Banda Arc. Netherlands Journal of Sea Research 24, 345–356. doi:10.1016/0077-7579(89)90160-9

Linthout, K., Helmers, H., Andriessen, P., 1991. Dextral strike-slip in Central Seram and 3-4.5 Ma Rb/Sr ages in pre-triassic metamorphics related to early Pliocene counterclockwise rotation of the Buru-Seram microplate (E. Indonesia). Journal of Southeast Asian Earth Sciences 6, 335–342. doi:10.1016/0743-9547(91)90079-D

Linthout, K., Helmers, H., Wijbrans, J.R., Van Wees, J.D.A.M., 1996. $^{40}Ar/^{39}Ar$ constraints on obduction of the Seram ultramafic complex: consequences for the evolution of the southern Banda Sea. Geological Society, London, Special Publications 106, 455–464. doi:10.1144/GSL.SP.1996.106.01.28

McCaffrey, R., 1988. Active tectonics of the eastern Sunda and Banda arcs. Geophysics 93, 15163–15182.

Milsom, J., 2001. Subduction in eastern Indonesia: how many slabs? Tectonophysics 338, 167–178. doi:10.1016/S0040-1951(01)00137-8

Pezzati, G., Hall, R., Burgess, P., Pérez-Gussinyé, M., 2014. The Poso Basin in Gorontalo Bay, Sulawesi: Extension related to core complex formation on land. Indonesian Petroleum Association, Proceedings 38, IPA14-G-297.

Pezzati, G., Hennig, J., Advokaat, E., Hall, R., Burgess, P., Pérez-Gussinyé, M., 2015. Subsidence in Gorontalo Bay, Sulawesi (Indonesia) and metamorphic core complex exhumation on land. EGU General Assembly 2015, 7476.

Pholbud, P., Hall, R., Advokaat, E., Burgess, P., Rudyawan, A., 2012. A new interpretation of Gorontalo Bay, Sulawesi. Indonesian Petroleum Association, Proceedings 36, IPA12-G-039.

Pownall, J.M., 2015. UHT metamorphism on Seram, eastern Indonesia: reaction microstructures and P–T evolution of spinel-bearing garnet–sillimanite granulites from the Kobipoto Complex. Journal of Metamorphic Geology 33, 909–935. doi:10.1111/jmg.12153

Pownall, J.M., Hall, R., 2014. Neogene extension on Seram: A new tectonic model for the northern Banda Arc. Indonesian Petroleum Association, Proceedings 38, IPA14-G-305.

Pownall, J.M., Hall, R., Watkinson, I.M., 2013. Extreme extension across Seram and Ambon, eastern Indonesia: evidence for Banda slab rollback. Solid Earth 4, 277–314. doi:10.5194/se-4-277-2013

Pownall, J.M., Hall, R., Armstrong, R.A., Forster, M.A., 2014. Earth's youngest known ultrahigh-temperature granulites discovered on Seram, eastern Indonesia. Geology 42, 279–282. doi:10.1130/G35230.1

Pownall, J.M., Hall, R., Lister, G.S., 2016. Rolling open Earth's deepest forearc basin. Geology 44, 947–950. doi: 10.1130/G38051.1.

Pownall, J.M., Hall, R., Armstrong, R.A., *in review*. Hot lherzolite exhumation, UHT migmatite formation, and acid volcanism driven by Miocene rollback of the Banda Arc, eastern Indonesia. Submitted to Gondwana Research.

Priem, H.N.A., Andriessen, P.A.M., Boelrijk, N.A.I.M., Hebeda, E.H., Hutchinson, C.S., Verdurmen, E.A.T., Versschure, R.H., 1978. Isotopic evidence for a middle to late Pliocene age of the cordierite granite on Ambon, Indonesia. Geologie en Mijnbouw 57, 441–443.

Réhault, J.-P., Maury, R.C., Bellon, H., Sarmili, L., Burhanuddin, S., Joron, J.-L., Cotten, J., Malod, J.-A., 1994. La Mer de Banda Nord (Indonésie): un bassin arrière-arc du Miocène supérieur. Comptes Rendus de l'Académie des Sciences, Série IIA: Sciences de la Terre et des Planètes 318, 969–976.

Richards, S., Lister, G., Kennett, B., 2007. A slab in depth: Three-dimensional geometry and evolution of the Indo-Australian plate. Geochemistry, Geophysics, Geosystems 8. doi:10.1029/2007GC001657

Rudyawan, A., Hall, R., White, L., 2014. Neogene extension of the Central North Arm of Sulawesi, Indonesia. AGU Fall Meeting 2014, T43A-4681.

Ryan, W.B.F., Carbotte, S.M., Coplan, J.O., O'Hara, S., Melkonian, A., Arko, R., Weissel, R.A., Ferrini, V., Goodwillie, A., Nitsche, F., Bonczkowski, J., Zemsky, R., 2009. Global Multi-Resolution Topography synthesis. Geochemistry, Geophysics, Geosystems 10. doi:10.1029/2008GC002332

Sajeev, K., Williams, I.S., Osanai, Y., 2010. Sensitive high-resolution ion microprobe U-Pb dating of prograde and retrograde ultrahigh-temperature metamorphism as exemplified by Sri Lankan granulites. Geology 38, 971–974.

Spakman, W., Hall, R., 2010. Surface deformation and slab-mantle interaction during Banda arc subduction rollback. Nature Geoscience 3, 562–566. doi:10.1038/ngeo917

Spell, T.L., McDougall, I., 2003. Characterization and calibration of Ar-40/Ar-39 dating standards. Chemical Geology 198, 189–211.

Steiger, R.H., Jäger, E., 1977. Subcommission on geochronology: Convention on the use of decay constants in geo- and cosmoschronology. Earth and Planetary Science Letters 36, 359–362.

Tjokrosapoetro, S., Budhitrisna, T., 1982. Geology and Tectonics of the northern Banda Arc. Bulletin of the Indonesian Geological Research and Development Centre 6, 1–17.

Tjokrosapoetro, S., Achdan, A., Suwitodirdjo, K., Rusmana, E., Abidin, H.Z., 1993a. Geological map of the Masohi quadrangle, Maluku, 1:250,000. Geological Research and Development Centre, Bandung, Indonesia.

Tjokrosapoetro, S., Budhitrisna, T., Rusmana, E., 1993b. Geology of the Buru Quadrangle, Maluku, 1:250,000. Geological Research and Development Centre, Bandung.

Valk, W., 1945. Contributions to the geology of West Seran, in: Rutten, L., Hotz, W. (Eds.), Geological, Petrographical, and Palaeontological Results of Explorations, Carried Out From September 1917 Till June 1919 in the Island of Ceram. De Bussy, Amsterdam, p. 104.

van Leeuwen, T., Allen, C.M., Kadarusman, A., Elburg, M., Palin, J.M., Muhardjo, Suwijanto, 2007. Petrologic, isotopic, and radiometric age constraints on the origin and tectonic history of the Malino Metamorphic Complex, NW Sulawesi, Indonesia. Journal of Asian Earth Sciences 29, 751–777. doi:10.1016/j.jseaes.2006.05.002

van Leeuwen, T., Allen, C.M., Elburg, M., Massonne, H.-J., Palin, J.M, Hennig, J., 2016. The Palu Metamorphic Complex, NW Sulawesi, Indonesia: Origin and evolution of a young metamorphic terrane with links to Gondwana and Sundaland. Journal of Asian Earth Sciences 115, 133–152.

Vielzeuf, D., Clemens, J.D., Pin, C., Moinet, E., 1990. Granites, granulites, and crustal differentiation. In: Vielzeuf, D., Vidal, Ph. (Eds.), Granulites and Crustal Evolution. pp. 59–85. Springer, Netherlands

Villeneuve, M., Martini, R., Bellon, H., Réhault, J.-P., Cornee, J.-J., Bellier, O., Burhannuddin, S., Hinschberger, F., Honthaas, C., Monnier, C., 2010. Deciphering of six blocks of Gondwanan origin within Eastern Indonesia (South East Asia). Gondwana Research 18, 420–437. doi:10.1016/j.gr.2009.12.011

Watkinson, I.M., 2011. Ductile flow in the metamorphic rocks of central Sulawesi. In: Hall, R., Cottam, M.A., Wilson, M.E.J. (Eds.), The SE Asian Gateway: History and Tectonics of the Australia-Asia Collision. Geological Society, London, Special Publications 355, 157–176. doi:10.1144/SP355.8

Watkinson, I.M., Hall, R., 2016. Fault systems of the eastern Indonesian triple junction: evaluation of Quaternary activity and implications for seismic hazards. In: Cummins, P. R, Meilano, I. (Eds.), Geohazards in Indonesia: Earth Science for Disaster Risk Reduction. Geological Society of London Special Publication.

White, R.W., Powell, R., 2002. Melt loss and the preservation of granulite facies mineral assemblages. Journal of Metamorphic Geology 20, 621–632.

Whitford, D.J., Jezek, P.A., 1979. Origin of late Cenozoic lavas from the Banda Arc, Indonesia: trace elements and Sr isotope evidence. Contributions to Mineralogy and Petrology 68, 141–150.

Zahirovic, S., Seton, M., Müller, R.D., 2014. The Cenozoic and Cretaceous tectonic evolution of Southeast Asia. Solid Earth 5, 227–273.

Figure Captions

Fig. 1 Tectonic map of Eastern Indonesia and the surrounding region showing the location of Seram and Ambon, located in the northern limb of the Banda Arc. Subduction zones and major faults are modified from Hall (2012). The location of the Banda Detachment, flooring the Weber Deep, is taken from Pownall et al. (2016). The digital elevation model uses Global Multi-Resolution Topography (GMRT) data from Ryan et al. (2009).

Fig. 2 (a) Geological map of Seram and Ambon (after Pownall et al., 2013), showing enlargements of (b) the southern Hoamoal Peninsula, and (c) the Kaibobo Peninsula. The key to all parts of the figure is shown bottom left. Sample locations (listed in Table 2) are marked on each part of the figure. Samples BK21 and BK18 are those of Linthout et al. (1996). Cross-section X–X′–X″, marked in part (c), is shown in Figure 13.

Fig. 3 Panoramic photo of the northern Kaibobo Peninsula taken from Gunung Hemahuhui, overlain with the approximate traces of geological contacts. Note that cordierite diatexites and lherzolites (comprising the Kobipoto Complex) are structurally below the Taunusa Complex, which forms the hanging wall to the Kaibobo Detachment.

Fig. 4 Kobipoto Complex samples. (a) Two generations of biotite growth in metatexite KP11-619 from the Kobipoto Mountains; (b) Spinel–sillimanite scheliere in diatexite SE10-178 from the Kaibobo Peninsula; (c) Mylonitised granite KB11-367 from the Tanjung Motianai Shear Zone (Kaibobo Peninsula) featuring biotite ‘fish’ (bt1) and biotite growth along the shear bands (bt2). See Table 2 for further sample information.

Fig. 5 Tehoru Formation samples. (a–c) Kyanite-staurolite-garnet schist HM11-177 featuring tightly crenulated white mica (wm1) and coarser white mica aggregates (wm2); (d, e) Garnet-biotite mylonite TS11-496 containing σ-type garnet porphyroblasts indicative of left-lateral shear; (f) Serpentinite boudin from the Kawa Shear Zone, located < 1 km to the north of sample TS11-496; (g–i) Garnet mylonite SER-26C, sampled from the shear zone south of Teluk Taluti (g). σ-type garnets and S–C fabric (which incorporates biotite in both S- and C-planes) is consistent with a left-lateral shear sense. The dashed white lines represent the strike of the schistosity. Photomicrographs in parts a–c are taken under cross-polarised light. See Table 2 for further sample information.

Fig. 6 Taunusa Complex samples. (a–c) Sillimanite-garnet gneiss KB11-234 containing fibrolitic sillimanite concentrated in shear bands. White mica growth is shown to predate biotite formation (c). (d–f) Sillimanite-garnet gneiss KB11-374 featuring large white mica fish (e) containing inclusions of sillimanite (f) and biotite grown in the strain shadows (d). (g–i) Andalusite-sillimanite-biotite schist SER-7 featuring the characteristic sillimanite-defined shear bands (h). (j–l) Garnet-cordierite-sillimanite metatexite KP11-581D, with coarse white mica grown in the leucosome, and crenulated white mica and sillimanite present in the melanosome. Photomicrographs in parts c, e, f, i, k, and l are taken under cross-polarised light. See Table 2 for further sample information.

Fig. 7 Lamprophyric rocks of the Kobipoto Mountians. (a) Phlogopite minette sample KP11-593 showing huge laths of bronze-coloured phlogopite. Note pen for scale. (b) Phlogopite-rich minette existing as veins through serpentinised lherzolites. (c) Photomicrograph of sample KP11-593 (XPL) showing very large euhedral phlogopite grains within a finer-grained groundmass predominantly of K-feldspar and apatite. See Table 2 for further sample information.

Fig. 8 Schematic cross-section demonstrating the main field relationships interpreted for Seram, showing the relationship between the Tehoru, Taunusa, and Kobipoto metamorphic complexes (after Pownall et al., 2013). The location of samples is purely diagrammatic.

Fig. 9 Apparent $^{40}Ar/^{39}Ar$ age spectra for samples younger than 12 Ma. (a) $^{40}Ar/^{39}Ar$ ages determined by Linthout et al. (1996) for Taunusa Complex gneiss (BK21) and Kobipoto Complex cordierite diatexite (BK18) from the Kaibobo Peninsula. (b–l) Apparent age spectra for 11 samples, interpreted using the method of Asymptotes and Limits (Forster and Lister, 2004). In instances where a single plateau age has been interpreted, the steps used to calculate this age are highlighted in dark blue. In instances where limits have been interpreted resulting from mixing of two gas populations, steps used to calculate each limit are marked in dark blue and light blue, respectively. Orange error bars are shown at 1σ. Yellow steps are not used in age calculations. The spectra are arranged to demonstrate cross-correlation of frequently measured ages. See Table 2 for individual interpretations. MSWD—mean square of weighted deviates.

Fig. 10 Apparent $^{40}Ar/^{39}Ar$ age spectra for samples recording *c.* 16 Ma ages. (a) $^{206}Pb/^{238}U$ zircon ages determined by Pownall et al. (2014) for Kobipoto Complex migmatites from the Kobipoto Mountains. (b–f) Apparent age spectra for 5 samples, interpreted using the method of Asymptotes and Limits (Forster and Lister, 2004). In instances where a single plateau age has been interpreted, the steps used to calculate this age are highlighted in dark blue. In instances where limits have been interpreted resulting from mixing of two gas populations, steps used to calculate each limit are marked in dark blue and light blue, respectively. Orange error bars are shown at 1σ. Yellow steps are not used in age calculations. The spectra are arranged to demonstrate cross-correlation of frequently measured ages. See Table 2 for individual interpretations. MSWD—mean square of weighted deviates.

Fig. 11 A comparison of $^{40}Ar/^{39}Ar$ ages determined by this study, $^{40}Ar/^{39}Ar$ ages published by Linthout et al. (1996), and $^{206}Pb/^{238}U$ zircon ages determined by Pownall et al. (2014). Error bars are shown at 1σ. Note the clustering of frequently measured ages at *c.* 16 Ma, 5.8–5.6 Ma, 4.5–4.4 Ma, and 3.5–3.4 Ma. The timings of North Banda Basin opening (12.5–7.15 Ma) and South Banda Basin opening (6.5–3.5 Ma) are taken from Hinschberger et al. (2000) and Hinschberger et al. (2001), respectively.

Fig. 12 Tectonic map of Seram (from Pownall et al., 2013) annotated with $^{40}Ar/^{39}Ar$ ages determined by this study. The ages support the interpretation that the strike-slip faults (red) in central Seram post-date movement along the detachment faults (green) in western Seram, and that the Kawa Shear Zone may therefore have overprinted similar extensional detachments in central Seram. Frequently measured ages, often demonstrating a remarkable degree of correlation between samples with large separation distances, are coloured as follows: red—*c*. 16 Ma, blue—5.8–5.6 Ma, purple—4.5–4.4 Ma, and green—3.5–3.4 Ma.

Fig. 13 Cross-section X–X′–X″ across the Kaibobo Detachment, Kaibobo Peninsula, annotated with photomicrographs labelled with respective $^{40}Ar/^{39}Ar$ ages for biotite and white mica. See Fig. 2c for location of the section.

Fig. 14 Block model for Seram and Ambon (adapted from Pownall et al., 2014) showing the timing of UHT metamorphism, detachment faulting, and strike-slip shearing as determined by this $^{40}Ar/^{39}Ar$ study. KSZ—Kawa Shear Zone; SCLM–Subcontinental lithospheric mantle.

Fig. 15 Tectonic reconstruction of Eastern Indonesia from Australia–SE Asia collision at *c*. 23 Ma (based on Hall, 2012) representing graphically the events correlated in Figure 11. NBB—North Banda Basin; SBB—South Banda Basin; BR—Banda Ridges.

Tables

Table 1: Previously-published ages for metamorphic rocks on Seram and Buru

Table 2: $^{40}Ar/^{39}Ar$ geochronology sample list and interpretation of apparent age spectra

1249 **Supplementary Data**

1251 **Supplementary Data File 1:** XRF analysis of lamprophyre sample KP11-593

1253 **Supplementary Data File 2:** $^{40}Ar/^{39}Ar$ geochronology data tables

Figure 1

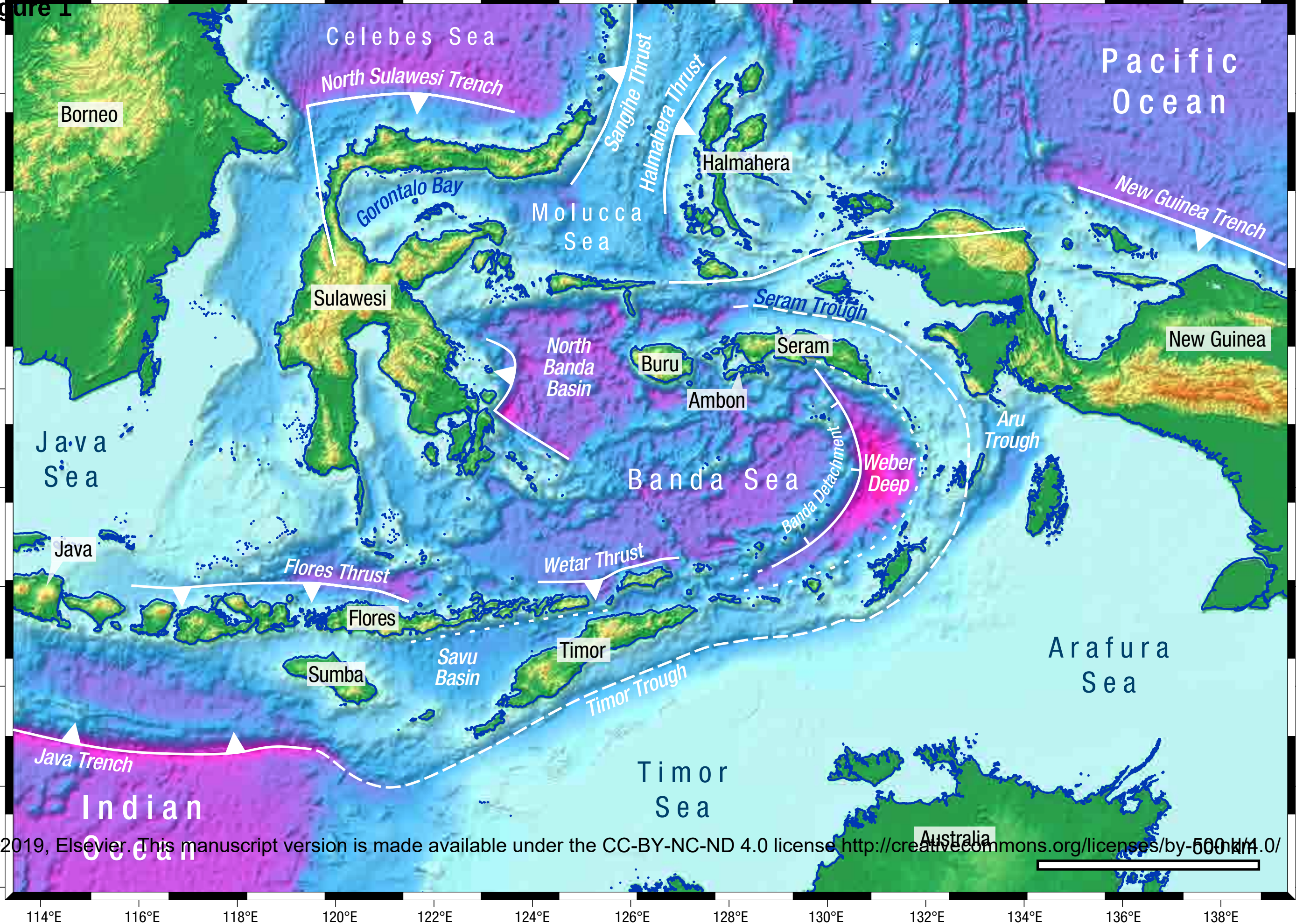
Celebes Sea
Pacific Ocean
North Sulawesi Trench
Sangihe Thrust
Halmahera Thrust
Borneo
Halmahera
Gorontalo Bay
Molucca Sea
New Guinea Trench
Sulawesi
Seram Trough
North Banda Basin
Buru
Seram
New Guinea
Ambon
Aru Trough
Java Sea
Weber Deep
Banda Detachment
Banda Sea
Java
Wetar Thrust
Flores Thrust
Flores
Timor
Savu Basin
Sumba
Arafura Sea
Timor Trough
Java Trench
Timor Sea
Indian Ocean
Australia
500 km
2°N
0°
2°S
4°S
6°S
8°S
10°S
12°S
14°S
114°E
116°E
118°E
120°E
122°E
124°E
126°E
128°E
130°E
132°E
134°E
136°E
138°E

Figure 2

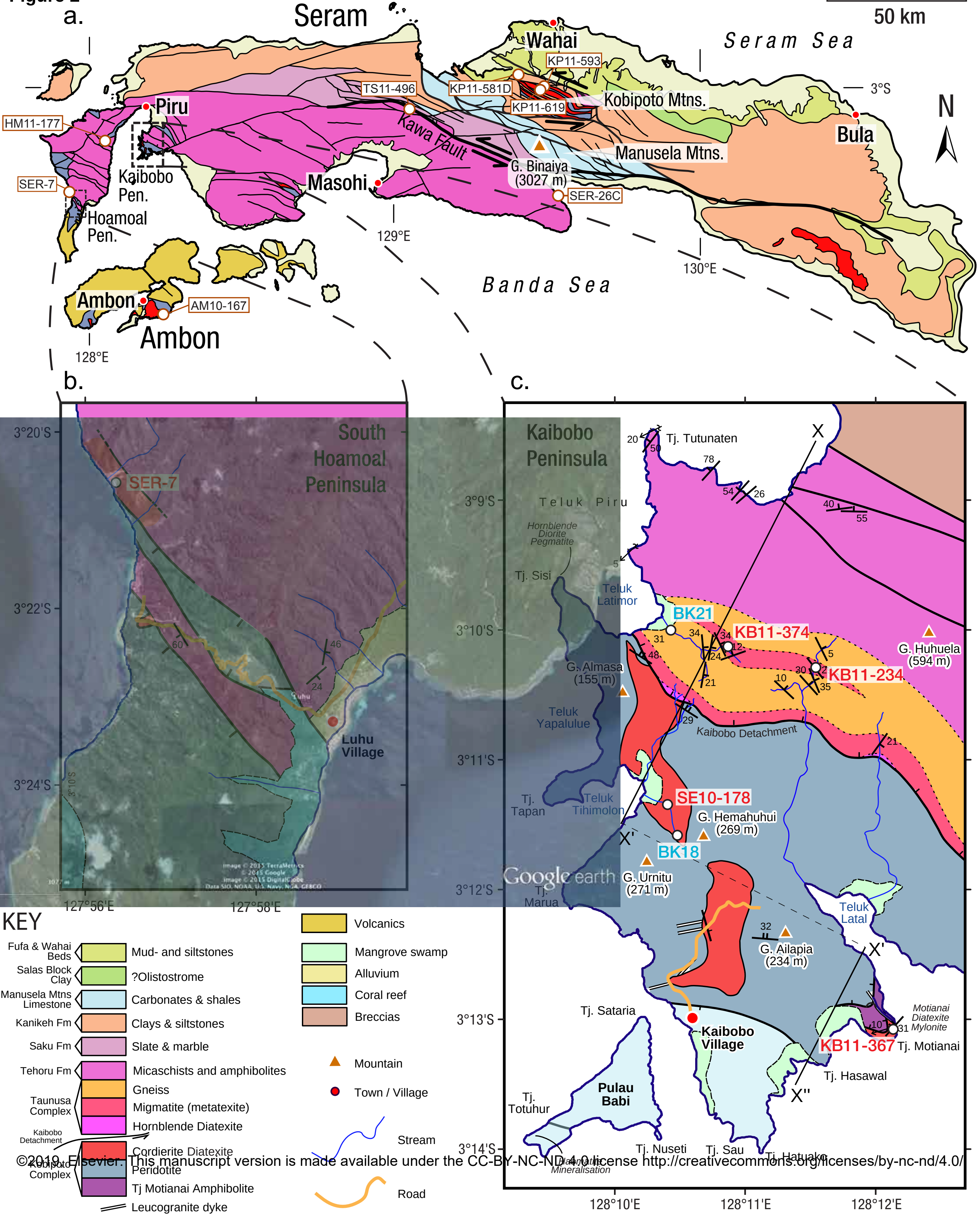

a.
Seram
Seram Sea
Banda Sea
50 km
N
3°S
129°E
130°E
128°E
Wahai
KP11-593
KP11-581D
KP11-619
TS11-496
Kobipoto Mtns.
Kawa Fault
Manusela Mtns.
G. Binaiya (3027 m)
SER-26C
Bula
Piru
HM11-177
Kaibobo Pen.
SER-7
Hoamoal Pen.
Masohi
Ambon
AM10-167
b.
3°20'S
3°22'S
3°24'S
127°56'E
127°58'E
South Hoamoal Peninsula
SER-7
Luhu Village
c.
Kaibobo Peninsula
Teluk Piru
Tj. Tutunaten
Hornblende Diorite Pegmatite
Tj. Sisi
Teluk Latimor
BK21
KB11-374
KB11-234
G. Huhuela (594 m)
G. Almasa (155 m)
Teluk Yapalulue
Kaibobo Detachment
SE10-178
Tj. Tapan
Teluk Tihimolon
G. Hemahuhui (269 m)
BK18
G. Urnitu (271 m)
Tj. Marua
G. Ailapia (234 m)
Teluk Latal
Tj. Sataria
Kaibobo Village
Motianai Diatexite Mylonite
KB11-367
Tj. Motianai
Tj. Hasawal
Pulau Babi
Tj. Totuhur
Tj. Nuseti
Tj. Sau
Tj. Hatuako
Mineralisation
X
X'
X''
3°9'S
3°10'S
3°11'S
3°12'S
3°13'S
3°14'S
128°10'E
128°11'E
128°12'E
Google earth
KEY
Fufa & Wahai Beds
Mud- and siltstones
Salas Block Clay
?Olistostrome
Manusela Mtns Limestone
Carbonates & shales
Kanikeh Fm
Clays & siltstones
Saku Fm
Slate & marble
Tehoru Fm
Micaschists and amphibolites
Taunusa Complex
Gneiss
Migmatite (metatexite)
Hornblende Diatexite
Kaibobo Detachment
Kobipoto Complex
Cordierite Diatexite
Peridotite
Tj Motianai Amphibolite
Leucogranite dyke
Volcanics
Mangrove swamp
Alluvium
Coral reef
Breccias
Mountain
Town / Village
Stream
Road

Figure 3

Gunung Huhuela
594 m
Gunung Almasa
155 m
Teluk Piru
TAUNUSA COMPLEX
Kaibobo Detachment
Crd Diatexite
Lherzolite
KOBIPOTO COMPLEX
N
Gunung Hemahuhui
269 m

Figure 4


KB11-619: Grt–Crd–Sil metatexite
SE10-178: Crd diatexite
KB11-367: Mylonitised Crd diatexite
a.
b.
c.
bt1
bt2
crd (pin)
ilm
sil
1 mm
bt
sil
sp
ilm
200 µm
bt2
bt1
crd
1 mm
SW
NE

Figure 5

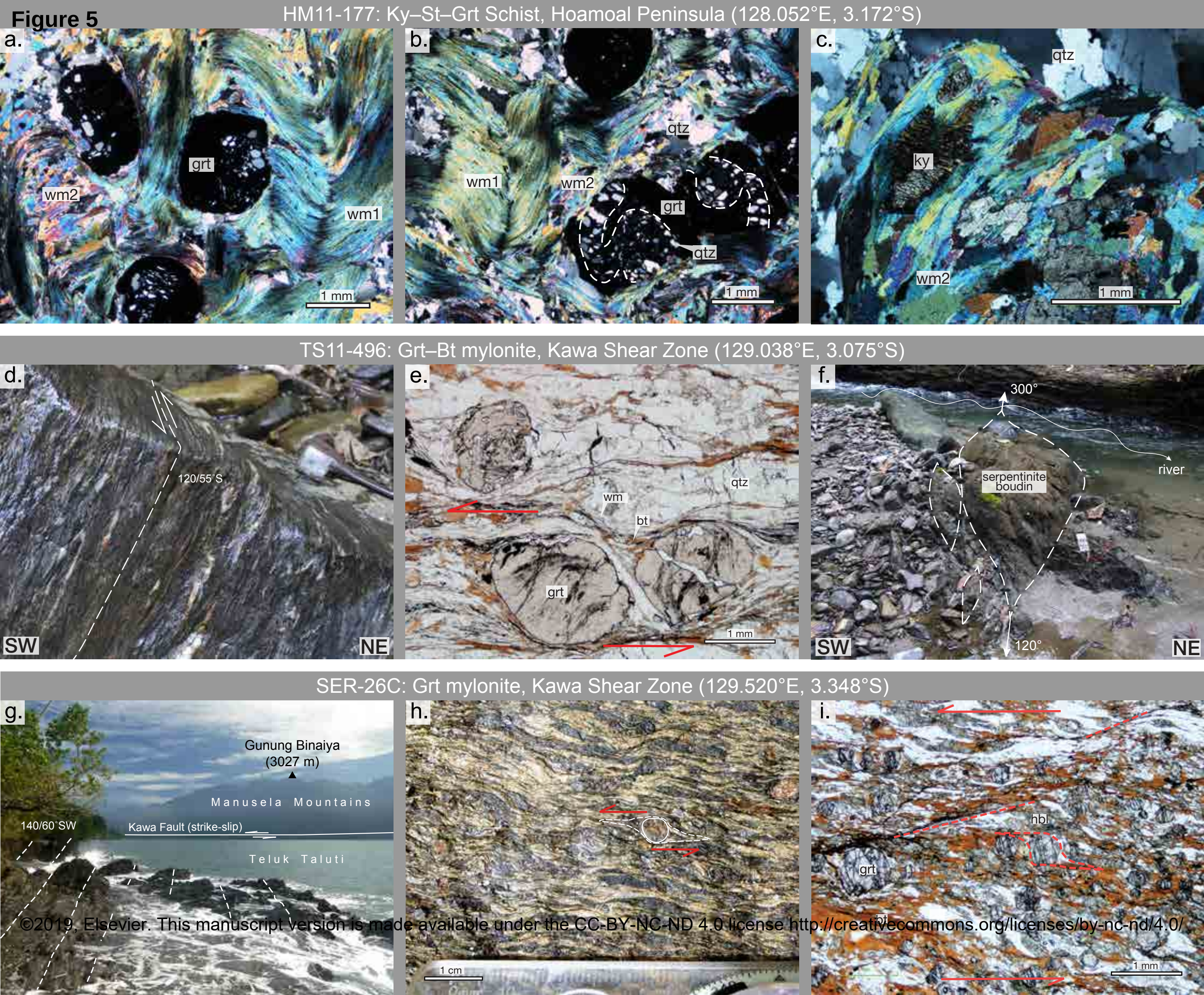
HM11-177: Ky–St–Grt Schist, Hoamoal Peninsula (128.052°E, 3.172°S)
a.
grt
wm2
wm1
1 mm
b.
qtz
wm1
wm2
grt
qtz
1 mm
c.
qtz
ky
wm2
1 mm
TS11-496: Grt–Bt mylonite, Kawa Shear Zone (129.038°E, 3.075°S)
d.
120/55˚S
SW
NE
e.
qtz
wm
bt
grt
1 mm
f.
300°
river
serpentinite boudin
SW
120°
NE
SER-26C: Grt mylonite, Kawa Shear Zone (129.520°E, 3.348°S)
g.
Gunung Binaiya
(3027 m)
Manusela Mountains
140/60˚SW
Kawa Fault (strike-slip)
Teluk Taluti
h.
1 cm
i.
hbl
grt
bt
1 mm

Figure 6

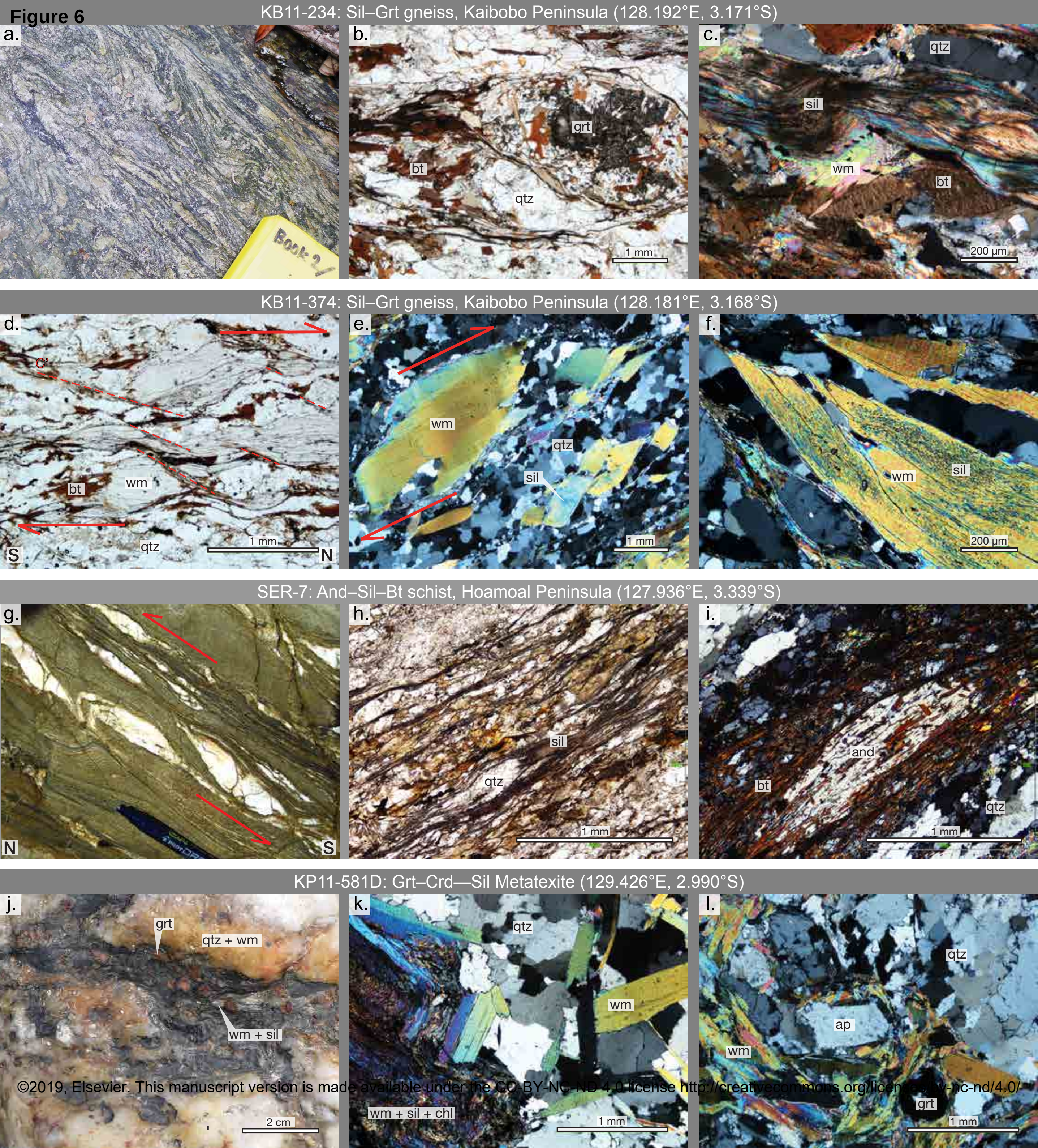
KB11-234: Sil–Grt gneiss, Kaibobo Peninsula (128.192°E, 3.171°S)
a.
Book 2
b.
grt
bt
qtz
1 mm
c.
qtz
sil
wm
bt
200 µm
KB11-374: Sil–Grt gneiss, Kaibobo Peninsula (128.181°E, 3.168°S)
d.
C'
bt
wm
qtz
S
1 mm
N
e.
wm
qtz
sil
1 mm
f.
wm
sil
200 µm
SER-7: And–Sil–Bt schist, Hoamoal Peninsula (127.936°E, 3.339°S)
g.
N
S
h.
sil
qtz
1 mm
i.
and
bt
qtz
1 mm
KP11-581D: Grt–Crd—Sil Metatexite (129.426°E, 2.990°S)
j.
grt
qtz + wm
wm + sil
2 cm
k.
qtz
wm
wm + sil + chl
1 mm
l.
qtz
ap
wm
grt
1 mm

Figure 7


KP11-593: Phlogopite Minette (129.480°E, 3.001°S)
a.
b.
serpentinised
lherzolite
~2 cm
c.
phlog
ap
kfs
pl
1 mm

Figure 8

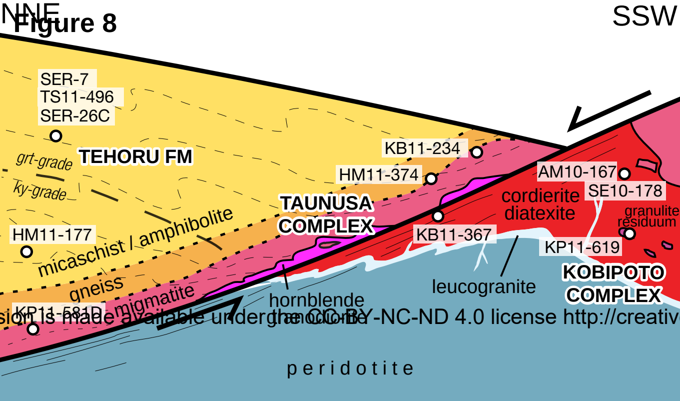
NNE
SSW
SER-7
TS11-496
SER-26C
TEHORU FM
grt-grade
ky-grade
HM11-177
micaschist / amphibolite
gneiss
migmatite
KP11-581D
KB11-234
HM11-374
TAUNUSA
COMPLEX
KB11-367
hornblende
AM10-167
SE10-178
cordierite
diatexite
granulite
residuum
KP11-619
leucogranite
KOBIPOTO
COMPLEX
peridotite

Figure 9

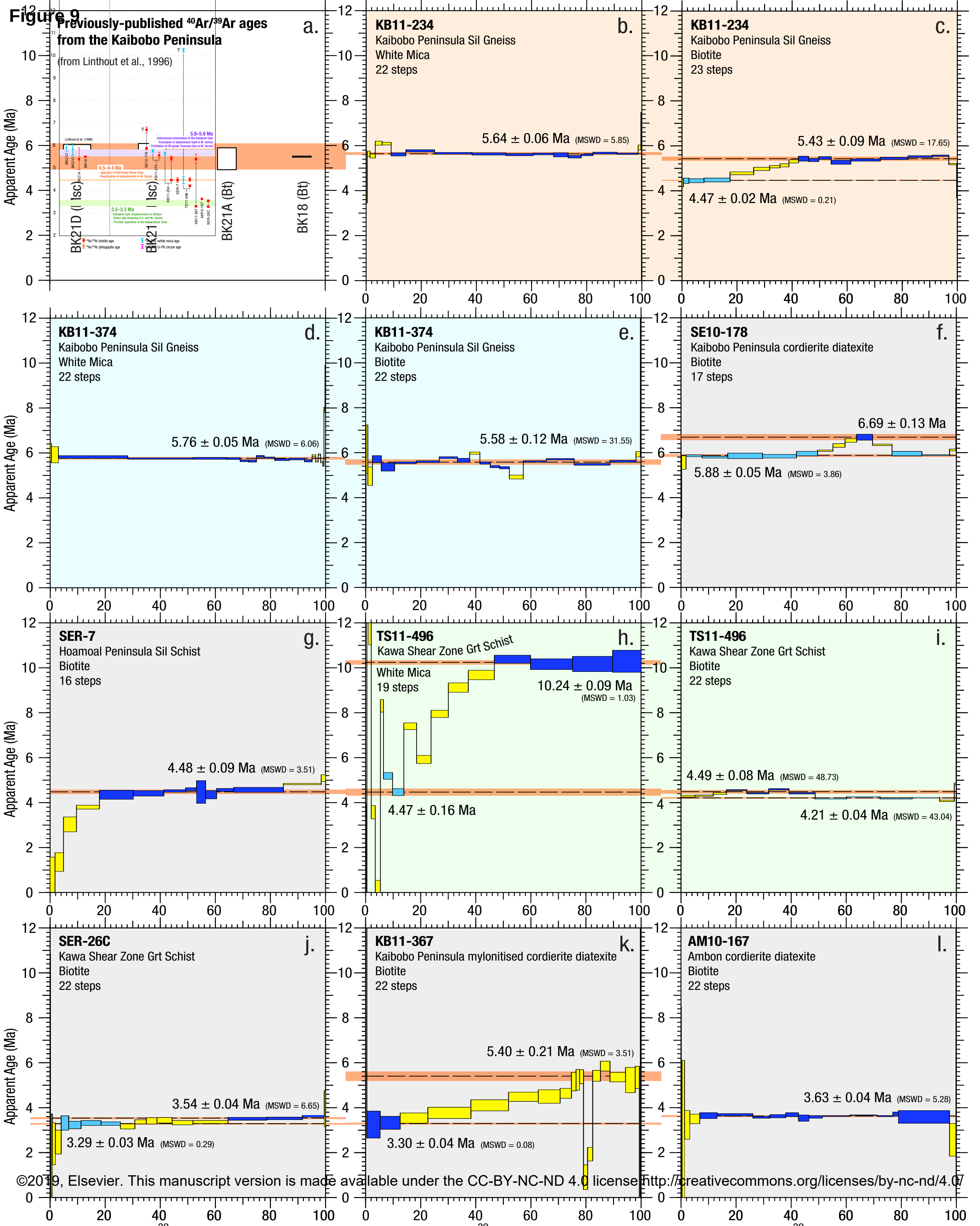

Previously-published $^{40}Ar/^{39}Ar$ ages from the Kaibobo Peninsula
(from Linthout et al., 1996)
a.
BK21D (I lsc)
BK21 I lsc)
BK21A (Bt)
BK18 (Bt)
KB11-234
Kaibobo Peninsula Sil Gneiss
White Mica
22 steps
b.
5.64 ± 0.06 Ma (MSWD = 5.85)
KB11-234
Kaibobo Peninsula Sil Gneiss
Biotite
23 steps
c.
5.43 ± 0.09 Ma (MSWD = 17.65)
4.47 ± 0.02 Ma (MSWD = 0.21)
KB11-374
Kaibobo Peninsula Sil Gneiss
White Mica
22 steps
d.
5.76 ± 0.05 Ma (MSWD = 6.06)
KB11-374
Kaibobo Peninsula Sil Gneiss
Biotite
22 steps
e.
5.58 ± 0.12 Ma (MSWD = 31.55)
SE10-178
Kaibobo Peninsula cordierite diatexite
Biotite
17 steps
f.
6.69 ± 0.13 Ma
5.88 ± 0.05 Ma (MSWD = 3.86)
SER-7
Hoamoal Peninsula Sil Schist
Biotite
16 steps
g.
4.48 ± 0.09 Ma (MSWD = 3.51)
TS11-496
Kawa Shear Zone Grt Schist
White Mica
19 steps
h.
10.24 ± 0.09 Ma (MSWD = 1.03)
4.47 ± 0.16 Ma
TS11-496
Kawa Shear Zone Grt Schist
Biotite
22 steps
i.
4.49 ± 0.08 Ma (MSWD = 48.73)
4.21 ± 0.04 Ma (MSWD = 43.04)
SER-26C
Kawa Shear Zone Grt Schist
Biotite
22 steps
j.
3.54 ± 0.04 Ma (MSWD = 6.65)
3.29 ± 0.03 Ma (MSWD = 0.29)
KB11-367
Kaibobo Peninsula mylonitised cordierite diatexite
Biotite
22 steps
k.
5.40 ± 0.21 Ma (MSWD = 3.51)
3.30 ± 0.04 Ma (MSWD = 0.08)
AM10-167
Ambon cordierite diatexite
Biotite
22 steps
l.
3.63 ± 0.04 Ma (MSWD = 5.28)
Apparent Age (Ma)
% ^{39}Ar released

Figure 10

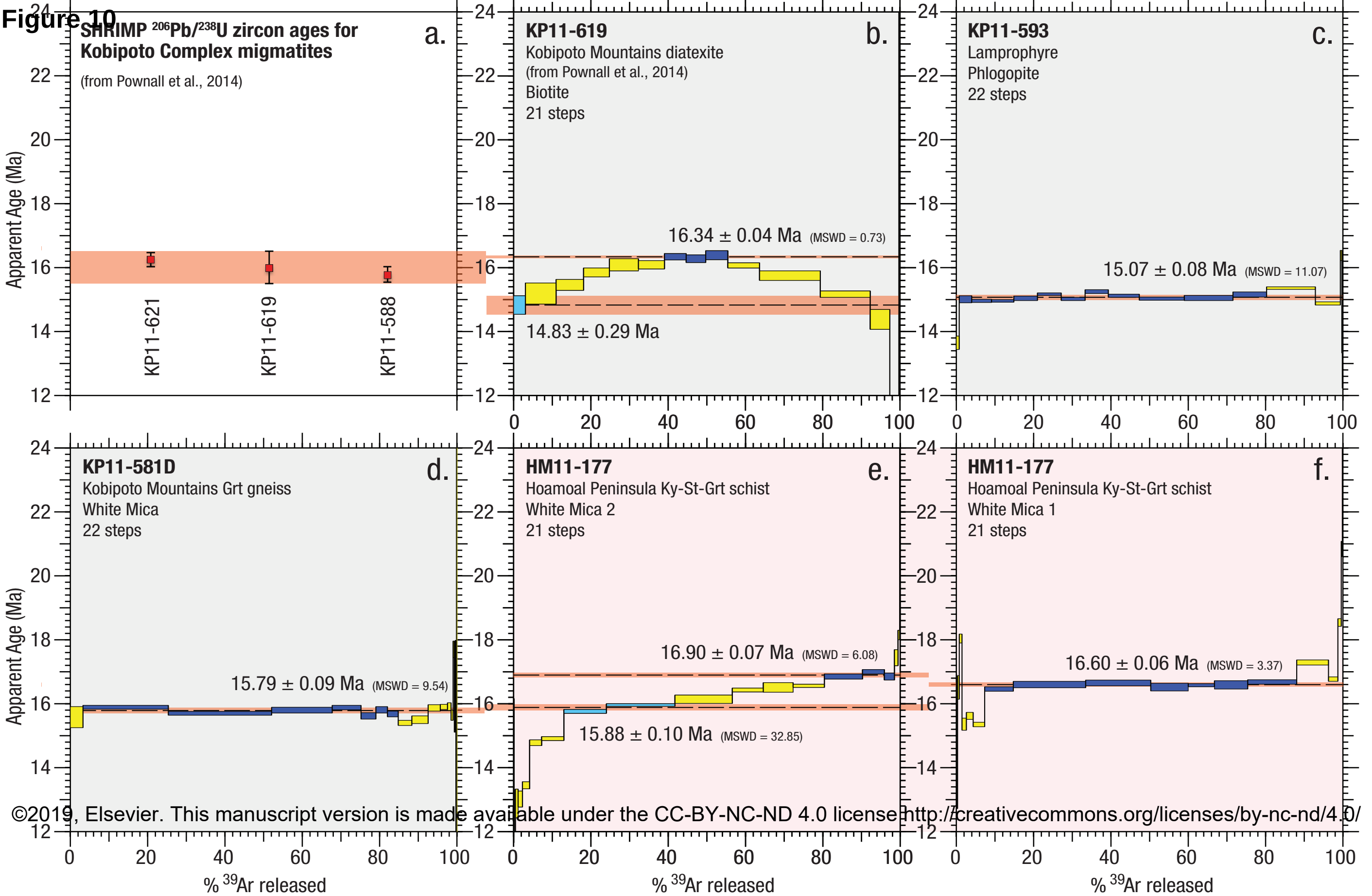
SHRIMP $^{206}Pb/^{238}U$ zircon ages for Kobipoto Complex migmatites
(from Pownall et al., 2014)
a.
KP11-621
KP11-619
KP11-588
Apparent Age (Ma)
KP11-619
Kobipoto Mountains diatexite
(from Pownall et al., 2014)
Biotite
21 steps
b.
16.34 ± 0.04 Ma (MSWD = 0.73)
14.83 ± 0.29 Ma
KP11-593
Lamprophyre
Phlogopite
22 steps
c.
15.07 ± 0.08 Ma (MSWD = 11.07)
KP11-581D
Kobipoto Mountains Grt gneiss
White Mica
22 steps
d.
15.79 ± 0.09 Ma (MSWD = 9.54)
HM11-177
Hoamoal Peninsula Ky-St-Grt schist
White Mica 2
21 steps
e.
16.90 ± 0.07 Ma (MSWD = 6.08)
15.88 ± 0.10 Ma (MSWD = 32.85)
HM11-177
Hoamoal Peninsula Ky-St-Grt schist
White Mica 1
21 steps
f.
16.60 ± 0.06 Ma (MSWD = 3.37)
% ^{39}Ar released

Figure 11

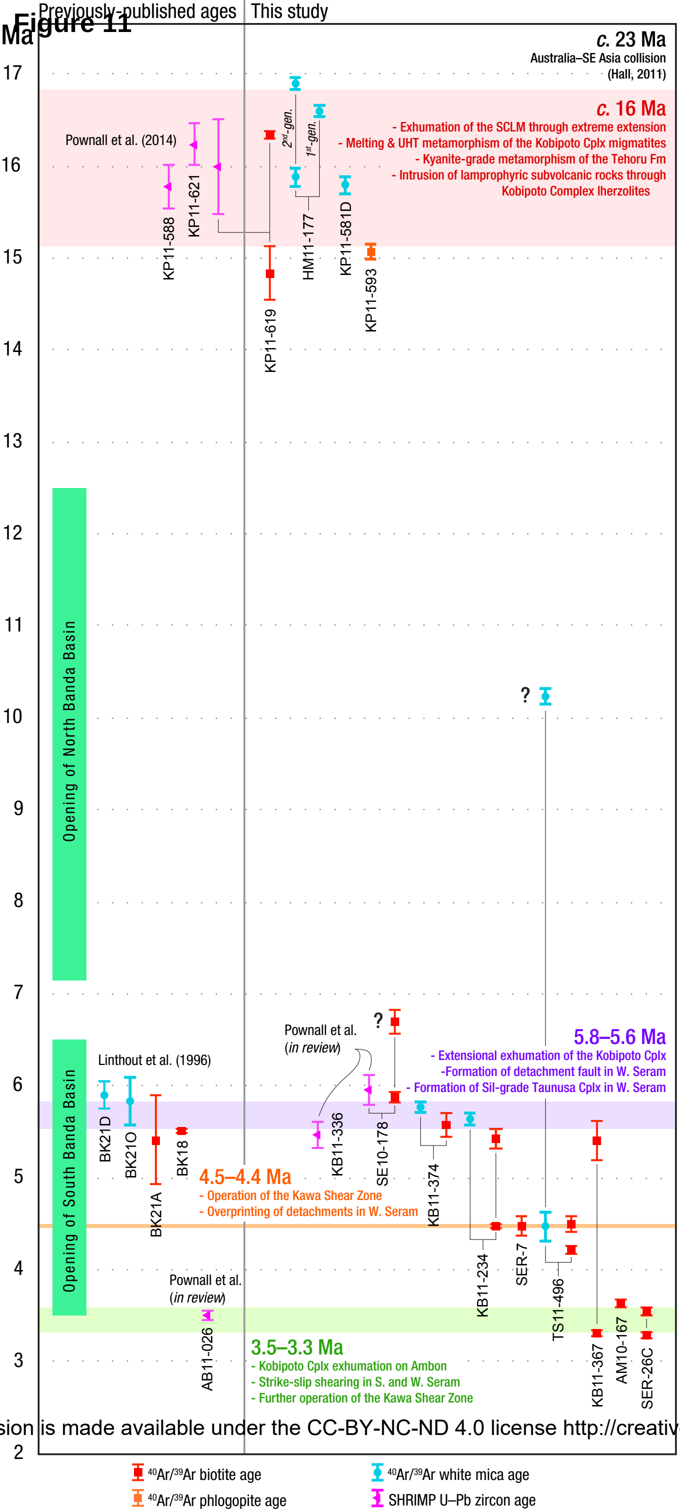
Previously-published ages
This study
Ma
17
16
15
14
13
12
11
10
9
8
7
6
5
4
3
2
c. 23 Ma
Australia–SE Asia collision
(Hall, 2011)
c. 16 Ma
- Exhumation of the SCLM through extreme extension
- Melting & UHT metamorphism of the Kobipoto Cplx migmatites
- Kyanite-grade metamorphism of the Tehoru Fm
- Intrusion of lamprophyric subvolcanic rocks through
Kobipoto Complex lherzolites
Pownall et al. (2014)
KP11-588
KP11-621
KP11-619
2nd-gen.
1st-gen.
HM11-177
KP11-581D
KP11-593
Opening of North Banda Basin
Opening of South Banda Basin
?
5.8–5.6 Ma
- Extensional exhumation of the Kobipoto Cplx
-Formation of detachment fault in W. Seram
- Formation of Sil-grade Taunusa Cplx in W. Seram
Linthout et al. (1996)
Pownall et al.
(in review)
BK21D
BK21O
BK21A
BK18
KB11-336
SE10-178
KB11-374
KB11-234
SER-7
TS11-496
KB11-367
AM10-167
SER-26C
4.5–4.4 Ma
- Operation of the Kawa Shear Zone
- Overprinting of detachments in W. Seram
Pownall et al.
(in review)
AB11-026
3.5–3.3 Ma
- Kobipoto Cplx exhumation on Ambon
- Strike-slip shearing in S. and W. Seram
- Further operation of the Kawa Shear Zone
40Ar/39Ar biotite age
40Ar/39Ar phlogopite age
40Ar/39Ar white mica age
SHRIMP U–Pb zircon age

Figure 12

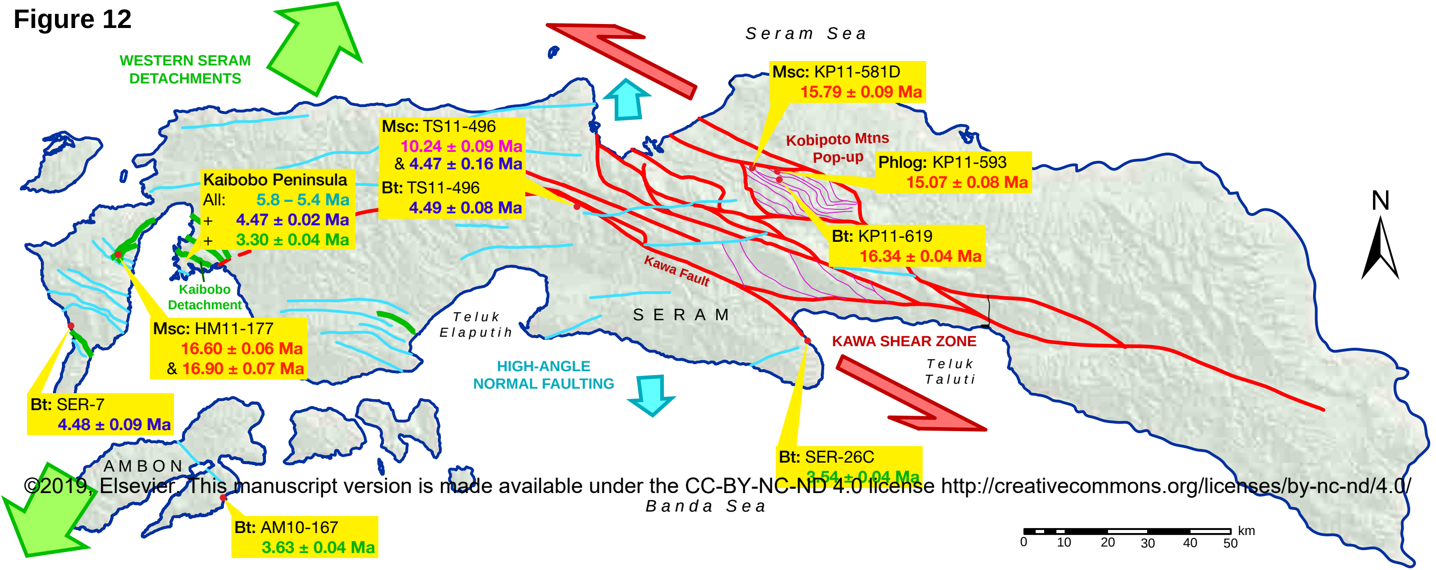
WESTERN SERAM DETACHMENTS
Seram Sea
Msc: KP11-581D
15.79 ± 0.09 Ma
Msc: TS11-496
10.24 ± 0.09 Ma
& 4.47 ± 0.16 Ma
Bt: TS11-496
4.49 ± 0.08 Ma
Kobipoto Mtns
Pop-up
Phlog: KP11-593
15.07 ± 0.08 Ma
Kaibobo Peninsula
All: 5.8 – 5.4 Ma
+ 4.47 ± 0.02 Ma
+ 3.30 ± 0.04 Ma
Bt: KP11-619
16.34 ± 0.04 Ma
N
Kawa Fault
Kaibobo
Detachment
Teluk
Elaputih
SERAM
Msc: HM11-177
16.60 ± 0.06 Ma
& 16.90 ± 0.07 Ma
KAWA SHEAR ZONE
Teluk
Taluti
HIGH-ANGLE
NORMAL FAULTING
Bt: SER-7
4.48 ± 0.09 Ma
AMBON
Bt: SER-26C
3.54 ± 0.04 Ma
Banda Sea
Bt: AM10-167
3.63 ± 0.04 Ma
km
0 10 20 30 40 50

Figure 13

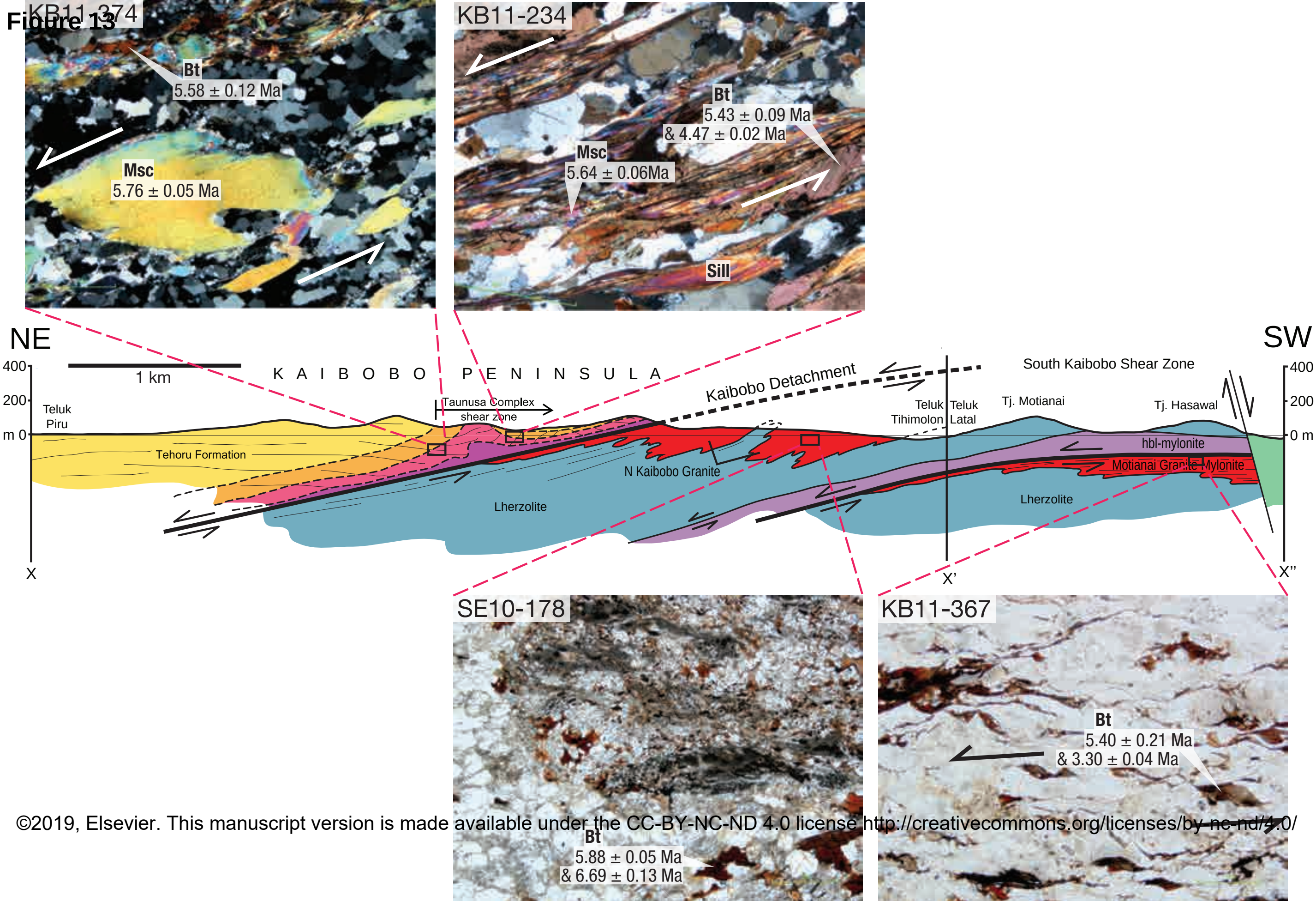

KB11-374
Bt
5.58 ± 0.12 Ma
Msc
5.76 ± 0.05 Ma
KB11-234
Bt
5.43 ± 0.09 Ma
& 4.47 ± 0.02 Ma
Msc
5.64 ± 0.06Ma
Sill
NE
SW
400
200
m 0
1 km
K A I B O B O P E N I N S U L A
Teluk
Piru
Taunusa Complex
shear zone
Kaibobo Detachment
South Kaibobo Shear Zone
Teluk
Tihimolon
Teluk
Latal
Tj. Motianai
Tj. Hasawal
400
200
0 m
Tehoru Formation
N Kaibobo Granite
hbl-mylonite
Motianai Granite Mylonite
Lherzolite
Lherzolite
X
X'
X''
SE10-178
Bt
5.88 ± 0.05 Ma
& 6.69 ± 0.13 Ma
KB11-367
Bt
5.40 ± 0.21 Ma
& 3.30 ± 0.04 Ma

Figure 14

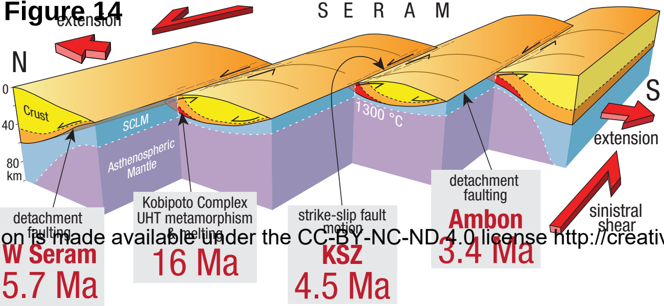

S E R A M
extension
N
S
0
40
80
km
Crust
SCLM
Asthenospheric Mantle
1300 °C
extension
sinistral shear
detachment faulting
W Seram
5.7 Ma
Kobipoto Complex UHT metamorphism & melting
16 Ma
strike-slip fault motion
KSZ
4.5 Ma
detachment faulting
Ambon
3.4 Ma

Figure 15

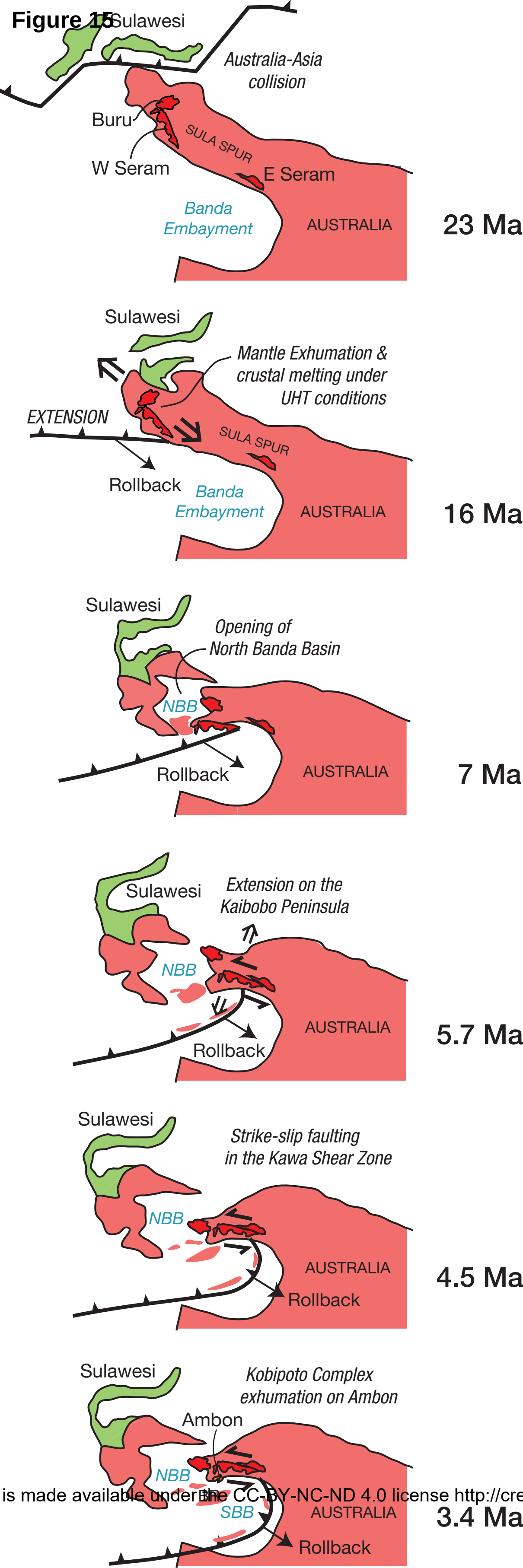

Sulawesi
Australia-Asia
collision
Buru
W Seram
SULA SPUR
E Seram
Banda
Embayment
AUSTRALIA
23 Ma
Sulawesi
Mantle Exhumation &
crustal melting under
UHT conditions
EXTENSION
SULA SPUR
Rollback
Banda
Embayment
AUSTRALIA
16 Ma
Sulawesi
Opening of
North Banda Basin
NBB
Rollback
AUSTRALIA
7 Ma
Sulawesi
Extension on the
Kaibobo Peninsula
NBB
AUSTRALIA
Rollback
5.7 Ma
Sulawesi
Strike-slip faulting
in the Kawa Shear Zone
NBB
AUSTRALIA
Rollback
4.5 Ma
Sulawesi
Kobipoto Complex
exhumation on Ambon
Ambon
NBB
SBB
AUSTRALIA
Rollback
3.4 Ma

Table 1

Authors	Sample No.	Rock	Geological unit	Location	Long. (˚E)	Lat. (˚S)	Age (Ma)			
							Rb–Sr	K–Ar	$^{40}Ar/^{39}Ar$	SHRIMP U–Pb zircon
Linthout et al. (1989)		Grt mica schist	Tehoru Formation	Central Seram				5–4 (Bt & Ms, prelim.)		
Linthout et al. (1991)	86 SNE 3	Grt mica schist	Tehoru Formation	Central Seram			3.4 ± 0.3 (Bt)	4.8 ± 0.4 (Bt)		
	86 SNE 9		Tehoru Formation	Central Seram			4.8 ± 0.3 (Bt)	3.0 ± 0.2 (Bt)		
	86 SNE 9		Tehoru Formation	Central Seram			5.4 ± 0.6 (Ms)			
Linthout et al. (1996)	BK21D	Sil gneiss	Taunusa Complex	Kaibobo Peninsula	128.17*	3.17*			5.90 ± 0.14 (Ms, l.s.h.)	
	BK21D	Sil gneiss	Taunusa Complex	Kaibobo Peninsula	128.17*	3.17*			2.91 ± 0.21 (Bt, l.s.h.)	
	BK21O	Sil gneiss	Taunusa Complex	Kaibobo Peninsula	128.17*	3.17*			5.83 ± 0.26 (Ms, l.s.h.)	
	BK21A	Sil-And gneiss	Taunusa Complex	Kaibobo Peninsula	128.17*	3.17*			6.64 ± 1.22 (Ms, l.s.h.)	
	BK21A	Sil-And gneiss	Taunusa Complex	Kaibobo Peninsula	128.17*	3.17*			5.41 ± 0.48 (Bt, l.s.h.)	
	BK18	Crd diatexite	Kobipoto Complex	Kaibobo Peninsula	128.17*	3.19*			5.51 ± 0.02 (Bt, l.s.f.)	
Pownall et al. (2014)	KP11-588	Grt-Sil granulite	Kobipoto Complex	Kobipoto Mountains	129.4786	3.0019				15.77 ± 0.24
	KP11-619	Grt-Crd-Sil metatexite	Kobipoto Complex	Kobipoto Mountains	129.4735	3.0168			16.34 ± 0.04 (Bt, f.s.h.)	16.00 ± 0.52
	KP11-621	Crd diatexite	Kobipoto Complex	Kobipoto Mountains	129.4785	3.0022				16.24 ± 0.23
Pownall et al. (*in review*)	SE10-178	Diatexite	Kobipoto Complex	Kaibobo Peninsula	128.1736	3.1884				5.95 ± 0.16
	KB11-336	Diatexite	Kobipoto Complex	Kaibobo Peninsula	128.1787	3.2005				5.47 ± 0.14
	AB11-026	Leucogranite	Kobipoto Complex	Latimor (Ambon)	128.2210	3.7192				3.49 ± 0.05
	AB11-384	Ambonite	high-K volcanics †	Hitu (Ambon)	128.0640	3.5930				1.94 ± 0.11

*estimated from map in Figure 2 of Linthout et al. (1996)

† as defined by Honthaas et al. (1999)

l.s.h.—laser step heating; f.s.h.—furnace step heating; l.s.f.—laser single fusion

prelim.—preliminary result

Table 2

Sample No.	Mineral	Rock	Geological unit	Location	Long. (˚E)	Lat. (˚S)	Prep. Method	Batch	Sample mass (mg)	Apparent age spectra Fig.	Interpreted $^{40}Ar/^{39}Ar$ ages (1σ errors)
SER-26C	biotite	Grt-Hbl mica schist	Tehoru Fm	Tehoru area	129.5204	3.3484	1	ANU#7	68.8	9j	Mixing between two gas reservoirs of similar $^{40}Ar/^{39}Ar$ ages: ***3.54 ± 0.04 Ma*** and ***3.29 ± 0.03 Ma***
TS11-496	white mica	Grt mica schist	Tehoru Fm	Kawa Shear Zone	129.0378	3.0751	1	ANU#13	90.9	9h	A ***10.24 ± 0.09 Ma*** $^{40}Ar/^{39}Ar$ age mixing with a younger gas population whose $^{40}Ar/^{39}Ar$ age tends to a ***4.47 ± 0.16 Ma*** lower limit
	biotite						1	ANU#13	62.2	9i	Mixing between two gas reservoirs of similar $^{40}Ar/^{39}Ar$ ages: ***4.49 ± 0.08 Ma*** and ***4.21 ± 0.04 Ma***
HM11-177	white mica (1st gen.)	Ky-St-Grt mica schist	Tehoru Fm	Hoamoal Pen.	128.0517	3.1719	2	ANU#13	111.4	10f	Single age of ***16.60 ± 0.06 Ma*** calculated from heating steps that collectively released ~80% of total ^{39}Ar
	white mica (2nd gen.)						2	ANU#13	91.5	10e	A ***16.90 ± 0.07 Ma*** $^{40}Ar/^{39}Ar$ age mixing with a younger ***15.88 ± 0.10 Ma*** $^{40}Ar/^{39}Ar$ age
KP11-581D	white mica	Grt-Sil metatexite	?Tehoru Fm	Kobipoto Mtns	129.4256	2.9902	2	ANU#13	31.5	10d	Single $^{40}Ar/^{39}Ar$ age of ***15.79 ± 0.09 Ma*** calculated from heating steps that collectively released ~80% of total ^{39}Ar
KB11-234	white mica	Sil-Grt gneiss	Taunusa Cplx	Kaibobo Pen.	128.1924	3.1708	1	ANU#13	42.1	9b	Single $^{40}Ar/^{39}Ar$ age of ***5.64 ± 0.06 Ma*** calculated from heating steps that collectively released ~90% of total ^{39}Ar
	biotite						1	ANU#13	89.7	9c	Spectrum converges on two limits due to a ***5.43 ± 0.09 Ma*** $^{40}Ar/^{39}Ar$ age mixing with a younger ***4.47 ± 0.02 Ma*** $^{40}Ar/^{39}Ar$ age
KB11-374	white mica	Sil-Grt gneiss	Taunusa Cplx	Kaibobo Pen.	128.1813	3.1682	2	ANU#13	52.0	9d	Single $^{40}Ar/^{39}Ar$ age of ***5.76 ± 0.05 Ma*** calculated from heating steps that collectively released ~90% of total ^{39}Ar
	biotite						2	ANU#13	12.6	9e	Single $^{40}Ar/^{39}Ar$ age of ***5.58 ± 0.12 Ma*** calculated from heating steps that collectively released ~80% of total ^{39}Ar
SER-7	biotite	Sil-Bt schist	Taunusa Cplx	Hoamoal Pen.	127.9359	3.3394	1	ANU#7	47.8	9g	Spectrum rises to an upper limit relating to an $^{40}Ar/^{39}Ar$ age of ***4.48 ± 0.09 Ma*** calculated from heating steps that collectively released ~60% of total ^{39}Ar
KB11-367	biotite	mylonitised diatexite	Kobipoto Cplx	Kaibobo Pen.	128.2024	3.2173	2	ANU#13	11.4	9k	A ***5.40 ± 0.21 Ma*** age mixing with a younger ***3.30 ± 0.04 Ma*** age. The two steps at ~80% of total ^{39}Ar release are spurious and are likely due to sample contamination
KP11-619	biotite	metatexite	Kobipoto Cplx	Kobipoto Mtns	129.4735	3.0168	1	ANU#13	2.7	10b	Spectrum produced by mixing between two argon reservoirs: one with an $^{40}Ar/^{39}Ar$ age of ***16.34 ± 0.04 Ma***, and one with an $^{40}Ar/^{39}Ar$ age of ***14.83 ± 0.29 Ma***
AM10-167	biotite	cordierite diatexite	Kobipoto Cplx	Ambon	128.2447	3.7379	1	ANU#7	51.3	9l	Single $^{40}Ar/^{39}Ar$ age of ***3.63 ± 0.04 Ma*** calculated from heating steps that collectively released ~90% of total ^{39}Ar
SE10-178	biotite	cordierite diatexite	Kobipoto Cplx	Kaibobo Pen.	128.1736	3.1884	1	ANU#7	120.0	9f	A ***5.88 ± 0.05 Ma*** age mixing slightly with a Ar population whose age converges to an upper limit of ***6.69 ± 0.13 Ma***
KP11-593	phlogopite	lamprophyre	Kobipoto Cplx	Kobipoto Mtns	129.4802	3.0006	2	ANU#13	100.5	10c	Single $^{40}Ar/^{39}Ar$ age of ***15.07 ± 0.08 Ma*** calculated from heating steps that collectively released ~80% of total ^{39}Ar

Fm—formation; Cplx—complex; gen.—generation; pen.—peninsula; mtns—mountains